4-2016

Dynamic sensor tasking and IMM EKF estimation for tracking impulsively maneuvering satellites

Arthur A. Lace
Purdue University

Graduate School Form
30 Updated 12/26/2015

PURDUE UNIVERSITY
GRADUATE SCHOOL
Thesis/Dissertation Acceptance

This is to certify that the thesis/dissertation prepared

By Arthur A Lace

Entitled

Dynamic Sensor Tasking and IMM EKF Estimation for Tracking Impulsively Maneuvering Satellites

For the degree of Master of Science in Aeronautics and Astronautics

Is approved by the final examining committee:

Inseok Hwang
Chair

Carolin E. Frueh

Dengfeng Sun

To the best of my knowledge and as understood by the student in the Thesis/Dissertation Agreement, Publication Delay, and Certification Disclaimer (Graduate School Form 32), this thesis/dissertation adheres to the provisions of Purdue University's "Policy of Integrity in Research" and the use of copyright material.

Approved by Major Professor(s): Inseok Hwang

Approved by: Weinong Wayne Chen 4/18/2016

Head of the Departmental Graduate Program Date

DYNAMIC SENSOR TASKING
AND IMM EKF ESTIMATION
FOR TRACKING IMPULSIVELY MANEUVERING SATELLITES

A Thesis

Submitted to the Faculty

of

Purdue University

by

Arthur A. Lace

In Partial Fulfillment of the

Requirements for the Degree

of

Master of Science in Aeronautics and Astronautics

May 2016

Purdue University

West Lafayette, Indiana

ACKNOWLEDGMENTS

Sangjin Lee provided a great deal of assistance during the writing of this thesis. His research into IMM EKF satellite tracking was the initial inspiration for this work. Meetings and discussion with him are part of what enabled this paper to be written. The time he was willing to spare while working on his own doctoral thesis was greatly appreciated.

Inseok Hwang's guidance as a thesis advisor was invaluable in understanding satellite tracking and tasking as a guidance, navigation, and control problem, enabling the creation of this thesis. His criticisms were also essential in refining this thesis into its present form.

Robert Lace and Mina Adsit provided essential support during the process of writing this paper. Without their assistance maintaining a positive mentality throughout this process would have been nearly impossible. Robert's assistance with editing was also critical in making sure a much reduced number of errors made it into the final paper.

TABLE OF CONTENTS

LIST OF TABLES

LIST OF FIGURES

Figure Page

Figure Page

Figure Page

Figure Page

SYMBOLS

$\boldsymbol{x}$	System state
$\boldsymbol{P}$	State estimate covariance
$\boldsymbol{r}$	Position
$\boldsymbol{v}$	Velocity
$\boldsymbol{y}$	Sensor measurements
$\boldsymbol{Y}$	Combined sensor measurements
ρ	Sensor measurement range
ψ	Sensor measurement longitude
θ	Sensor measurement latitude
h	Sensor dynamics function
$\boldsymbol{C}$	Linearized sensor dynamics
Ω	Fisher Information matrix
$\mu_{i,j}$	Information gain
γ	Probability of mode transition
$\mathcal{N}$	Gaussian normal distribution
$\boldsymbol{\mu}$	Maneuver trigger mean
$\boldsymbol{L}$	Maneuver trigger variable matrix
m	Mode probability
$\boldsymbol{Q}$	State error covariance
$\boldsymbol{R}$	Sensor error covariance
f	System dynamics function
$\boldsymbol{F}$	Linearized system dynamics matrix
$\boldsymbol{K}$	Kalman gain
μ	Earth's gravitational parameter

ABBREVIATIONS

ECF	Earth centered earth fixed reference frame
ECI	Earth centered inertial reference frame
EKF	Extended Kalman filter
GEO	Geostationary earth orbit
IMM	Interacting multiple model
LEO	Low earth orbit
LHLV	Local horizontal local vertical reference frame
RMS	Root mean squared
SBSS	Space Based Space Surveillance

ABSTRACT

Lace, Arthur A. M.S.A.A., Purdue University, May 2016. Dynamic Sensor Tasking and IMM EKF Estimation for Tracking Impulsively Maneuvering Satellites. Major Professor: Inseok Hwang.

In order to efficiently maintain space situational awareness, care must be taken to optimally allocate expensive observation resources. In most situations the available sensors capable of tracking spacecraft have their time split between many different monitoring responsibilities. Tracking maneuvering spacecraft can be especially difficult as the schedule of maneuvers may not be known and will often throw off previous orbital models. Effectively solving this tasking problem is an ongoing focus of research in the area of space situational awareness. Most methods of automated tasking do not make use of interacting multiple model extended Kalman filter techniques to better track satellites during maneuvers. This paper proposes a modification to a Fisher information gain and estimated state covariance based sensor tasking method to take maneuver probability and multiple model dynamics into account. By incorporating the probabilistic maneuvering model, sensor tasking can be improved during satellite maneuvers using constrained resources. The proposed methods are verified through the use of numerical simulations with multiple maneuvering satellites and both orbital and ground-based sensors.

1. INTRODUCTION

1.1 Motivation

It is essential to effectively track satellites and other spacecraft to ensure the safety of both future and current space missions. Estimating the orbits of satellites without the use of on-board telemetry is a task that requires limited and expensive observational resources. Making the best use of these resources is an important component of maintaining space situational awareness (SSA). To this end, dynamic optimal sensor allocation can be utilized as a component of an effective tracking system using distributed sensor resources. Efficient automated sensor tasking research is a major focus of several recent developments in SSA [1] [2].

The current development of automated sensor tasking methods for tracking potentially maneuvering or station keeping satellites using maneuver probability metrics is somewhat underdeveloped. The quick detection of changes in orbit can be important in crowded orbital zones or regions where high positioning precision is important [2]. Modern systems such as the Space-Based Space Surveillance (SBSS) system can be used as a basis for modeling distributed sensor systems [3].

1.2 Maneuvering Satellite Tracking

Maintaining space situational awareness is an important component of effectively managing the increasingly complex and valuable infrastructure in earth orbit. Satellite telemetry is an important component of tracking satellites, but needs to be augmented and verified by independent observations to ensure satellites are performing as expected. By the nature of iterative probability, the more satellites are in space and the longer they are in continuous operation, the greater chance there is for the

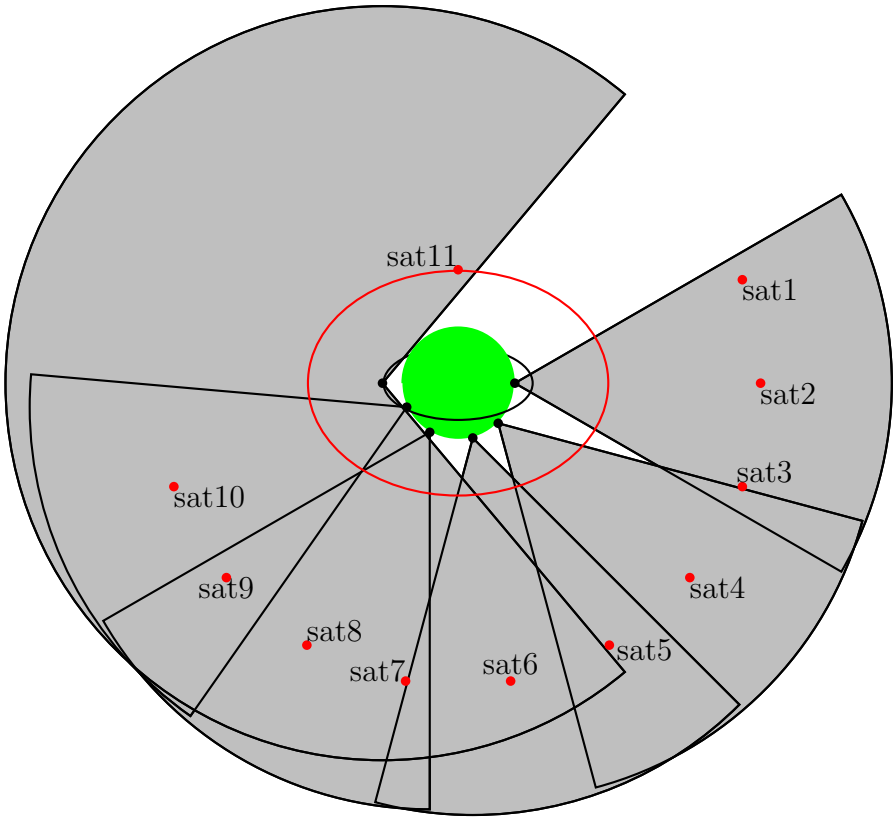

Figure 1.1. Sensor and satellite configuration where earth orbiting or ground-based sensors (black) observe certain limited regions (gray) and attempt to track target satellites (red)

occurrence of accidents. To mitigate the potential for complications, techniques used to track and verify the proper operation of satellites needs to continuously improve. Human error or malice can also foul up communications between satellite operating organizations, greatly increasing the risk of accidents or other misfortunes [2].

Satellites maneuver using impulsive or continuous propulsion systems in the vast majority of cases [4] [2]. In the case of modern continuous systems using low thrust propulsion methods, traditional extended Kalman filter (EKF) tracking methods can maintain high accuracies as gradual state changes can be accounted for using either the sensor data or adjustments to the system models [5]. However, in the case of

impulsive maneuvers, the ability to quickly detect and respond to rapid changes is an issue with state estimation techniques.

Impulsive maneuvers are a critical part of maintaining many satellites' orbits or of their transitions between orbits. Station keeping maneuvers can occur as often as four times a day in the case of classical geostationary earth orbit (GEO) station keeping [6]. Often an observer has no knowledge of the schedule or method of maneuvers for a given satellite. Because of the uncertainty inherent in when maneuvers may occur it is difficult or unwise to include maneuvers directly into the EKF satellite model. Probabilistic methods must be used to predict maneuvers instead.

1.3 Interacting Multiple Model Extended Kalman Filter

One of the more direct ways to account for partially known maneuvering models in satellite tracking is to use an interacting multiple model (IMM) EKF [7]. By using several EKF filters that utilize both maneuvering and non-maneuvering modes, the blending of the modes generates a more accurate depiction of the satellite motion during maneuvers. This IMM method is generally very useful when the potential maneuver can be represented as an increase in state error.

IMM tracking is a well known and understood method of dealing with systems that operate in distinct modes depending on certain state based parameters [8], especially in tracking maneuvering satellites [7]. Satellite behavior when not maneuvering is relatively deterministic, based on orbital mechanics and known disturbances while its maneuvering behavior is uncertain and heavily dependent on the type of satellite and its current state.

The design of a maneuver probability model is a key component of IMM EKF methods of state estimation [7]. Assigning a high probability to the likely points of maneuver allows the IMM EKF to properly adjust the estimation dynamics to better follow the maneuvering target. The maneuver probability models are based around having a high probability near the bounds of the geostationary operating window for

geostationary satellites or near an apsis point for satellites in other orbits. Maneuvering probability models have to change substantially between different satellite types as the expected behavior for GEO station keeping differs significantly from orbital transfers and other maneuvers.

1.4 Information Gain Sensor Allocation

The information gain method of sensor allocation is based on generating a metric related to improvement in estimation accuracy of the EKF from a potential measurement on each update step to use in the cost function of a linear programming optimization [9]. One common metric used to express the potential accuracy gain of a particular measurement is the Fisher information matrix, which is determined by the sensor dynamics and error of the system [1]. The current state estimate covariance matrix can also be used as a component of the information gain as a measure of the current uncertainty of a particular satellite.

By calculating the information gain for each sensor-target pair at each update step an optimal allocation of sensors can be generated. This tasking method has the advantage of using simple linear programming techniques once the information gain is calculated from the most recent state estimates. Fisher information gain is a well researched method of sensor allocation that is fairly simple to implement even with nonlinear orbital mechanics [1].

The Fisher information gain cannot be used alone for general satellite tracking problems without other metrics. Fisher information gain tasking identifies which potential measurements generate the greatest reduction in estimated state covariance based on the available sensors, but does not take into account whether a target has been observed recently. Without a state estimate covariance term in the information gain, certain hard to measure targets could potentially never be observed if there are not sufficient sensors to ensure that all targets are observed at every time step.

It is assumed in this paper that the sensor allocation is altered at every update step, which is not necessarily possible for several sensor technologies. However, simplifications of the sensor dynamics are necessary to keep the scope of the problem reasonable. Some adjustments to the IMM EKF model need to be made to account for the potential lack of sensor data at a given update step. This paper does not address the satellite acquisition and state initialization problem [10] and its integration into these methods could be subject of future research.

1.5 Sensor Systems

The primary source of satellite observations in the United States is the distributed network of sensors and satellites run by the US Air Force and related agencies. This collection of radar, optical, passive radio, and other sensors provides information on a wide variety of space objects [11]. Most of the current optical methods rely on detecting orbital tracks and collating track data from different observatories to determine positioning and orbital information [12]. SBSS and other observation systems track a wide variety of satellites including GEO targets as part of their mission [3]. Because this research is interested in tracking satellites in higher earth orbits optical sensors are the preferred sensor type [13].

Observation planning was historically done on a daily basis [11] but developments in automated sensor and distributed automation have enabled more advanced methods. To ensure automated systems are effectively used, their targets need to be selected intelligently. Greedy optimization algorithms based on target priority were initially used for satellite tracking but modern advancements in dynamic scheduling has allowed for more advanced solutions [9]. Unfortunately, there are limited research resources for dynamically tracking multiple potentially maneuvering spacecraft. Integrating improved maneuvering spacecraft tracking methods [14] into a dynamic tasking method could demonstrate improved performance and illustrating this possibility is one of the primary goals of this paper.

1.6 Proposed Tasking Method Improvement

Using IMM EKF methods designed to track maneuvering satellites, the performance of sensor networks tracking multiple targets can be improved. If a satellite is not observed soon after a maneuver, larger errors can be generated requiring a probabilistic component to be included in the information gain. Demonstrating improvements in tracking over single EKF methods in a sensor restricted system with multiple maneuvering satellites would confirm the effectiveness of IMM EKF tracking.

2. METHODOLOGY

2.1 Sensor Modeling

For every filter time step each target satellite i is observed using a subset of the available sensors j. These sensors can be either orbital observation platforms or ground-based satellite tracking resources, as seen in Figure 1.1.

The sensor dynamics need to be modeled in a manner approximating real world sensors. Optical sensors generally make use of arc tracking techniques to determine satellite orbits [11]. But to keep the sensor model manageable, the examples in this paper use a simplified representation of satellite observations. The sensor outputs are considered as simple range and angle measurements with associated error covariances [1] [7]. The range $\rho_{i,j}$, longitude $\psi_{i,j}$, and latitude $\theta_{i,j}$ angles are calculated in the

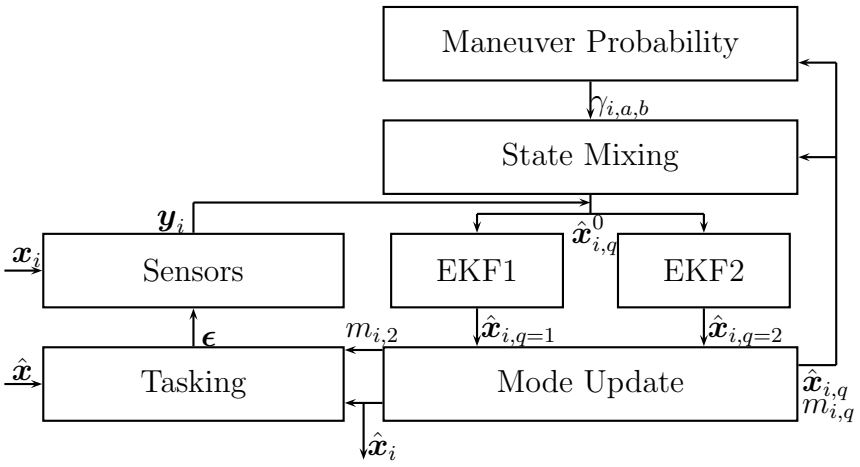

Figure 2.1. Tracking and tasking method block diagram

earth centered earth fixed (ECF) reference frame and can be converted to the other reference frames if needed.

The system state for satellite i is represented by $\boldsymbol{x}_i = [\boldsymbol{r_i}^T, \boldsymbol{v_i}^T]^T$ while the position of sensor j is represented by $\boldsymbol{r}_j$. The sensor dynamics are derived from system states composed of the position $\boldsymbol{r}_i = [x_i, y_i, z_i]^T$ and velocity $\boldsymbol{v}_i = [v_{x,i}, v_{y,i}, v_{z,i}]^T$ components in the current reference frame along with sensor positions $\boldsymbol{r}_j = [x_j, y_j, z_j]^T$.

$$\rho_{i,j} = \sqrt{(x_i - x_j)^2 + (y_i - y_j)^2 + (z_i - z_j)^2} \tag{2.1}$$

$$\psi_{i,j} = \tan^{-1}(\frac{y_i - y_j}{x_i - x_j}) \tag{2.2}$$

$$\theta_{i,j} = \tan^{-1}(\frac{z_i - z_j}{\sqrt{(x_i - x_j)^2 + (y_i - y_j)^2}}) \tag{2.3}$$

$$h_{i,j}(\boldsymbol{x}) = \begin{bmatrix} \rho_{i,j} \\ \psi_{i,j} \\ \theta_{i,j} \end{bmatrix} \tag{2.4}$$

The above sensor dynamics can then be converted to a linearized matrix $\hat{\boldsymbol{C}}_{i,j}$ that is determined specifically for each sensor-target pair. During tasking the satellite state values are based on the last estimate of the satellites state.

$$\hat{\boldsymbol{C}}^{\boldsymbol{r}}_{i,j} = \begin{bmatrix} \frac{\delta\rho_{i,j}}{\delta x_i} & \frac{\delta\rho_{i,j}}{\delta y_i} & \frac{\delta\rho_{i,j}}{\delta z_i} \\ \frac{\delta\psi_{i,j}}{\delta x_i} & \frac{\delta\psi_{i,j}}{\delta y_i} & \frac{\delta\psi_{i,j}}{\delta z_i} \\ \frac{\delta\theta_{i,j}}{\delta x_i} & \frac{\delta\theta_{i,j}}{\delta y_i} & \frac{\delta\theta_{i,j}}{\delta z_i} \end{bmatrix} \tag{2.5}$$

$$\hat{\boldsymbol{C}}^{\boldsymbol{r}}_{i,j} = \begin{bmatrix} \frac{x_i - x_j}{\rho_{i,j}} & \frac{y_i - y_j}{\rho_{i,j}} & \frac{z_i - z_j}{\rho_{i,j}} \\ \frac{-(y_i - y_j)}{(x_i - x_j)^2 + (y_i - y_j)^2} & \frac{x_i - x_j}{(x_i - x_j)^2 + (y_i - y_j)^2} & 0 \\ \frac{-(x_i - x_j)(z_i - z_j)}{\sqrt{(x_i - x_j)^2 + (y_i - y_j)^2}\rho_{i,j}^2} & \frac{-(y_i - y_j)(z_i - z_j)}{\sqrt{(x_i - x_j)^2 + (y_i - y_j)^2}\rho_{i,j}^2} & \frac{\sqrt{(x_i - x_j)^2 + (y_i - y_j)^2}}{\rho_{i,j}} \end{bmatrix} \tag{2.6}$$

$$\hat{\boldsymbol{C}}_{i,j} = \left[\hat{\boldsymbol{C}}^{\boldsymbol{x}}_{i,j}, \boldsymbol{0}^{3\times 3}\right] \tag{2.7}$$

The $\hat{\boldsymbol{C}}_{i,j}$ matrix is used as part of the sensor tasking as well as in the EKF using the propagated system state estimate. The sensor model is the same no matter the type of object being tracked within the scope of this paper.

2.2 Reference Frames

The tracking and tasking methods described in this paper make use of three different orbital reference frames. The tasking problem is handled in the ECF reference frame for easy positioning of ground-based observational resources and simplified handling of GEO satellites. The orbital simulations and the low earth orbit (LEO) orbit case tracking method make use of the earth centered inertial (ECI) frame due to the ease of general orbital simulations. The GEO satellite tracking makes use of the local horizontal local vertical(LHLV) reference frame centered at the satellites' target orbital position. In the LHLV reference frame x is along the orbital track, y is along the axis from the earth center to the orbital target, and z is perpendicular to the orbital plane.

The conversion between the ECF and the LHLV reference frames used in the GEO satellite tracking is primarily dependent on the target longitude L_i and radius R_g of the geostationary orbit [15]. Neither ECF nor LHLV are inertial reference frames, but they are contained within the same non-inertial frame.

$$x_{ECF} = \cos(L_i)(x_{LHLV} + R_g) - \sin(L_i)y_{LHLV} \tag{2.8}$$

$$y_{ECF} = \sin(L_i)(x_{LHLV} + R_g) + \cos(L_i)y_{LHLV} \tag{2.9}$$

$$z_{ECF} = z_{LHLV} \tag{2.10}$$

$$C_{ECF}^{LHLV} = \begin{bmatrix} \cos(L_i) & -\sin(L_i) & 0 \\ \sin(L_i) & \cos(L_i) & 0 \\ 0 & 0 & 1 \end{bmatrix} \tag{2.11}$$

$$\boldsymbol{v}_{ECF} = C_{ECF}^{LHLV}\boldsymbol{v}_{LHLV} \tag{2.12}$$

Converting between ECF and ECI is more elaborate due to the change between a non-inertial and inertial frames. This frame conversion requires the inclusion of the

rotation rate of the earth against the inertial frame ω_e and the time elapsed since the initial alignment of the two frames $(t - t_{align})$.

$$C_{ECF}^{ECI}(k) = \begin{bmatrix} \cos(\omega_e(t - t_{align})) & \sin(\omega_e(t - t_{align})) & 0 \\ -\sin(\omega_e(t - t_{align})) & \cos(\omega_e(t - t_{align})) & 0 \\ 0 & 0 & 1 \end{bmatrix} \tag{2.13}$$

$$\boldsymbol{r}_{ECF}(k) = C_{ECF}^{ECI}(k)\boldsymbol{r}_{ECI}(k) \tag{2.14}$$

$$\boldsymbol{v}_{ECF}(k) = C_{ECF}^{ECI}(k)\left(\boldsymbol{v}_{ECI}(k) - cross(\begin{bmatrix} 0, & 0, & \omega_e \end{bmatrix}^T, \boldsymbol{r}_{ECI}(k))\right) \tag{2.15}$$

The state estimate covariance matrix also needs to be converted between reference frames using the basic covariance rotation method from reference frame a to ECF.

$$D_{ECF}^{a}(k) = \begin{bmatrix} C_{ECF}^{a}(k) & \mathbf{0} \\ \mathbf{0} & C_{ECF}^{a}(k) \end{bmatrix} \tag{2.16}$$

$$\boldsymbol{P}_{ECF} = D_{ECF}^{a}(k)^T \boldsymbol{P}_a D_{ECF}^{a}(k) \tag{2.17}$$

The sensor readings taken in the ECF frame also need to be converted, but this is simply a matter of altering the $\psi_{i,j}$ term by the appropriate amount. The latitude and range are the same in all reference frames used.

$$\psi_{i,j,ECI} = \psi_{i,j,ECF} + \omega_e(t - t_{align}) \tag{2.18}$$

$$\psi_{i,j,LHLV} = \psi_{i,j,ECF} - Li \tag{2.19}$$

2.3 Fisher Information Gain

Assigning sensors to track multiple targets can be formulated as a traditional linear optimization problem. Using a linear form allows simple and computationally efficient techniques such as linear programming to be used. However, to get good results from this assignment process, a consistent and effective method of assigning tasking gains is required.

One simple but very useful metric for the information gain where every satellite would have at least one sensor observing it is the Fisher information gain [9]. This is a metric that expresses the reduction of the state covariance matrix in the Kalman filter tracking that object for a potential observation.

The Fisher information matrix for each sensor satellite pair $\boldsymbol{\Omega}_{i,j}$ is dependent primarily on the sensor noise and the current system geometry. The Fisher information matrix is related to the change in covariance $\boldsymbol{P}_i$ at each update step where M_i sensors observe satellite i.

$$\boldsymbol{P}_i(k)^{-1} = \boldsymbol{P}_i(k|k-1)^{-1} + \sum_{j=1}^{M_i} \boldsymbol{\Omega}_{i,j} \tag{2.20}$$

The Fisher information matrix is derived from the sensor model error covariance $\boldsymbol{R}_j$ and the current estimate of the satellites position.

$$\boldsymbol{\Omega}_{i,j} = (\hat{\boldsymbol{C}}_{i,j})^T \boldsymbol{R}_j^{-1} (\hat{\boldsymbol{C}}_{i,j}) \tag{2.21}$$

The Fisher information gain includes no components of the IMM EKF tracking methodology or maneuver probability. Thus, the traditional implementation of Fisher information gain $\mu_{i,j}^F$ is not meaningfully different when using IMM EKF tracking methods [1]. The sum of all the diagonal elements of the Fisher information matrix is used as the Fisher information gain.

$$\mu_{i,j}^F = \mathrm{tr}(\boldsymbol{\Omega}_{i,j}) \tag{2.22}$$

In the scenario considered in this paper, every satellite cannot have at least one observation at every time step so purely Fisher information gain tasking will not function properly, so alternative methods need to be used.

2.4 Tasking Methodology

The tasking of the sensor network is based on the maximization problem using the information gain metric $\mu_{i,j}$. This gain value is calculated for each sensor-target

pair and is related to an estimate of how much reduction in error is gained from that particular observation and the current estimated error of the system. The tasking can be formulated as a linear optimization problem dependent on maximizing the sum of all the $\mu_{i,j}$ values associated with active observations. Every possible observation is represented as a variable $\epsilon_{i,j}$ [1] that equals one if sensor j observes satellite i, and is zero otherwise. The cost function for the optimization problem can be expressed as a simple summation to optimize the matrix ϵ. In this formulation there are N satellites and M sensors in the system.

$$J = \sum_{i=1}^{N} \sum_{j=1}^{M} \mu_{i,j} \epsilon_{i,j} \tag{2.23}$$

The optimization of ϵ is subject to the limitation that each sensor can only observe T targets at any given time. Many sensor-target pairs would not be valid observations due to range, angle, or visibility limitations. The limitations of ground-based sensors can be represented as range and angle limitations. Orbital sensors are approximated as range limited with a disk of the earth's equatorial radius approximating line of sight limitations. If visibility requirements are not satisfied, then the gain for that satellite sensor pair can be set to $\mu_{i,j} = -1$ to ensure good performance during the sensor allocation. The optimization constraints are therefore expressed as the target limit constraint and the potential range of $\epsilon_{i,j}$.

$$\sum_{i=1}^{N} \epsilon_{i,j} < T, j = 1, 2, ..., M \tag{2.24}$$

$$0 \leq \epsilon_{i,j} \leq 1 \tag{2.25}$$

Information gain generation using the current state estimates is the key component in accounting for the multiple model and maneuver probability elements of IMM EKF based tracking. Differences in how the information gain is generated are the primary differences between different tasking methods [9] . As discussed earlier, the purely Fisher information gain method does not work in systems with more targets than sensors and cannot directly account for maneuver probability and multiple model

methodology. Because of these limitations, modifications need to made to allow for effective tasking.

An ad-hoc improvement [1] incorporating the current state estimate covariance $\hat{\boldsymbol{P}}_i$ demonstrates enhanced performance and can handle systems where not all targets can be observed at any given time step. The scaling factors α and β are implementation dependent and good design practices associated with selecting them are not well defined [1]. The result is a metric that contains both the potential accuracy improvements from a particular observation and the estimated inaccuracy of the satellite being tracked.

$$\mu_{i,j}^{M} = \alpha \operatorname{tr}(\boldsymbol{\Omega}_{i,j}) + (1-\alpha)\beta \operatorname{tr}(\hat{\boldsymbol{P}}_i) \tag{2.26}$$

This Fisher information and covariance based tasking method does have certain advantages and disadvantages when implemented in a IMM EKF tracking system. Satellites with a high probability of maneuvering demonstrate much larger estimated state covariance values, the satellites are more highly prioritized as a result, indirectly incorporating maneuvering probability into the tasking. However, when very different types of satellites are being tracked using the same sensor network, the scale of the priorities can unfavorably focus on satellites with a higher expected error over satellites that are expected to maneuver. To prioritize the tracking of maneuvering satellites a more direct incorporation of the maneuvering probability needs to be added to the information gain.

An additional term $(1 + \Upsilon m_{q=2})$ introducing a stronger probability element as a potential weighting method in the information gain is the a novel contribution of this paper. The scaling value Υ determines the weighting of the probability of being in a maneuvering state $m_{q=2}$.

$$\mu_{i,j}^{L} = (1 + \Upsilon m_{q=2})(\alpha \operatorname{tr}(\boldsymbol{\Omega}_{i,j}) + (1-\alpha)\beta \operatorname{tr}(\hat{\boldsymbol{P}}_i)) \tag{2.27}$$

The above method only functions when used with state estimation methods that take the maneuver probability into account or that can otherwise generate that value.

This requirement limits the usefulness of this method to cases where the maneuvering behavior of the target is well understood, such as station keeping GEO satellites or satellites performing maneuvers near clear apsis points.

The use of a scaling factor based on the probability of maneuvering was motivated by the desire to retain the dynamics of the Fisher information and covariance based tasking method when the satellites are not near maneuvering points. When a satellite is near a point where maneuvers are expected those satellites are observed more frequently. Slightly fewer observations of other non-maneuvering satellites will result from this probability component of the tasking, so the average error of non-maneuvering satellites may increase slightly. But this is a reasonable trade off for better tracking of satellites during large maneuvers.

2.5 Maneuver Probability

The IMM EKF method makes use of two state estimators updated at every system step with different estimated state error matrices. A satellite can be considered to potentially operate in two modes, one where the satellite is maneuvering and another where it is not. The modes are differentiated using the variable q, which has a value of 1 for the non-maneuvering model and 2 for the maneuvering model. The probability of each mode cannot be accurately determined purely from the current state estimates as both the maneuvering and non-maneuvering modes have different state estimates. Instead, what can be determined from both state estimates is the probability of transitioning between the modes $\gamma_{i,a,b}(k)$ based on all previous measurements $\boldsymbol{Y}_i(k-1)$. Using this transition probability, the mode probabilities can be computed iteratively [7].

$$\gamma_{i,a,b}(k) = p(q(k) = b | q(k-1) = a, \boldsymbol{Y}_i(k-1)) \tag{2.28}$$

This mode transition probability distribution is based on the proximity of the state estimate to the trigger boundary associated with maneuvering behavior. The probability of mode transition is modeled as a Gaussian normal distribution centered on

the trigger boundary $\boldsymbol{\mu}_b$ with a covariance $\boldsymbol{\Sigma}$ determined by the nature of the maneuver condition. A $g(x)$ function determines what derived statistics are utilized by the trigger boundary. For example, the latitude and longitude based conditions could use $g(x)$ to generate the appropriate angle values. The $\boldsymbol{L}$ term is a matrix identifying which derived values are used as the trigger conditions.

$$\mathcal{N}_b(\boldsymbol{L}g(\boldsymbol{x}), \boldsymbol{\mu}, \boldsymbol{\Sigma}) \tag{2.29}$$

To take into account the uncertainty of the state estimate, the associated multivariate normal distribution of the current state estimate is used. The use of this value in a scenario with dynamic sensor tasking results in oscillatory behavior in the probability of maneuvering, as the current error of the state estimate can increase by large amounts during iterations where it is unobserved.

$$\mathcal{N}_p(\boldsymbol{x}, \hat{\boldsymbol{x}}_{i,q}(k-1), \hat{\boldsymbol{P}}_{i,q}(k-1)) \tag{2.30}$$

By integrating across the entirety of the real state space, one can determine the overall probability that the satellite is in the proximity of the trigger conditions for any given bound.

$$\gamma_{i,a,b}(k) = \int_{\mathbb{R}} \mathcal{N}_b(\boldsymbol{L}g(\boldsymbol{x}), \boldsymbol{\mu}, \boldsymbol{\Sigma}) \mathcal{N}_p(\boldsymbol{x}, \hat{\boldsymbol{x}}_{i,q}(k-1), \hat{\boldsymbol{P}}_{i,q}(k-1)) d\boldsymbol{x} \tag{2.31}$$

In the GEO case, the maneuver probability is dependent on the latitude and longitude of the current estimate of the satellite position. For the sake of simplification these angle limits can be approximated as displacement limits in the LHLV reference frame, specifically along the y and z axises. These limits forms a bounding box around the central point of the LHLV frame. There are a total of four different probability distributions at the corresponding positive and negative values of the allowable position error. Differing $\boldsymbol{L}$ matrices alter which variables are being considered.

$$\boldsymbol{L}_{EW} = \begin{bmatrix} 0 & 1 & 0 & 0 & 0 & 0 \end{bmatrix} \tag{2.32}$$

$$\boldsymbol{L}_{NS} = \begin{bmatrix} 0 & 0 & 1 & 0 & 0 & 0 \end{bmatrix} \tag{2.33}$$

In the GEO satellite case, $g(\boldsymbol{x})$ is an identity function as any transformations are handled earlier in the conversion to LHLV. When the geostationary satellite approaches the bounding box shown in Figure 2.2, the probability of transitioning to the maneuvering state increases.

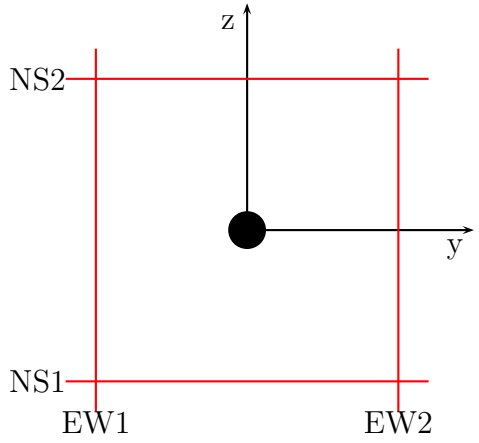

Figure 2.2. Geostationary mode transition boundaries in LHLV

In the case of a LEO satellite, the mode change probability can be based on proximity to the nearest apsis point of the orbit. Many impulsive maneuvers take place near apsis points in the satellite's orbit, such as Hohmann transfers. Finding this probability can be simplified via reference frame conversion to a LHLV frame, much like the GEO case such that the zero point of the y and z axes are at the nearest apsis point.

In the LEO case the probability of transitioning to the maneuvering state increases when the satellite is near the boundary seen in Figure 2.3. The reference frame transition is only done for the mode probability calculations for the LEO case and the rest of the satellite state estimation is done in the ECI frame. Because of the

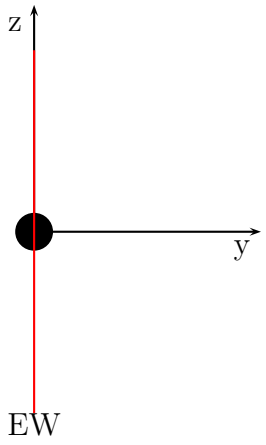

Figure 2.3. LEO mode transition boundary in LHLV around apsis point

high relative velocity of the satellite in the LHLV reference frame, a larger $\mathbf{\Sigma}$ value has to be used due to the sampling rate potentially missing the maneuvering point. Because this wider range results in a lower probability of maneuvering than is useful, an additional correction factor is included to increase the probability such that it approaches a consistent high value when near the apsis point.

The GEO probability results in four separate probabilities as each bound is calculated independently. Because only one maneuver can take place during any given short time frame, only the maximum probability is considered in the IMM EKF dynamics. More developed methods to resolve the multiple maneuvering probabilities would be the subject of future work.

As both the GEO and LEO probability models allow for a $g(x)$ that is an identity function the linear nature of the Gaussian distributions allows for a significant simplification of the probability dynamics [7]. The two probability distributions can be

combined into a single distribution with a mean $\lambda_{i,q}$ and covariance $\Lambda_{i,q}$ multiplied by a correction gain κ.

$$\Lambda_{i,q} = (\hat{\boldsymbol{P}}_{i,q}(k-1)^{-1} + \boldsymbol{L}^T\boldsymbol{\Sigma}^{-1}\boldsymbol{L})^{-1} \tag{2.34}$$

$$\lambda_{i,q} = \Lambda_{i,q}(\hat{\boldsymbol{P}}_{i,q}(k-1)^{-1}\hat{\boldsymbol{x}}_{i,q}(k-1) + \boldsymbol{L}^T\boldsymbol{\Sigma}^{-1}\boldsymbol{\mu}) \tag{2.35}$$

$$\kappa_1 = \frac{|\Lambda_{i,q}|^{\frac{1}{2}}}{(2\pi|\hat{\boldsymbol{P}}_{i,q}(k-1)||\boldsymbol{\Sigma}|)^{\frac{1}{2}}} \tag{2.36}$$

$$\kappa_2 = \exp(-\frac{1}{2}(\boldsymbol{\mu}^T\boldsymbol{\Sigma}^{-1}\boldsymbol{\mu} + \hat{\boldsymbol{x}}_{i,q}(k-1)^T\hat{\boldsymbol{P}}_{i,q}(k-1)^{-1}\hat{\boldsymbol{x}}_{i,q}(k-1) - \lambda_{i,q}^T\Lambda_{i,q}^{-1}\lambda_{i,q})) \tag{2.37}$$

$$\kappa = \kappa_1\kappa_2 \tag{2.38}$$

$$\mathcal{N}_b(\boldsymbol{L}g(\boldsymbol{x}), \boldsymbol{\mu}, \boldsymbol{\Sigma})\mathcal{N}_p(\boldsymbol{x}, \hat{\boldsymbol{x}}_{i,q}(k-1), \hat{\boldsymbol{P}}_{i,q}(k-1))d\boldsymbol{x} = \kappa\mathcal{N}_n(\boldsymbol{x}, \lambda_{i,q}, \Lambda_{i,q}) \tag{2.39}$$

As the probability is integrated over the whole real space associated with the state, the probability becomes the correction gain κ.

$$\gamma_{i,a,b}(k) = \kappa \tag{2.40}$$

2.6 Estimated State Mixing

Once the transition probabilities are determined, the mixing probabilities $m_{i,a|b}(k)$ are calculated using the previous state probability estimate $m_{i,a}(k-1)$ [7].

$$m_{i,a}(k-1) = p(q_i(k-1) = a|\boldsymbol{Y}_i(k-1)) \tag{2.41}$$

$$m_{i,a|b}(k) = p(q_i(k-1) = a|q_i(k) = b, \boldsymbol{Y}_i(k-1)) \tag{2.42}$$

$$m_{i,a|b}(k) = \frac{\gamma_{i,a,b}(k-1)m_{i,a}(k-1)}{\sum_{c=1}^{2}\gamma_{i,c,b}(k-1)m_{i,c}(k-1)} \tag{2.43}$$

This mixing probability allows for the previous estimated state and covariance of the system to be combined to generate the most likely system state for both modes of the current EKF estimation step.

$$\hat{\boldsymbol{x}}_{i,a}^{0} = \sum_{c=1}^{2} m_{i,c|a}(k)\hat{\boldsymbol{x}}_{i,c}(k-1) \tag{2.44}$$

$$\hat{\boldsymbol{P}}_{i,a}^{0} = \sum_{c=1}^{2} m_{i,c|a}(k)(\hat{\boldsymbol{P}}_{i,a}(k-1) + [\hat{\boldsymbol{x}}_{i,c}(k-1) - \hat{\boldsymbol{x}}_{i,a}^{0}][\hat{\boldsymbol{x}}_{i,c}(k-1) - \hat{\boldsymbol{x}}_{i,a}^{0}]^{T}) \tag{2.45}$$

2.7 Interacting Multiple Model Extended Kalman Filter

The IMM EKF method is used to track a maneuvering spacecraft more closely soon after an impulsive maneuver. A basic system model derived from orbital mechanics is used for the non-maneuvering mode and allows for tracking using Kalman filter techniques. At the same time, a similar model making use of a much higher state noise is also being tracked [7]. The state q describes the two different maneuvering modes where one is non-maneuvering and two is maneuvering. The primary difference between each mode is the $\boldsymbol{Q}_q$ state error covariance matrix, which is of a much higher magnitude in the maneuvering case. Additionally, this filtering method needs to be able to account for multiple or no sensor measurements at any given update step.

An EKF system model can be represented using the system state $\boldsymbol{x}(k) \in \mathbb{R}^{m\times 1}$ and the sensor outputs $\boldsymbol{y}(k) \in \mathbb{R}^{n\times 1}$. The state error $\boldsymbol{w}_q(k) \in \mathbb{R}^{m\times 1}$ with covariance $\boldsymbol{Q}_q \in \mathbb{R}^{m\times m}$ and sensor noise $\boldsymbol{v}(k) \in \mathbb{R}^{n\times 1}$ with covariance $\boldsymbol{R} \in \mathbb{R}^{n\times n}$ represents the unknown stochastic errors in the observations of the system. The control component $\Delta\boldsymbol{u} \in \mathbb{R}^{m\times 1}$ represents the maneuvers of the target. Due to the unknown nature of the maneuvering model outside of specific tracking applications, the maneuvering impulses cannot be directly incorporated into the EKF. The nonlinear system dynamics $f(\boldsymbol{x})$ and sensor dynamics $h(\boldsymbol{x})$ are used to represent the system dynamics and sensor dynamics of the given system. The full system model then takes the form seen in Equation 2.46 and Equation 2.47.

$$\boldsymbol{x}_i(k+1) = f_i(\boldsymbol{x}_i(k)) + \boldsymbol{w}_{q,i}(k) + \Delta\boldsymbol{u}_i(k) \tag{2.46}$$

$$\boldsymbol{y}_{i,j}(k) = h_{i,j}(\boldsymbol{x}(k)) + \boldsymbol{v}_{i,j}(k) \tag{2.47}$$

The propagated system state makes use of the state dynamics model. In the case with no sensor readings for a given satellite, this propagated value is the final value for the EKF update. This same propagation without update also applies to the state estimate covariance $\hat{\boldsymbol{P}}_i \in \mathbb{R}^{m \times m}$ propagation.

$$\hat{\boldsymbol{x}}_{i,q}(k|k-1) = f_i(\hat{\boldsymbol{x}}^0_{i,q}(k-1)) \tag{2.48}$$

The EKF makes use of the linearized dynamics of the system as part of the maximum likelihood Kalman filter estimation. The linearized sensor dynamics $\hat{\boldsymbol{C}}_{i,j}$, as seen in Equation 2.7, can be calculated for each sensor satellite pair. A total of u sensor readings for a given satellite can be combined into one larger matrix of $\boldsymbol{y}_i \in \mathbb{R}^{p \times 1}$ with an error covariance $\boldsymbol{R}_i \in \mathbb{R}^{p \times p}$, where $p = n * u$, with a trace composed of each sensor's error covariance matrices. The sensor dynamics are combined accordingly, becoming a larger matrix $\hat{\boldsymbol{C}}_i \in \mathbb{R}^{p \times m}$. The linearized state dynamics $\boldsymbol{F}_i$ are required as part of the estimated state covariance $\hat{\boldsymbol{P}}_i$ update process.

$$\boldsymbol{F}_{i,q}(k) = \left.\frac{\partial f}{\partial \boldsymbol{x}}\right|_{\hat{\boldsymbol{x}}_{i,q,m}(k)} \tag{2.49}$$

$$\hat{\boldsymbol{P}}_{i,q}(k|k-1) = \boldsymbol{F}_{i,q}(k-1)\hat{\boldsymbol{P}}^0_{i,q}(k-1)(\boldsymbol{F}_{i,q}(k-1))^T + \boldsymbol{Q}_q \tag{2.50}$$

To account for the sensor readings of the satellite at each time step, estimated sensor readings are used along with the Kalman gain $\boldsymbol{K}_{q,i}$to determine the appropriate changes to the state estimate and estimate covariance to adjust the current maximum likelihood state estimate.

$$\boldsymbol{K}_{q,i} = \hat{\boldsymbol{P}}_{i,q}(k|k-1)\hat{\boldsymbol{C}}^T_{i,q}(\hat{\boldsymbol{C}}_{i,q}\hat{\boldsymbol{P}}_{i,q}(k|k-1)\hat{\boldsymbol{C}}^T_{i,q} + \boldsymbol{R}_i) \tag{2.51}$$

$$\hat{\boldsymbol{x}}_{i,q}(k) = \hat{\boldsymbol{x}}_q(k|k-1) + \boldsymbol{K}_{i,q}(\boldsymbol{y}_i - h(\hat{\boldsymbol{x}}_{i,q}(k|k-1))) \tag{2.52}$$

$$\hat{\boldsymbol{P}}_{i,q}(k) = (\boldsymbol{I} - \boldsymbol{K}_{i,q}\hat{\boldsymbol{C}}_{i,q})\hat{\boldsymbol{P}}_{i,q}(k|k-1) \tag{2.53}$$

2.8 Estimated State Fusion

After the EKF update is complete, a final estimate that is a fusion of the two state estimates using the mode probabilities is generated [7]. Mode probabilities are

dependent on the previous mode filter iteration probabilities and the probability that the given sensor readings match the expected state. Additionally, both of the modes' state estimates and covariances are retained for the next EKF update.

The state probability has to be updated to take into account the transition probabilities calculated earlier, before being used to find the overall state estimate.

$$p(\boldsymbol{y}_i(k)|q(k)=a,\boldsymbol{Y}_i(k-1)) = \mathcal{N}_s(\boldsymbol{y}_i(k) - h_i(\hat{\boldsymbol{x}}_a(k|k-1),\boldsymbol{0},\boldsymbol{S}_a(k)) \tag{2.54}$$

$$\boldsymbol{S}_a(k) = \hat{\boldsymbol{C}}_{i,q}\hat{\boldsymbol{P}}_{i,q}(k|k-1)\hat{\boldsymbol{C}}_{i,q}^T + \boldsymbol{R}_i \tag{2.55}$$

The normalizing variable s normalizes the results such that $\sum_{c=1}^{2} m_{i,c}(k) = 1$.

$$p(q(k)=b|\boldsymbol{Y}_i(k-1)) = \sum_{c=1}^{2} \gamma_{i,c,b}(k) m_{i,c}(k) \tag{2.56}$$

$$m_{i,a}(k) = \frac{1}{s} p(\boldsymbol{y}_i(k)|q(k)=a,\boldsymbol{Y}_i(k-1)) p(q(k)=a|\boldsymbol{Y}_i(k-1)) \tag{2.57}$$

The probability update gives us the probability of each of the two modes at time step k. This then allows for the merging of the two estimates to create the overall state estimate, which is used for future tracking allocation and monitoring the satellite's position.

$$\hat{\boldsymbol{x}}_i(k) = \sum_{c=1}^{2} \hat{\boldsymbol{x}}_{i,c}(k) m_{i,c}(k) \tag{2.58}$$

$$\hat{\boldsymbol{P}}_i(k) = \sum_{c=1}^{2} \left(\hat{\boldsymbol{P}}_{i,c}(k) + [\hat{\boldsymbol{x}}_{i,c}(k) - \hat{\boldsymbol{x}}(k)][\hat{\boldsymbol{x}}_{i,c}(k) - \hat{\boldsymbol{x}}(k)]^T \right) m_{i,c}(k) \tag{2.59}$$

3. NUMERICAL SIMULATION

3.1 Simulation Overview

Due to the complexities of demonstrating the analytical behavior of extremely nonlinear and discontinuous state estimators, numerical simulations were used to demonstrate the effectiveness of the tasking methods. A somewhat abstracted representation of potential observational resources are used, along with a set of geostationary satellites and a low earth orbit maneuvering satellite as tracking targets as seen in Figure 1.1.

The simulation configuration is based on a general overview of the SBSS program published by Boeing [3]. Four satellites in $630km$ altitude sun synchronous orbits are used as orbital sensors. In this implementation each satellite occupies a different quarter of the same orbit. The five ground telescopes in the simulation are approximately located at longitudes corresponding the east($-75°$) and west($-120°$) coasts of the United States, Greenland($-45°$), northern Europe($0°$), and Hawaii($-155°$). However, the sensor positions are approximated at the equator. The ground sensors are modeled as capable of viewing a 30 deg cone with a range of $40000km$ and able to track a single target. The orbital sensors are able to view in all directions with a range of $80000km$ and able to track a single target. These details of sensor capabilities are heavily abstracted as details on modern, real world sensor capabilities are often classified.

The weighting coefficients used during sensor assignment are set somewhat arbitrarily and could be refined in future work. The weighting coefficients used in the covariance and probability based tasking methods using Equations 2.26 and 2.27 can be seen in Table 3.1.

Symbol	Value
α	0.5
β	1
Υ	1

Table 3.1. Tasking coefficients

The ten target GEO satellites in the example configuration are located at 20° intervals from 20° longitude to −160°, where ground sensors have the opportunity to view them. These GEO satellites are numbered 1 through 10. The initial states of the satellites are set at zero in their LHLV reference frame. However, to keep all the satellites from maneuvering at once due to roughly similar drift rates, every satellite after the first is altered to have an initial condition two hours into its simulation later than the previous one.

Additionally, one LEO satellite numbered Satellite 11 is initially in an orbit of eccentricity 0.17 with a semilatus rectum of $8371km$, performing a transfer with maneuvers at times $703800s$ and $708100s$ with a magnitude $200\frac{m}{s}$ along and against the satellite direction of motion respectively.

A sampling period of 10 seconds is used as an approximation of the sensor networks observation interval. The sensor covariance of measurement noise R_j is set based on other work with similar sensor dynamics [1] [7]. All sensors have the same error and dynamics as an approximation of a unified sensor network. A more detailed simulation in potential future work could make use of sensor characteristics that represent specific installations.

$$\boldsymbol{R}_j = \begin{bmatrix} \sigma_\rho^2 & 0 & 0 \\ 0 & \sigma_\psi^2 & 0 \\ 0 & 0 & \sigma_\theta^2 \end{bmatrix} = \begin{bmatrix} 10^{-2}km^2 & 0 & 0 \\ 0 & 16 \times 10^{-12}rad^2 & 0 \\ 0 & 0 & 16 \times 10^{-12}rad^2 \end{bmatrix} \tag{3.1}$$

The mode dependent state error covariance is the primary difference in the modeling between the two different state estimators and is derived from other work [7] but

increased in magnitude. Finding the correct tasking method coefficients and adjustments to work with a smaller state error covariance matrix would require additional research.

$$\boldsymbol{Q}_1 = \begin{bmatrix} 10^2 km^2 & 0 & 0 & 0 & 0 & 0 \\ 0 & 10^2 km^2 & 0 & 0 & 0 & 0 \\ 0 & 0 & 10^2 km^2 & 0 & 0 & 0 \\ 0 & 0 & 0 & (0.1\frac{km}{s})^2 & 0 & 0 \\ 0 & 0 & 0 & 0 & (0.1\frac{km}{s})^2 & 0 \\ 0 & 0 & 0 & 0 & 0 & (0.1\frac{km}{s})^2 \end{bmatrix} \tag{3.2}$$

The covariance for the maneuvering model is much higher in order to model the greater state uncertainty around the point of maneuver.

$$\boldsymbol{Q}_2 = 100\boldsymbol{Q}_1 \tag{3.3}$$

3.2 Orbital Mechanics Modeling

A simplified orbital mechanics model is used for both the target satellites and LEO observation platforms [16] [17] [15]. Outside of the standard two body orbital dynamics, the model accounts for third body perturbations of the sun and moon, the non-spherical dynamics of the earth, resistance due to the earth's atmosphere, and solar radiation pressure [4]. A more elaborate and accurate simulation or real world satellite state data could be a potential improvement for future work in verifying tracking method validity.

The orbital simulations is run using continuous time system acceleration dynamics in MATLAB. Thus, only the acceleration components for each perturbation needs to be calculated using the current state variables and certain earth orbit parameters [15]. The satellite specific parameters such as A_{sat} C_{Dsat} or m_{sat} are very rough estimates derived from the LaoSat-1 [18].

Symbol	Parameter	Value	Units
ω_e	Earth's Rotation Rate	7.292×10^{-5}	$\frac{rad}{s}$
μ	Earth's Gravitational Parameter	3.986×10^{14}	$\frac{m^3}{s^2}$
μ_M	Moon's Gravitational Parameter	4.903×10^{12}	$\frac{m^3}{s^2}$
μ_S	Sun's Gravitational Parameter	1.327×10^{20}	$\frac{m^3}{s^2}$
R_e	Earth's Average Equatorial Radius	6.378×10^{6}	m
r_M	Average Earth-Moon Distance	3.850×10^{8}	m
r_S	Average Earth-Sun Distance	1.496×10^{11}	m
J_2	Earth's Oblateness Parameter	1.0826×10^{-3}	$-$
h_{a0}	Atmospheric Cutoff Altitude	7×10^{5}	m
H_a	Atmospheric Scale Height	8.866×10^{4}	m
ρ_0	Cutoff Density	3.164×10^{-13}	$\frac{kg}{m^3}$
L_s	Sun Luminosity	3.8395×10^{26}	W
c	Speed of Light	2.998×10^{8}	$\frac{m}{s}$
A_{sat}	Satellite Area	28.4	m^2
C_{Dsat}	Satellite Drag Coefficient	1	$-$
m_{sat}	Satellite Mass	4200	kg

Table 3.2. Satellite simulation parameters

The general acceleration dynamics of a satellite $f_s(\boldsymbol{x}, t)$ are the sum of the various separate dynamics components. The current state $\boldsymbol{x}$ is composed of the position $\boldsymbol{r}$ and velocity $\boldsymbol{v}$ components where the magnitude of those two vectors are r and v respectively.

$$f_s(\boldsymbol{x}, t) = \boldsymbol{a}_{2body}(\boldsymbol{x}, t) + \boldsymbol{a}_{3B}(\boldsymbol{x}, t) + \boldsymbol{a}_{J_2}(\boldsymbol{x}, t) + \boldsymbol{a}_{drag}(\boldsymbol{x}, t) + \boldsymbol{a}_{rad}(\boldsymbol{x}, t) \tag{3.4}$$

The two body gravitational model makes use of the gravitational attraction between the satellite and the earth and represents the primary acceleration in the orbit.

$$\boldsymbol{a}_{2body}(\boldsymbol{x},t) = -\frac{\mu}{r^3}\boldsymbol{r} \tag{3.5}$$

The third body gravitational perturbations from the sun and the moon are modeled using the position of those bodies approximated as circular orbits in the ECI frame with a radius of the average distance of those bodies from the earth. This simple time based calculation generates a vector of the bodies' position in the ECI frame of $\boldsymbol{r}_{3B}$. The acceleration for the body can be calculated as the difference between the acceleration of the satellite and the acceleration of the earth due to the body.

$$\boldsymbol{a}_{3B}(\boldsymbol{x},t) = -\mu_{3B}\left(\frac{\boldsymbol{r}-\boldsymbol{r}_{3B}}{||\boldsymbol{r}-\boldsymbol{r}_{3B}||^3} + \frac{\boldsymbol{r}_{3B}}{r_{3B}^3}\right) \tag{3.6}$$

This third body acceleration is calculated for both the sun and moon, neglecting all other gravitational bodies.

The non-spherical dynamics of the earth are primarily dependent on the current position of the satellite relative to the earth.

$$\boldsymbol{a}_{J_2}(\boldsymbol{x},t) = -\frac{3\mu R_e^2 J_2}{2r^5}\begin{bmatrix}(1-5(\frac{z}{r})^2)x\\(1-5(\frac{z}{r})^2)y\\(3-5(\frac{z}{r})^2)z\end{bmatrix} \tag{3.7}$$

Atmospheric drag is not a substantial factor for GEO satellites due to their position in high earth orbit. However drag needs to be included for the sake of completeness and for modeling the LEO satellite. This calculation is also the least accurate component of the model due to the extremely rough estimates of the satellite parameters and very simplistic atmospheric density and aerodynamic models. Both the

atmospheric models and the solar radiation models assume a constant satellite profile as an approximation.

$$B = \frac{C_{Dsat} A_{sat}}{m_{sat}} \tag{3.8}$$

$$\rho(r) = \rho_0 \exp\left(\frac{h_{a0} - r}{H_a}\right) \tag{3.9}$$

$$\boldsymbol{v}_{rel} = \boldsymbol{v} - cross([0, 0, \omega_e]^T, \boldsymbol{r}) \tag{3.10}$$

$$\boldsymbol{a}_{drag}(\boldsymbol{x}, t) = -\frac{1}{2}\rho(r) B v_{rel} \boldsymbol{v}_{rel} \tag{3.11}$$

The solar pressure of the sun's radiation is simulated using a similarly simplified model. The third body position vector $\boldsymbol{r}_{3B}$ for the sun $\boldsymbol{r}_S$ is used. The solar pressure model is another calculation where a more advanced satellite and disturbance model would result in more accurate simulations.

$$P_{sat} = \frac{A_{sat}}{m_{sat}}; \tag{3.12}$$

$$p_{srp} = \frac{L_s}{4c\pi||(\boldsymbol{r} - \boldsymbol{r}_S)||^2} \tag{3.13}$$

$$\boldsymbol{a}_{rad}(\boldsymbol{x}, t) = p_{srp} P_{sat} \frac{(\boldsymbol{r} - \boldsymbol{r}_S)}{||(\boldsymbol{r} - \boldsymbol{r}_S)||} \tag{3.14}$$

3.3 Maneuver Modeling

To model the maneuvering behavior of GEO station keeping satellites, a simple two burn correction method is used. A simplified version of the linearized state transition model, along with a propagated state estimate, can be utilized to determine the state after the assigned maneuver duration. The propagated state $\delta \boldsymbol{r}^{prop}(t)$ can then be used along with the linearized dynamics and numerical minimization techniques, to determine the appropriate velocity change vector needed to return to the desired system state.

Converting to the LHLV reference frame results in orbital dynamics that can be linearized to a closed form solution $\Psi(\tau)$ for a given maneuver time frame τ, which is from the current time t to the time of the maneuver t_n, and the rotation rate of the

earth ω_e. This transition matrix is calculated in terms of the change in position $\delta \boldsymbol{r}$ due to impulsive velocity $\Delta \boldsymbol{V}$ changes and is derived from Hills equations [19].

$$\delta \boldsymbol{r}(t) = \delta \boldsymbol{r}^{prop}(t) + \sum_{n=1}^{2} \Psi(t - t_n) \Delta V_n Heaviside(t - t_n) \tag{3.15}$$

$$\Psi(\tau) = \begin{bmatrix} \frac{\sin(\omega_e)\tau}{\omega_e} & \frac{2}{\omega_e}(1 - cos(\omega_e \tau)) & 0 \\ -\frac{2}{\omega_e}(1 - cos(\omega_e \tau)) & \frac{4\sin(\omega_e \tau) - 3\omega_e \tau}{\omega_e} & 0 \\ 0 & 0 & \frac{\sin(\omega_e \tau)}{\omega_e} \end{bmatrix} \tag{3.16}$$

The appropriate ΔV value is then found by solving a nonlinear minimization problem with a cost function J to minimize fuel consumption.

$$J = \sum_{n=1}^{2} \Delta V_n^T \Delta V_n \tag{3.17}$$

This minimization is subject to a constraint such that the position at the end of the maneuver period is within a set range δr_{max} of the target point with the distance from the target point being $\delta r(t)$.

$$\delta r(t) < \delta r_{max} \tag{3.18}$$

The calculated maneuver is triggered whenever the satellite moves outside of the allowable bounds of $115km$ in approximated latitude and longitude error from the target point. The maneuver attempts to get the satellite within $\delta r_{max} = 5km$ in a time period of 3 days and a typical 9 day period after simulation initialization can be seen in Figure 3.1.

This above station keeping method does not produce good long term results. However, alternative methods [6] [15] [20] demonstrated difficulties during implementation and were discarded as options because they were problematic to implement. But the station keeping serves as an adequate example of a maneuvering GEO satellite to demonstrate the maneuver probability dependent tracking that is the focus of this paper.

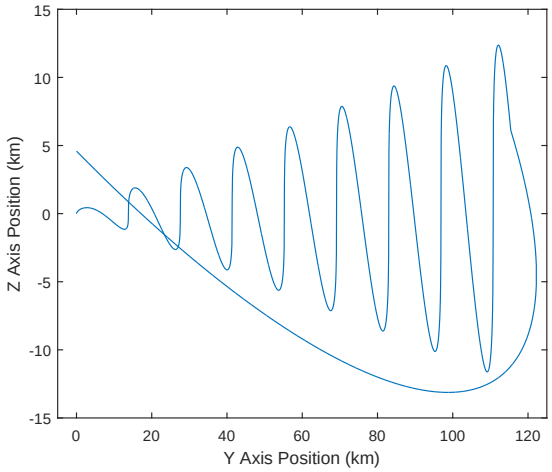

Figure 3.1. Station keeping maneuver of GEO Satellite 2 over the course of 9 days in LHLV reference frame

To represent maneuvering a LEO satellite, a hand tuned maneuver between two elliptical orbits is used. This maneuver has a much higher impulse than station keeping maneuvers and serves as the primary illustration of tracking error of maneuvering satellites. The behavior of the LEO satellite during the maneuver can be seen in Figure 3.2.

3.4 State Probability

The LEO and GEO satellites perform very different types of maneuvers, but all of the maneuvering conditions can be approximated as trigger bounds where a maneuver is likely to occur. As discussed in section 2.5, probability bounds are represented as a probability distribution along the relevant state axis. The GEO case, bounds have a variance of $\Sigma_{GEO} = 4km^2$ located at $\boldsymbol{\mu}_{b,GEO} = 115km$ in the east-west and north-south directions. In the LEO case, the bound is located at a zero point $\boldsymbol{\mu}_{b,LEO} = 0km$

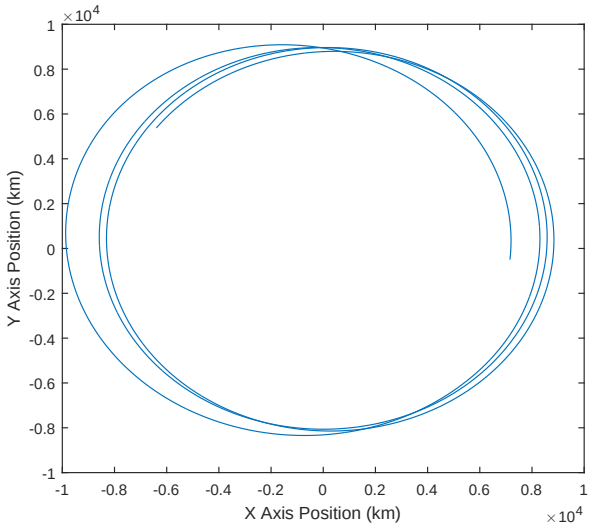

Figure 3.2. Orbital transfer maneuver of LEO Satellite 11 in the ECF frame during the time period between $700000s - 730000s$

on the EW axis and has a variance of $\Sigma_{LEO} = (1000km)^2$ and a correction factor such that the peak value of $\gamma_{i,1,2}(k)$ is 0.7.

$$\gamma_{i,1,2}(k) = \int_{\mathbb{R}} \mathcal{N}_b(\boldsymbol{L}g(\boldsymbol{x}), \boldsymbol{\mu}, \boldsymbol{\Sigma})\mathcal{N}_p(\boldsymbol{x}, \hat{\boldsymbol{x}}_{i,1}(k-1), \hat{\boldsymbol{P}}_{i,1}(k-1))d\boldsymbol{x} \tag{3.19}$$

$$\gamma_{i,2,2}(k) = \int_{\mathbb{R}} \mathcal{N}_b(\boldsymbol{L}g(\boldsymbol{x}), \boldsymbol{\mu}, \boldsymbol{\Sigma})\mathcal{N}_p(\boldsymbol{x}, \hat{\boldsymbol{x}}_{i,2}(k-1), \hat{\boldsymbol{P}}_{i,2}(k-1))d\boldsymbol{x} \tag{3.20}$$

$$\gamma_{i,1,2}(k) = 1 - \gamma_{i,1,1}(k) \tag{3.21}$$

$$\gamma_{i,2,2}(k) = 1 - \gamma_{i,2,1}(k) \tag{3.22}$$

To prevent irregular numerical errors from occurring, the transition probability is restricted between 0.01 and 0.99. The probability of the LEO case is only calculated if the eccentricity of the orbit is greater than 0.075. These restrictions could be minimized with additional fine tuning of the probability models.

3.5 Extended Kalman Filter Details

To attain the forms described in section 2.7, the GEO and LEO satellites need to be tracked using different nonlinear dynamics models due to differences in reference frame. Additionally, discrete models need to be used with the EKF [7]. The initial state estimate used is the true state of the satellite, as the acquisition and state initialization problems [10] are beyond the scope of this paper. The initial state estimate error covariance was set to be the state error covariance for the non-maneuvering mode.

Symbol	Parameter	Value	Units
R_c	Target Radius	4.2164×10^4	km
μ	Earth's Gravitational Parameter	3.986×10^5	$\frac{km^3}{s^2}$
Δt	Measurement Sample Period	10	s

Table 3.3. IMM EKF parameters

To account for the motion of the GEO satellite in the LHLV reference frame, the mean motion n has to be included in the equations. The state for a satellite i is used in the following equations, so the specific satellite is not identified.

$$n = \left(\frac{\mu}{r(k)^3}\right)^{0.5} \tag{3.23}$$

$$\delta v_x = 2nv_y(k) + n^2x(k) - \frac{\mu(R_c + x(k))}{((R_c + x(k))^2 + y(k)^2 + z(k)^2)^{0.5}} \tag{3.24}$$

$$\delta v_y = -2nv_y(k) + n^2x(k) - \frac{\mu y(k)}{((R_c + x(k))^2 + y(k)^2 + z(k)^2)^{0.5}} \tag{3.25}$$

$$\delta v_z = -\frac{\mu z(k)}{((R_c + x(k))^2 + y(k)^2 + z(k)^2)^{0.5}} \tag{3.26}$$

$$\boldsymbol{x}(k+1) = \begin{bmatrix} x(k+1) \\ y(k+1) \\ z(k+1) \\ v_x(k+1) \\ v_y(k+1) \\ v_z(k+1) \end{bmatrix} = \begin{bmatrix} x(k) + \Delta t v_x(k) \\ y(k) + \Delta t v_y(k) \\ z(k) + \Delta t v_z(k) \\ v_x(k) + \Delta t \delta v_x \\ v_y(k) + \Delta t \delta v_y \\ v_z(k) + \Delta t \delta v_z \end{bmatrix} + \boldsymbol{w}(k) + \begin{bmatrix} \mathbf{0} \\ \Delta \boldsymbol{V} \end{bmatrix} \tag{3.27}$$

The LEO satellite tracking makes use of two body orbital mechanics with less complications due to its being tracked in the ECI frame.

$$n_h = -\frac{\mu}{r(k)^3} \tag{3.28}$$

$$\boldsymbol{x}(k+1) = \begin{bmatrix} x(k+1) \\ y(k+1) \\ z(k+1) \\ v_x(k+1) \\ v_y(k+1) \\ v_z(k+1) \end{bmatrix} = \begin{bmatrix} x(k) + \Delta t v_x(k) \\ y(k) + \Delta t v_y(k) \\ z(k) + \Delta t v_z(k) \\ v_x(k) + \Delta t n_h x(k) \\ v_y(k) + \Delta t n_h y(k) \\ v_z(k) + \Delta t n_h z(k) \end{bmatrix} + \boldsymbol{w}(k) + \begin{bmatrix} \mathbf{0} \\ \Delta \boldsymbol{V} \end{bmatrix} \tag{3.29}$$

There are a few ad-hoc modifications made to the EKF method to mitigate numerical issues that cropped up when observing satellites that had been unobserved for an extended period. This sudden error correction was primarily an issue only with the purely Fisher information based method and certain rare cases with other methods. The first modification to the EKF method mirrors the upper triangular component

of the updated covariance matrix of the state estimate to ensure symmetry. If any of the eigenvalues of the covariance matrix are negative due to numerical errors, an identity matrix multiplied by a correction term equal to the highest magnitude of the negative eigenvalues is added to the covariance.

3.6 Simulation Results

Multiple simulations of tracking the same state data are performed with random noise to get a reasonable example of the average behavior of the tracking methods. A $3 \times 10^4 s$ interval from $700000s$ to $730000s$ into the orbital simulation that contains multiple satellite maneuvers is used to illustrate tasking method effectiveness. Overall, six maneuvers are performed at times listed in Table 3.4 within the tasking period.

Time (s)	Sat#
703800	11
708100	11
719570	3
720750	1
721550	10
725350	2

Table 3.4. Satellite maneuver times

The purely Fisher information based tasking seen in Equation 2.22 demonstrated, as expected, substantial errors in Figure 3.3 due to extended periods without observations of certain satellites. Purely Fisher information based tasking is not a useful demonstration of tasking method effectiveness.

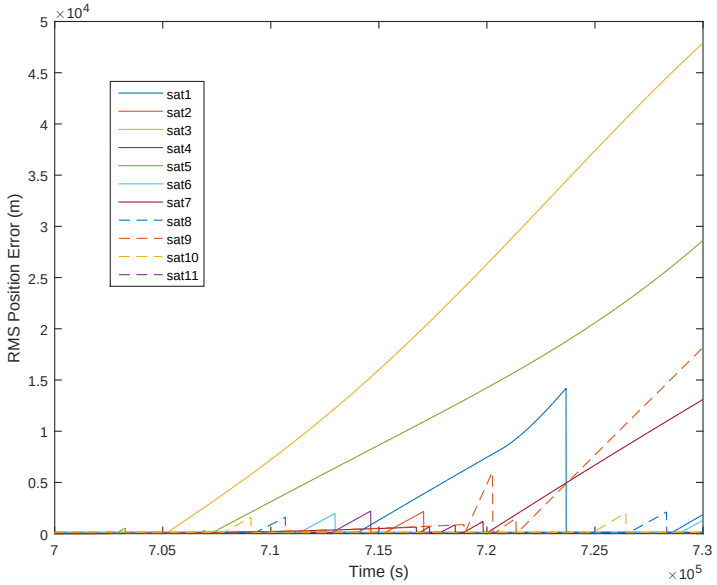

Figure 3.3. RMS position error for all satellites averaged over 100 simulations using only Fisher information based tasking

3.6.1 Single EKF Tasking

Using the method seen in Equation 2.26, which included the current state estimate covariance [1], the long periods without observation are not a problem and effective tasking results can be seen. A single EKF based tracking and tasking method used in previous research [1] serves as a baseline comparison for the performance of tracking in a system with dynamic sensor allocation. This Fisher information and covariance method has previously demonstrated accurate tracking of multiple non-maneuvering satellites and the errors it demonstrates when used in a maneuvering system illustrate the kind of problems the probabilistic IMM EKF tracking methods are designed to minimize.

For small maneuvers, such as satellite station keeping, the single EKF method demonstrates good tracking as in Figure 3.4 and 3.5. However, larger maneuvers such as the LEO satellite's transfer, has significant velocity error that takes upwards of $300s$ to be corrected (Figure 3.9). Position error during maneuvers (Figure 3.7) is

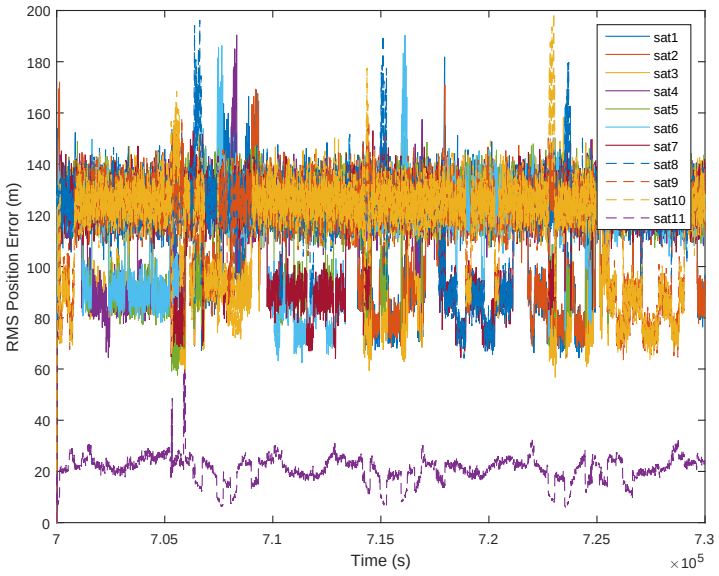

Figure 3.4. RMS position error for all satellites averaged over 100 simulations using Fisher information and covariance based sensor tasking with a single EKF estimator

less substantial, but that is more an artifact of this method's tendency to prioritize the closer LEO satellites due to their much higher Fisher information gain. When a satellite is being continuously observed, position error is reasonable after maneuvers. But if the tasking method does not ensure continuous measurements, substantial errors can result, as can be seen with the Fisher and covariance based IMM EKF tasking method. The satellite tasking demonstrates oscillatory behavior (Figure 3.6) where the number of observations alternates between a higher and lower number of sensor observations at each time step. These oscillations are a result of the covariance behavior, as steps with less observations result in covariance spikes that are mitigated by performing more observations of that satellite in the next step.

One trend that can be observed is the LEO satellite non-maneuvering velocity error in Figure 3.8 is much higher than the average error of the GEO satellites. The larger LEO velocity error is due to the higher effect of atmospheric drag, the higher relative velocities, and the fact that the satellite can be observed by more

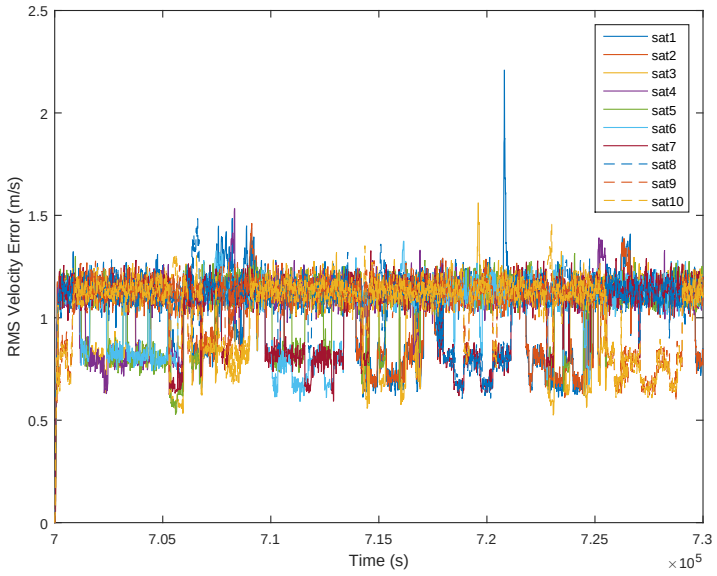

Figure 3.5. RMS velocity error for all satellites' except Satellite 11 averaged over 100 simulations using Fisher information and covariance based sensor tasking with a single EKF estimator

sensors on one side of the planet due to all ground-based sensors being located in the western hemisphere. This discrepancy in sensor availability is the cause of the periodic oscillation of the velocity error. The LEO satellite has a lower degree of position error as the sensor angle measurement error has a diminished effect on the corresponding position estimate.

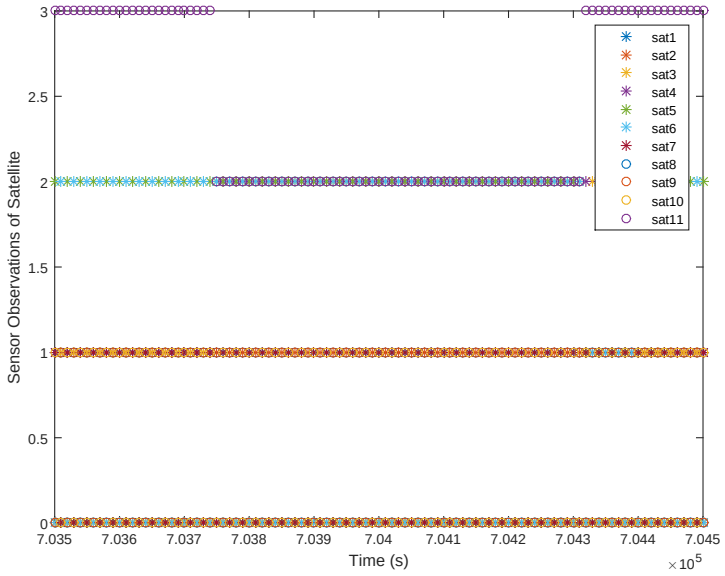

Figure 3.6. Number of sensor observations of a given satellite averaged over 100 simulations using Fisher information and covariance based sensor tasking with a single EKF estimator

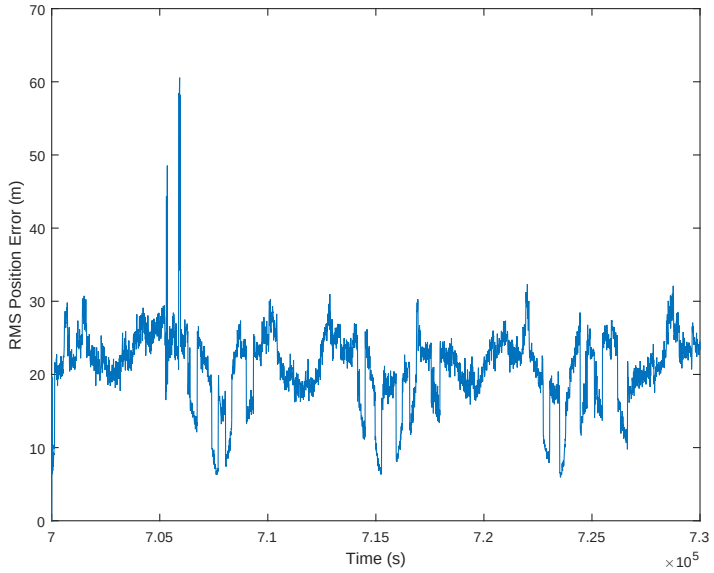

Figure 3.7. Satellite 11 RMS position error averaged over 100 simulations using Fisher information and covariance based sensor tasking with a single EKF estimator

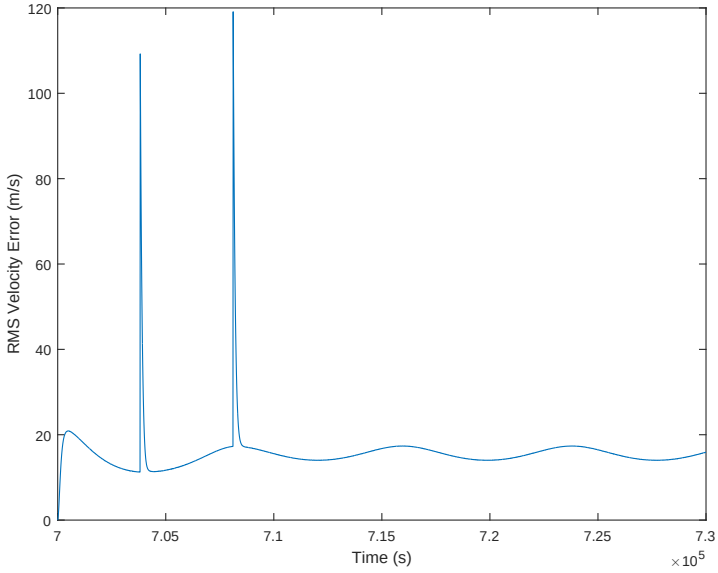

Figure 3.8. Satellite 11 RMS velocity error averaged over 100 simulations using Fisher information and covariance based sensor tasking with a single EKF estimator

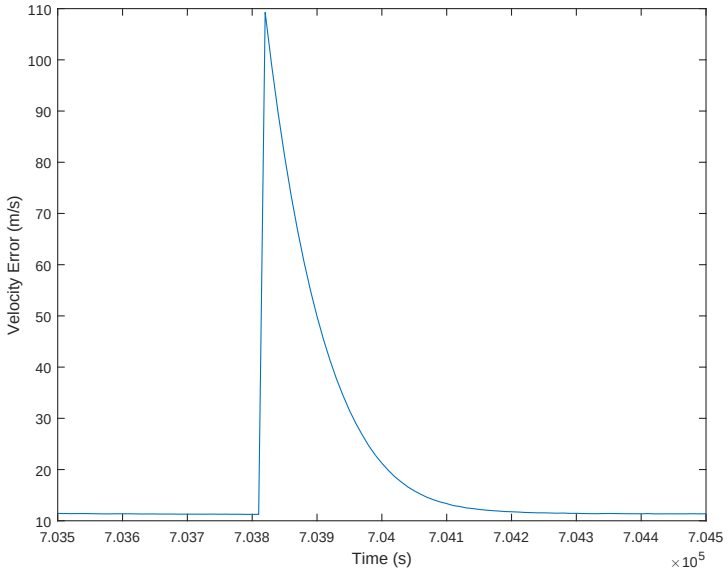

Figure 3.9. Satellite 11 RMS velocity error averaged over 100 simulations using Fisher information and covariance based sensor tasking with a single EKF estimator during first LEO maneuver

3.6.2 Fisher and Covariance Tasking

An IMM EKF tracking method can be used to reduce the error of the satellites' state estimate during maneuvers in the case of continuously observed satellites [7]. But when the tracking has to account for periods without observation or with multiple satellite observations, certain issues with the satellite state estimate covariance matrix become apparent. Because of the higher state error of the maneuvering mode EKF a satellite's state estimate covariance is much higher near maneuvering boundaries and the satellite is appropriately more highly prioritized by the tasking method. This increase in covariance is most pronounced after a satellite has not been observed for an iteration as the error covariance directly after multiple measurements is low (Figures 3.18 and 3.17). These oscillations in state estimate covariance have the potential to leave satellites unobserved for several time steps after a significant maneuver as can be seen in Figure 3.12. Infrequent observations after maneuvers could also easily occur with the single EKF method if the satellites are in very different orbital positions relative to the available sensors. Any strong bias towards certain satellites could result in steps with no observations, even soon after a maneuver.

The position error results in Figure 3.10 demonstrate a wider range of errors than the single EKF method. Several satellites have lower error than the group average. This difference in error is primarily due to the probability of maneuvering affecting the covariance of the satellite state resulting more observations for certain satellites. The position error of the LEO satellite during the first maneuver (Figure 3.15) demonstrates substantial error spikes due to brief periods without observation before the velocity error can be corrected, demonstrating a substantial issue with the tracking method.

The spike in velocity error for Satellite 11 seen in Figure 3.16 during the first maneuver demonstrates a reduction in the time required to return to the normal levels of error. In this case the Satellite 11 velocity estimate only takes around $160s$ instead of $300s$ to return to normal. This improvement in velocity tracking is offset

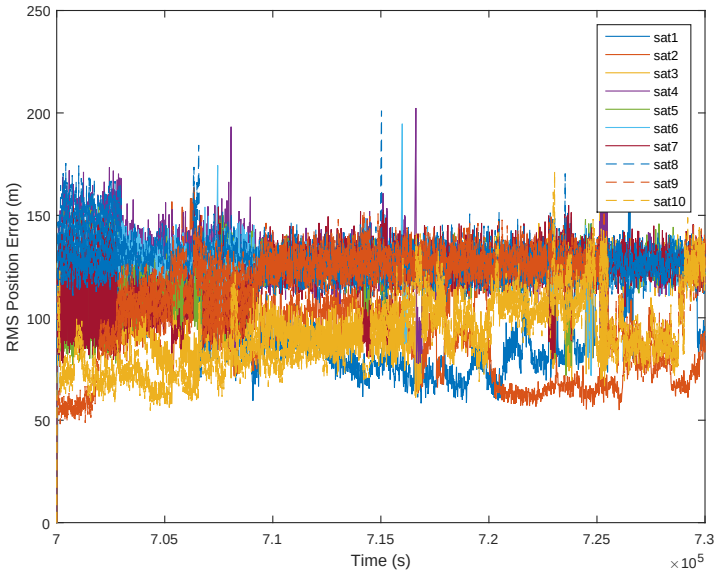

Figure 3.10. RMS position error for all satellites except Satellite 11 averaged over 100 simulations using Fisher information and covariance based sensor tasking

by spikes in position error due to the periods without observations. To improve the tracking of maneuvering satellites, the probability of maneuvering can be included in the information gain term, as was addressed earlier in Equation 2.27.

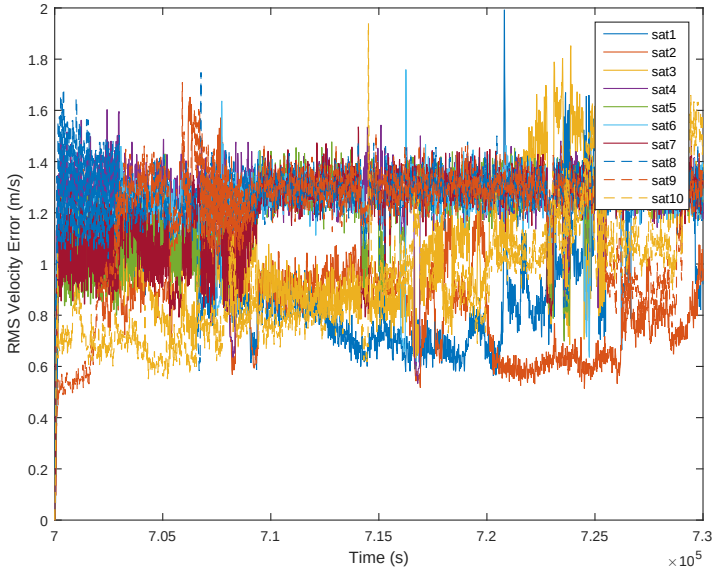

Figure 3.11. RMS velocity error for all satellites except Satellite 11 averaged over 100 simulations using Fisher information and covariance based sensor tasking

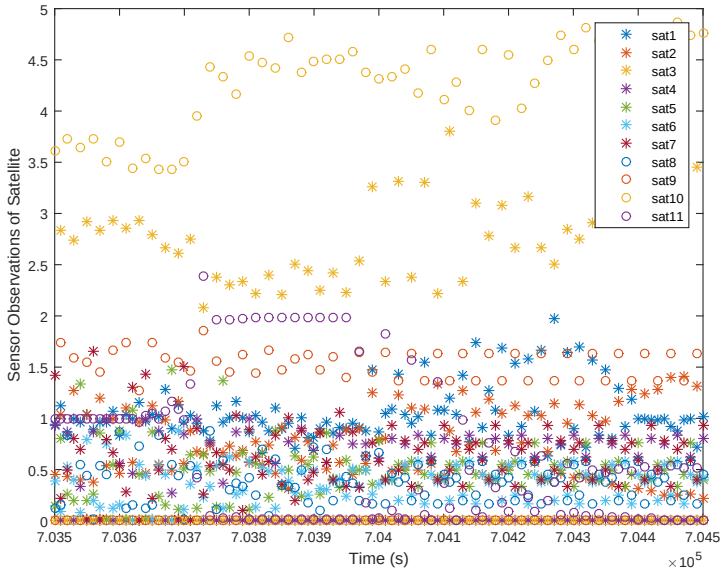

Figure 3.12. Number of sensor observations of a given satellite averaged over 100 simulations using Fisher information and covariance based sensor tasking

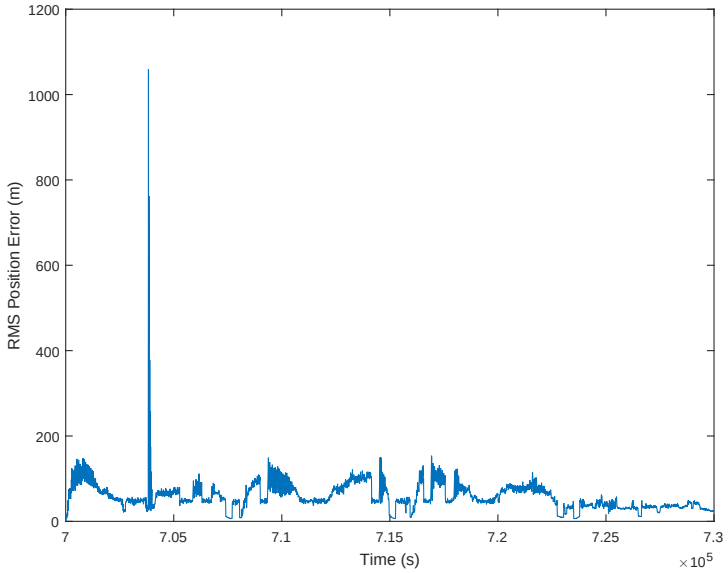

Figure 3.13. Satellite 11 RMS position error averaged over 100 simulations using Fisher information and covariance based sensor tasking

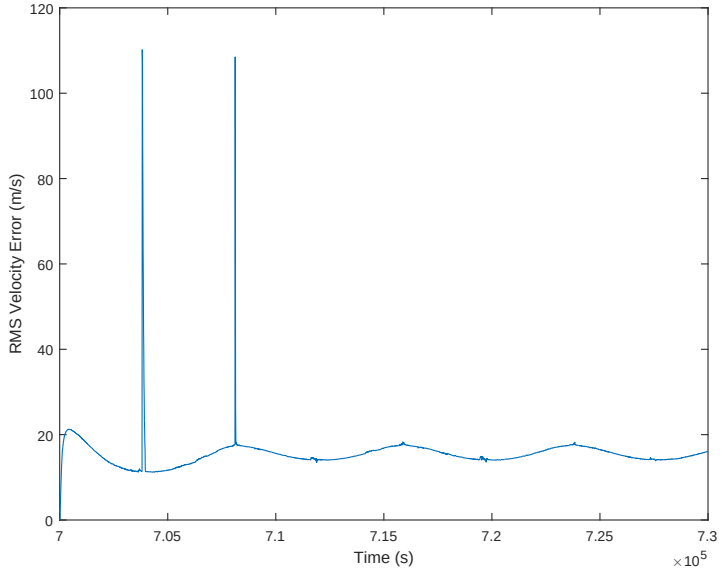

Figure 3.14. Satellite 11 RMS velocity error averaged over 100 simulations using Fisher information and covariance based sensor tasking

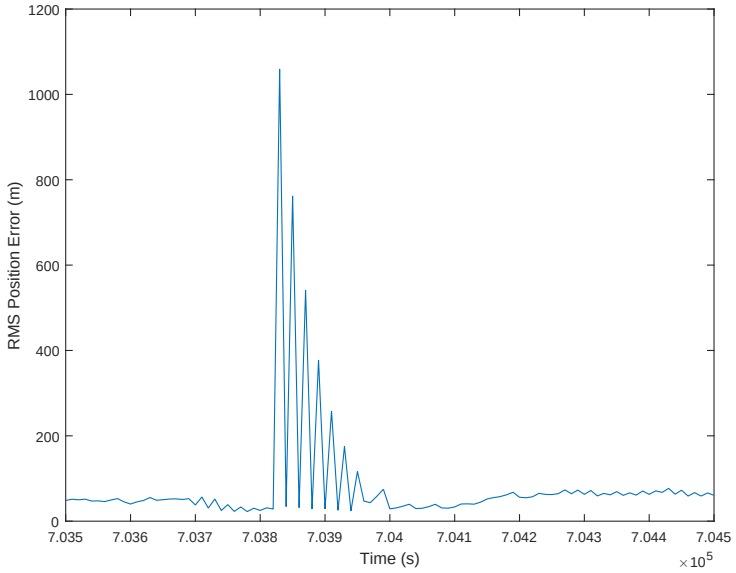

Figure 3.15. Satellite 11 RMS position error averaged over 100 simulations using Fisher information and covariance based sensor tasking around the first LEO maneuver

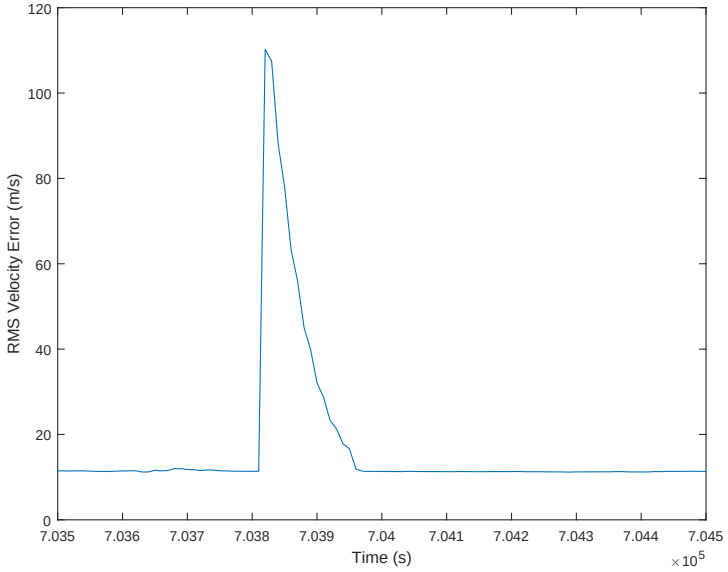

Figure 3.16. Satellite 11 RMS velocity error averaged over 100 simulations using Fisher information and covariance based sensor tasking around the first LEO maneuver

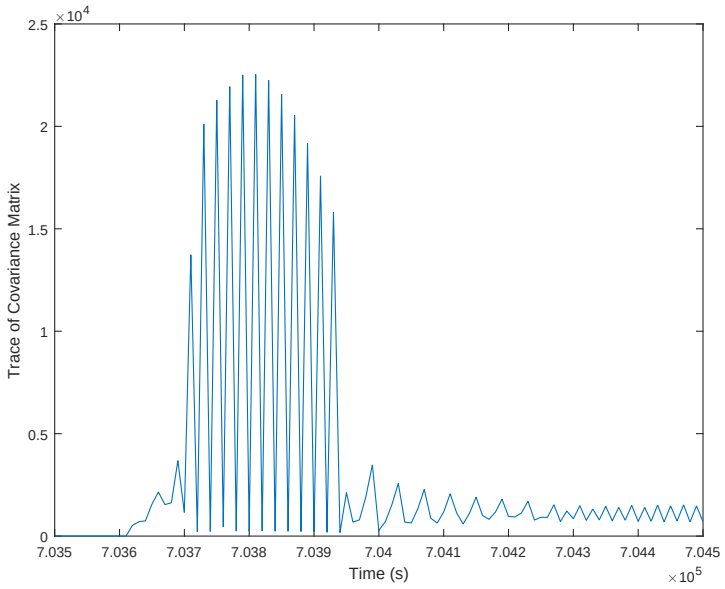

Figure 3.17. Average trace of the covariance matrix for Satellite 11 over 100 simulations using Fisher information and covariance based sensor tasking

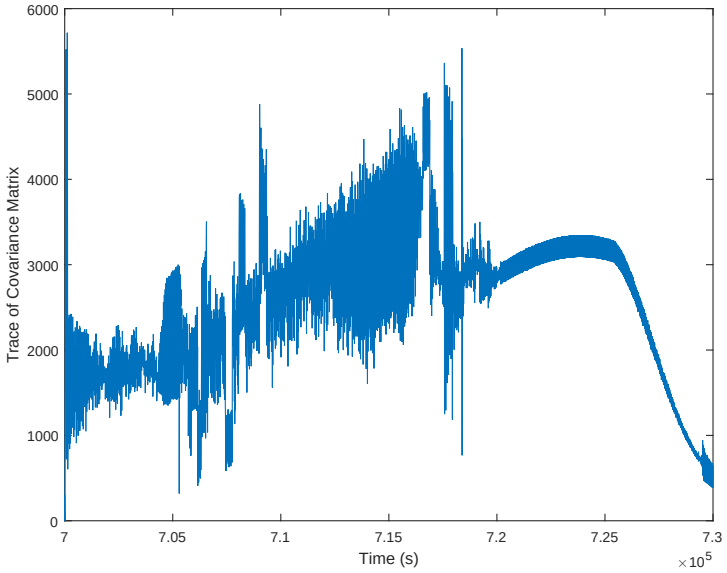

Figure 3.18. Average trace of the covariance matrix for Satellite 2 over 100 simulations using Fisher information and covariance based sensor tasking

3.6.3 Fisher, Probability and Covariance Tasking

To improve the behavior of tracking maneuvering satellites, the method proposed by this paper makes use of a probability component in the information gain as seen in Equation 2.27. Because the probability of maneuvering is just an additional gain applied to the tasking optimization gain, more satellite observations are allocated to satellites near maneuvering states, reducing the error around maneuvering by making it more likely the satellite will be continuously observed while the velocity error is being corrected after the maneuver.

This probability dependent tasking method demonstrates improved velocity error convergence rates. In Figure 3.23, error convergence time going down to $50s$ while avoiding the oscillatory position errors of the other IMM EKF method (Figures 3.22 and 3.24). These results appear very promising as it is an improvement in the maneuver tracking behavior while maintaining similar non-maneuvering tracking performance.

In Figure 3.21 a much more consistent spread of potentially maneuvering satellite observations than previous methods (Figure 3.12) can be seen. However, the spikes in velocity error of Satellite 10 (Figure 3.20) are the result of the tasking method allocating the non-maneuvering satellites as a lower priority. The constants used in Table 3.1 could be fine tuned to specific applications, minimizing these kinds of minor errors and could be the subject of future work.

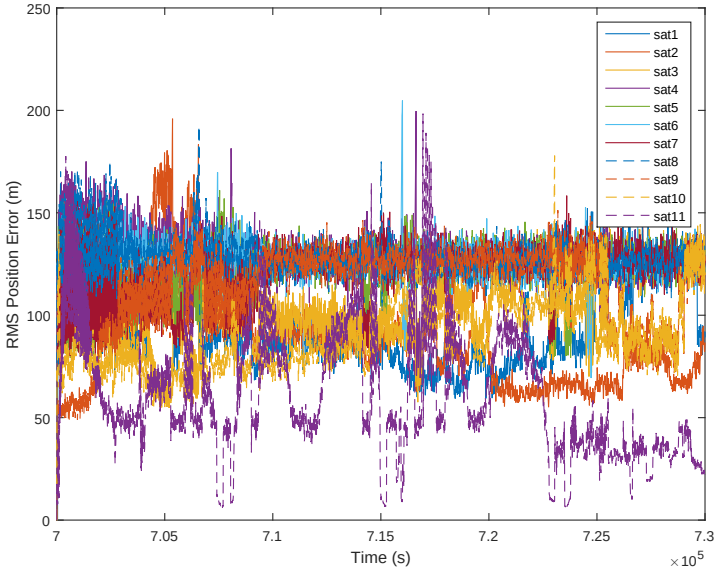

Figure 3.19. RMS position error for all satellites averaged over 100 simulations using probability, Fisher information, and covariance based sensor tasking

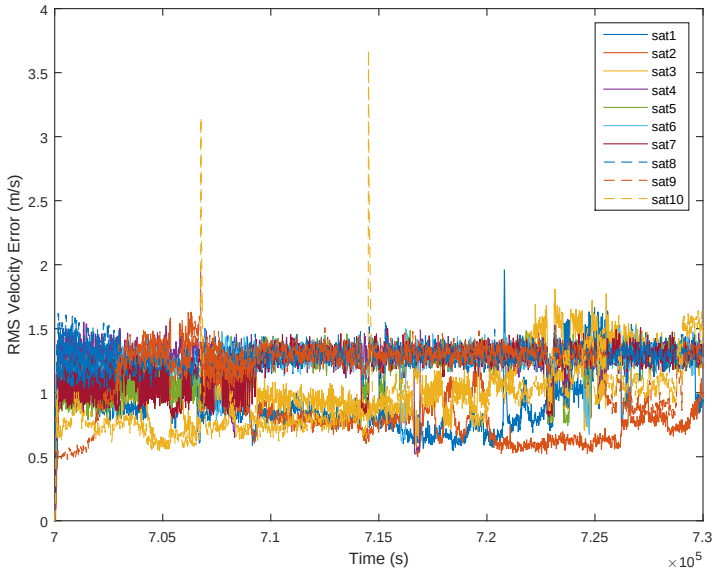

Figure 3.20. RMS velocity error for all satellites except Satellite 11 averaged over 100 simulations using probability, Fisher information, and covariance based sensor tasking

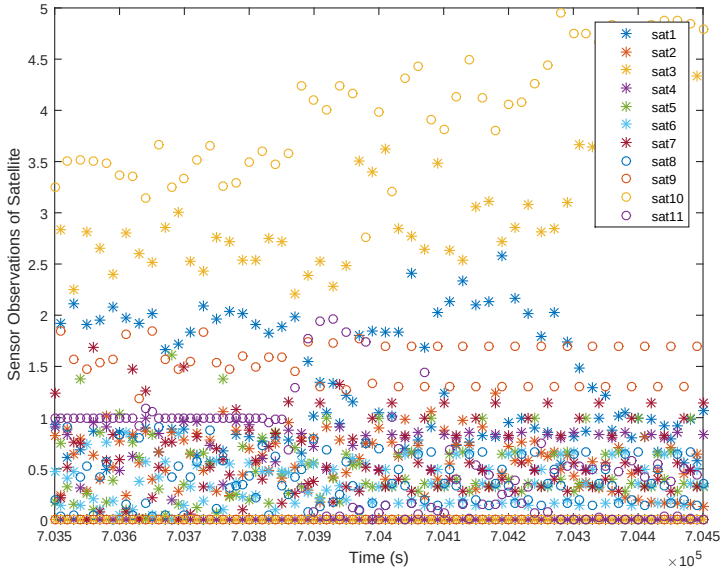

Figure 3.21. Number of sensor observations on a given satellite averaged over 100 simulations using probability, Fisher information, and covariance based sensor tasking

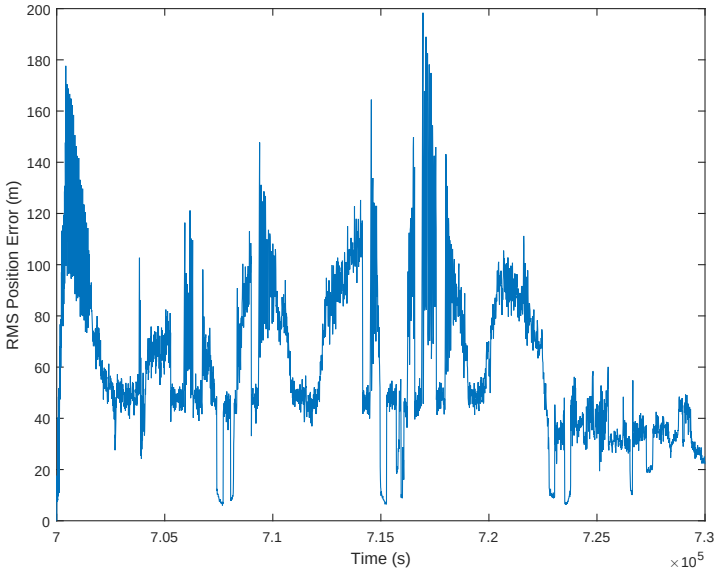

Figure 3.22. Satellite 11 RMS position error averaged over 100 simulations using probability, Fisher information, and covariance based sensor tasking

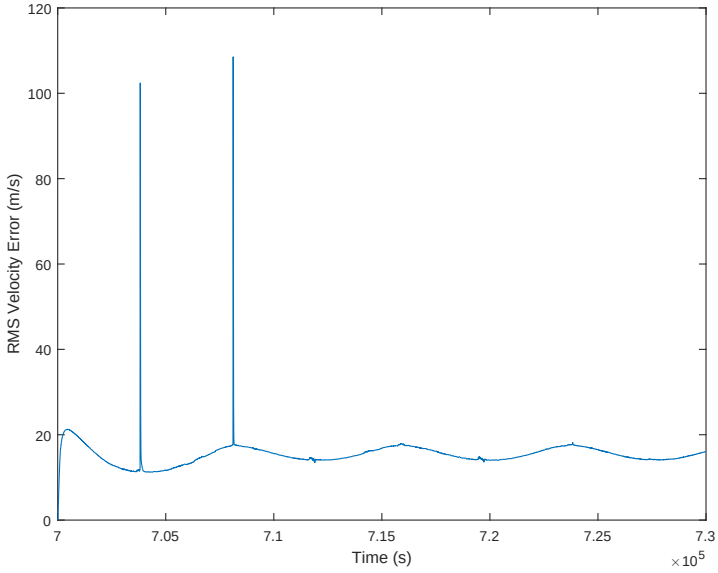

Figure 3.23. Satellite 11 RMS velocity error averaged over 100 simulations using probability, Fisher information, and covariance based sensor tasking

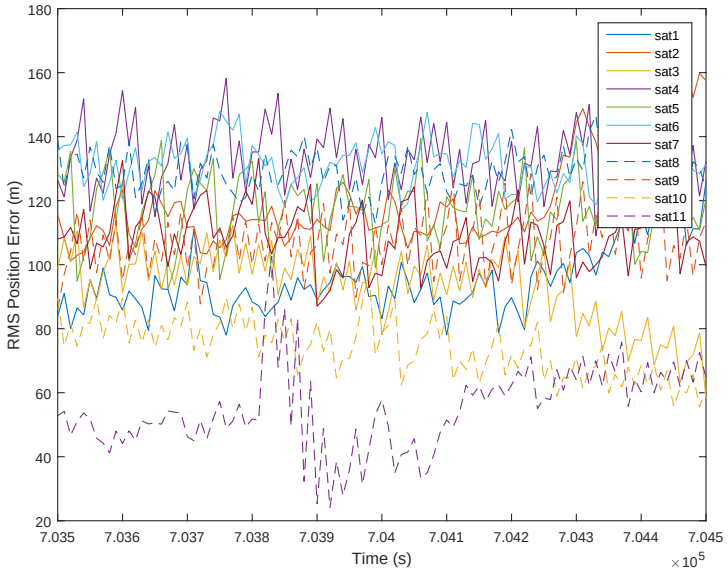

Figure 3.24. RMS position error for all satellites averaged over 100 simulations using probability, Fisher information, and covariance based sensor tasking near the first LEO maneuver

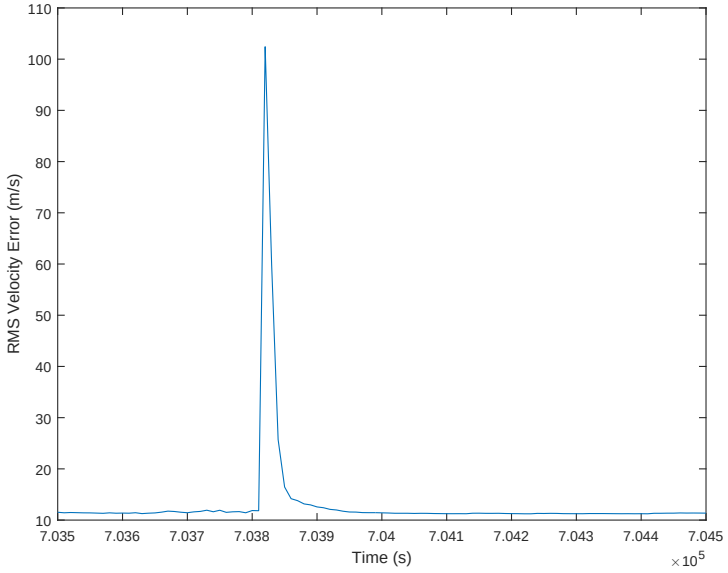

Figure 3.25. Satellite 11 RMS velocity error averaged over 100 simulations using probability, Fisher information, and covariance based sensor tasking near the first LEO maneuver

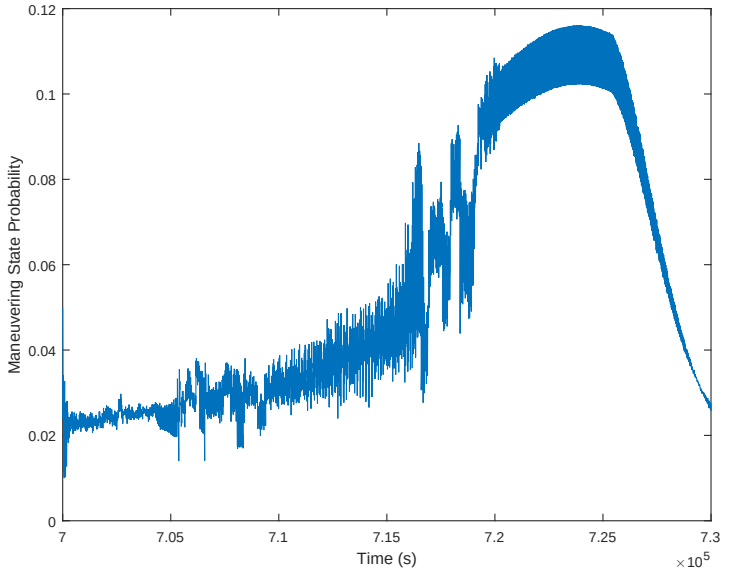

Figure 3.26. Average probability of the maneuvering mode for Satellite 2 over 100 simulations using probability, Fisher information, and covariance based sensor tasking

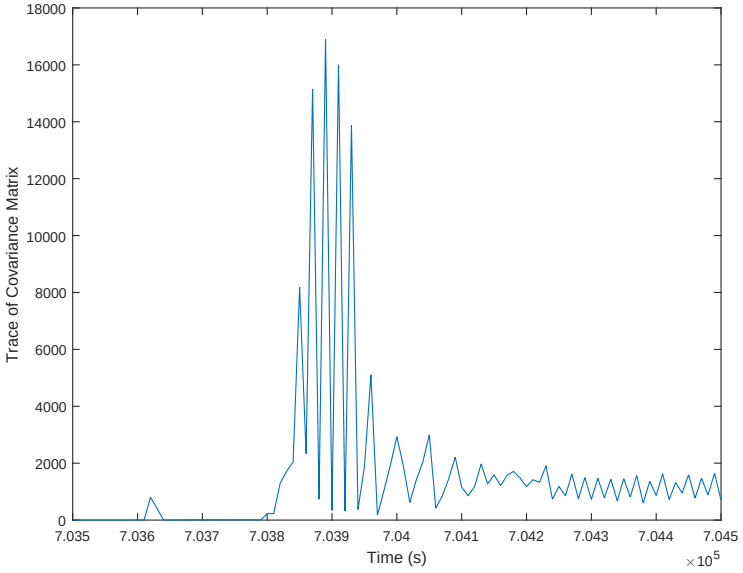

Figure 3.27. Trace of estimated state covariance for Satellite 11 averaged over 100 simulations using probability, Fisher information, and covariance based sensor tasking

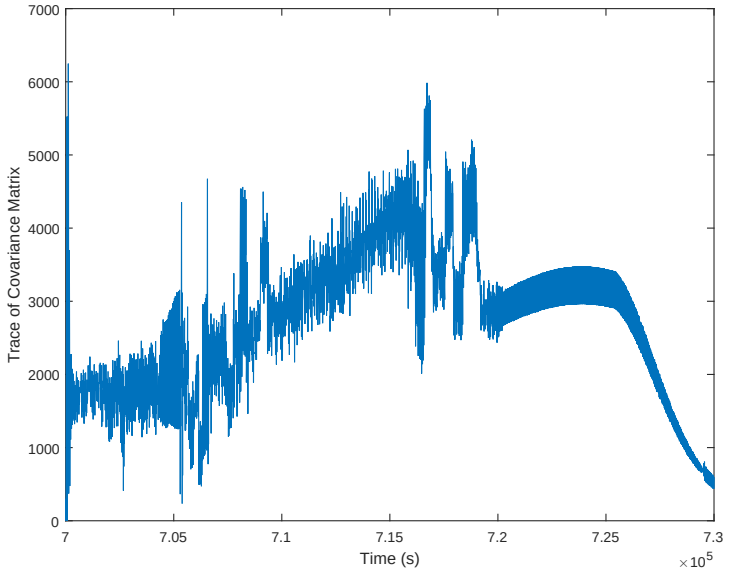

Figure 3.28. Average trace of estimated state covariance for Satellite 2 over 100 simulations using probability, Fisher information, and covariance based sensor tasking

3.6.4 Method Comparisons

Given the high variability of error with multiple satellites being tracked it is somewhat difficult to clearly ascertain the relative performance of different satellite tasking and tracking methods. The average of the RMS position and velocity errors across all satellites is calculated to compare the tasking performance between the different methods. The specific tasking behavior of each satellite can be seen in Appendix A.

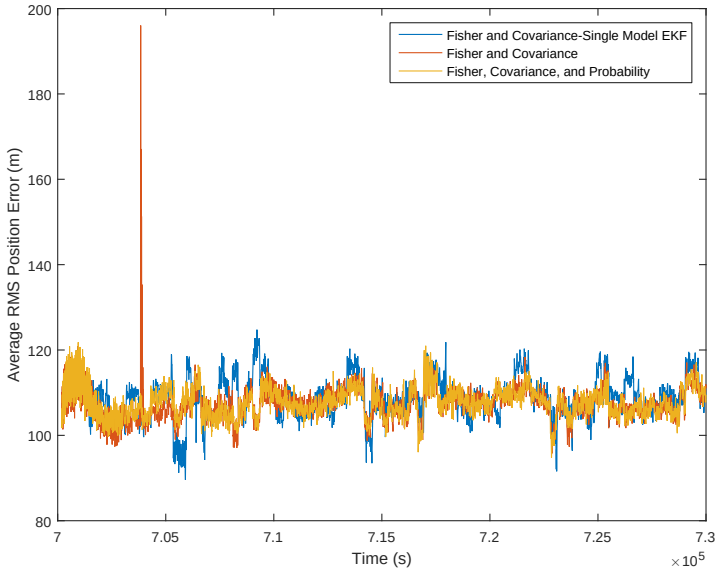

Figure 3.29. Average of all satellites' position error over 100 simulations for all tasking methods

As can be seen in Figure 3.29, at time periods with no maneuvers, the performance of all three methods is roughly similar with the single EKF method exhibiting a greater range of errors and a slightly higher mean. The largest obvious difference between the methods is the substantial position error in the IMM EKF method without the direct probability component, previously seen in Figure 3.15. This spike of position error is not present with other methods and are the result of lack of observation directly after a maneuver as can be seen in Figure 3.31. The visible spike in this

metric is heavily weighted towards the error of Satellite 11 while the average value is heavily dependent on the less accurate tracking of the GEO satellites.

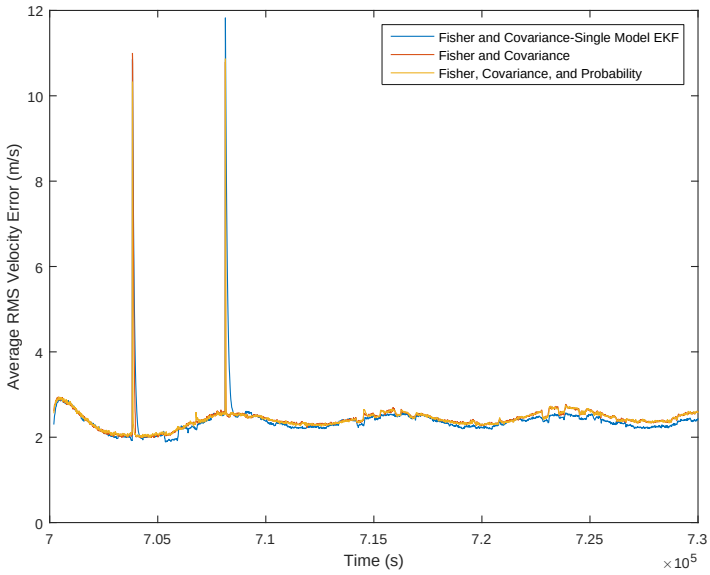

Figure 3.30. Average of all satellites' velocity error over 100 simulations for all tasking methods

The velocity error averages in Figure 3.30 also demonstrates spikes due to the Satellite 11 maneuvers. The overall average of the velocity error appears to be dominated by the Satellite 11 error. It appears that outside of LEO maneuvers, the single EKF model performs slightly better than the IMM methods but that is a result of multiple potentially maneuvering satellites being present in the later section of the time period simulated, see for example Figure 3.26. As the potentially maneuvering satellites are observed more closely at the expense of other satellites, there is a slight increase in average velocity error as these maneuvers are not substantial enough to seriously disrupt the single EKF satellite tracking. The improvement in position error is of a comparable degree to the increase in velocity error during this period (Table 3.5). These very small loses could likely be reduced by fine tuning the satellite probability models and tasking coefficients with different priorities based on the satel-

Method	Error Metric	Value	Standard Deviation
Single EKF	Mean Position Error	$108.7346m$	$4.8029m$
	Max Position Error	$199.2855m$	–
	Mean Velocity Error	$2.3908\frac{m}{s}$	$0.5420\frac{m}{s}$
	Max Velocity Error	$119.1369\frac{m}{s}$	–
IMM Fisher and Covariance	Mean Position Error	$107.4954m$	$4.11049m$
	Max Position Error	$1059.6797m$	–
	Mean Velocity Error	$2.4291\frac{m}{s}$	$0.3898\frac{m}{s}$
	Max Velocity Error	$110.2265\frac{m}{s}$	–
IMM Fisher, Covariance, and Probability	Mean Position Error	$107.6523m$	$3.4713m$
	Max Position Error	$204.7985m$	–
	Mean Velocity Error	$2.41675\frac{m}{s}$	$0.2969\frac{m}{s}$
	Max Velocity Error	$108.5713\frac{m}{s}$	–

Table 3.5. Method error comparison from $700500s$ to $730000s$

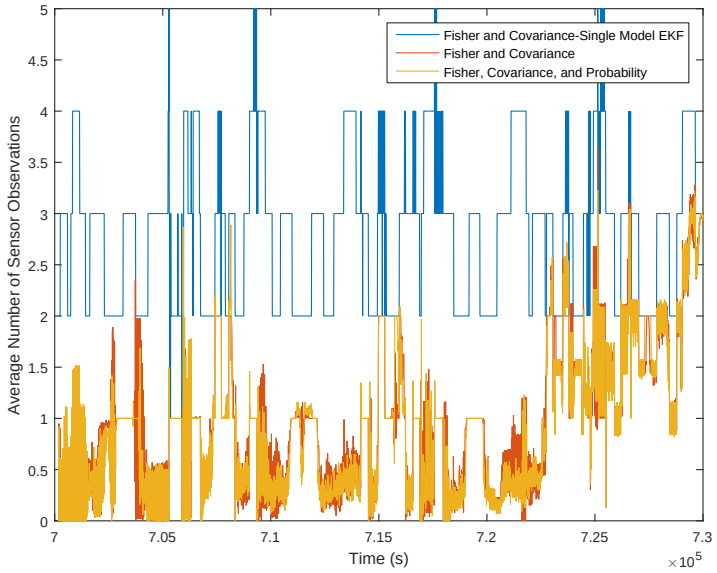

Figure 3.31. Average number of observations of Satellite 11 over 100 simulations for all tasking methods

lite type. Such modifications could be the subject of future work to bring velocity tracking results closer to the single EKF method while still allowing for improved maneuver tracking behavior. Over the full simulation period, the results of the single and IMM EKF methods are comparable, which is expected as improvements from the IMM method are primarily seen around maneuvers.

In an attempt to better illustrate the differences between the probability based and covariance based tracking methods, a shorter time frame around the large Satellite 11 maneuvers can be seen in Figure 3.32 and Figure 3.33 for the first maneuver, and in Figure 3.35 and Figure 3.36 for the second maneuver. The mean and max errors for these time periods can also be found in Table 3.6 and Table 3.7, respectively. The large spikes in the Fisher and covariance IMM EKF method position error are the primary issue that can be detected near the first maneuver. The error is the result of the oscillatory tasking behavior that can be seen in Figure 3.34 and as without the additional probability component in tasking the error there are steps

where no observations which causes the large position errors to occur. The position error performance near maneuvers is in favor of the IMM EKF method that directly incorporates probability.

Near maneuvers, the velocity tracking is best done with the method directly employing probability, while other methods demonstrate worse performance. The improvement in velocity error settling time with the IMM methods is quite substantial, potentially reducing the settling time by a factor of around six (Figure 3.36). The period limited averages of position and velocity error seen in Table Table 3.6 and Table 3.7 reflect these improvements with the greatest difference in error is seen in the method directly incorporating probability.

One performance metric that is lost when converting to the average error across all satellites is the maximums errors of each satellite that can be seen in Figures 3.4, 3.10, and 3.19. The maximum position and velocity errors seen for any particular satellite appear to be relatively consistent between different tasking methods with some potential reductions in the number of error spikes using the IMM EKF methods. As the many maximums in position error do not correspond to satellite maneuvers, other methods than maneuver prediction will need to be applied to minimize these errors.

3.7 Discussion

The baseline performance of velocity and position error away from large maneuvers is comparable to what is seen in other work using similar sensor error dynamics observing geostationary satellites [7] [12]. Because the error results are very heavily dependent on particular satellite configurations, it is difficult to make direct comparisons to the results of other research [1]. The average error values seen in this paper is slightly worse than single sensor single target results, but that is to be expected in sensor limited systems with higher state error covariance values. The differences between the IMM EKF methods and the single EKF method are a better indicator

Method	Error Metric	Value	Standard Deviation
Single EKF	Mean Position Error	$106.8932m$	$3.3337m$
	Max Position Error	$147.1400m$	–
	Mean Velocity Error	$2.7291\frac{m}{s}$	$1.7837\frac{m}{s}$
	Max Velocity Error	$109.2691\frac{m}{s}$	–
IMM Fisher and Covariance	Mean Position Error	$106.8130m$	$12.5088m$
	Max Position Error	$1059.6797m$	–
	Mean Velocity Error	$2.5414\frac{m}{s}$	$1.6706\frac{m}{s}$
	Max Velocity Error	$110.2265\frac{m}{s}$	–
IMM Fisher, Covariance, and Probability	Mean Position Error	$105.8925m$	$2.2275m$
	Max Position Error	$160.2447m$	–
	Mean Velocity Error	$2.1986\frac{m}{s}$	$0.93674\frac{m}{s}$
	Max Velocity Error	$109.2691\frac{m}{s}$	–

Table 3.6. Method error comparison from $703500s$ to $704500s$

Method	Error Metric	Value	Standard Deviation
Single EKF	Mean Position Error	$108.8932m$	$4.2465m$
	Max Position Error	$190.4877m$	–
	Mean Velocity Error	$3.3492\frac{m}{s}$	$1.9087\frac{m}{s}$
	Max Velocity Error	$119.1369\frac{m}{s}$	–
IMM Fisher and Covariance	Mean Position Error	$104.7563m$	$3.5236m$
	Max Position Error	$193.2763m$	–
	Mean Velocity Error	$2.6795\frac{m}{s}$	$0.9298\frac{m}{s}$
	Max Velocity Error	$108.5308\frac{m}{s}$	–
IMM Fisher, Covariance, and Probability	Mean Position Error	$104.9494m$	$2.4846m$
	Max Position Error	$181.4694m$	–
	Mean Velocity Error	$2.6772\frac{m}{s}$	$0.9381\frac{m}{s}$
	Max Velocity Error	$108.5713\frac{m}{s}$	–

Table 3.7. Method error comparison from $707800s$ to $708800s$

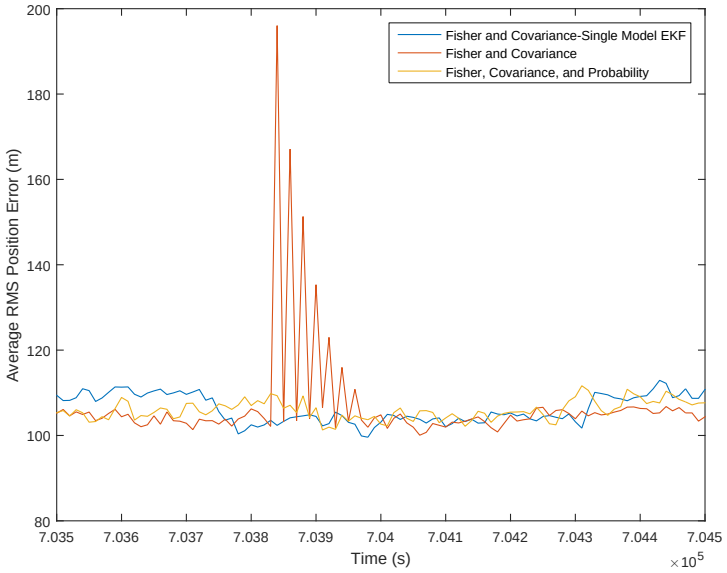

Figure 3.32. Average of all satellites' position error over 100 simulations for all tasking methods near the first LEO maneuver

of performance improvements. The improvements in average position error near maneuvers can result in improvements on the order of a tenth of the non-maneuvering error as seen in Figure 3.35 which is an improvement in line with other notable developments [1]. With alternative satellite simulation configurations the improvements from IMM EKF tracking can be even greater as can be seen in Appendix B.

The improvement in velocity error settling time after substantial maneuvers from around five minutes to less than one (Figure 3.33) is significant on the scale of the continuous observation times used in arc tracking methods that often continuously observe for five or more minutes [12]. This faster tracking performance would potentially allow for the allocation of shorter observation times, increasing the efficiency of tasking methods. Refinements in the tasking model in future work could also take this into account by adjusting the probability of maneuvering model to have lower boundary covariance.

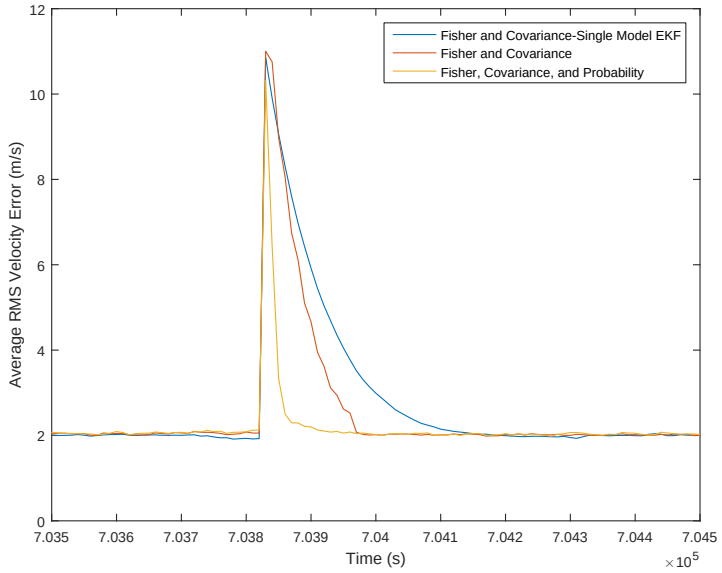

Figure 3.33. Average of all satellites' velocity error over 100 simulations for all tasking methods near the first LEO maneuver

The mitigation of the massive position error spikes seen in Figure 3.15 is a major improvement in the probability based tasking method proposed by this paper. Any tasking method that does not include maneuver prediction or detection methodologies runs the risk of this type of error, as there are no tasking components to ensure that satellites are continuously observed around a maneuver. The improved velocity error settling time from IMM EKF methods helps some with this issue but without continuous observations the improvements are reduced as can be seen in Figure 3.33. Additionally in Figure 3.34 it is apparent that the improved performance in large maneuver tracking occurs with less observations than the single EKF method indicating a substantial increase in tracking method performance. The second LEO maneuver avoids this same oscillatory behavior due to the satellite being continuously observed by a ground-based sensor as can be seen in Appendix A. The probability component in the information gain allows the simple linear optimization techniques to achieve this goal with a minimum of other modifications while maintaining similar perfor-

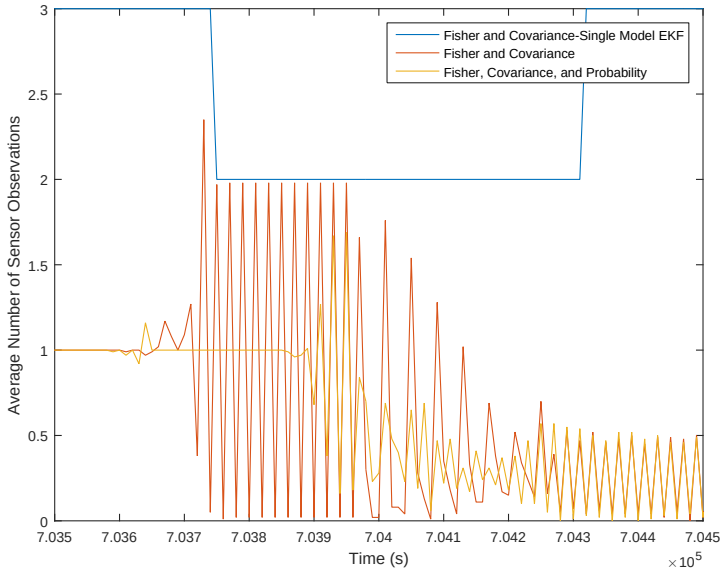

Figure 3.34. Average number of observations of Satellite 11 over 100 simulations for all tasking methods near the first LEO maneuver

mance away from maneuvers. Potential improvements in the tasking method could use requirements that satellites above a certain maneuvering probability thresholds are guaranteed continuous observations if possible. This requirement based tasking modification could be a potential future research subject but would require additional research into conflicting requirements management.

In future work the exact values of the tasking coefficients seen in Table 3.1, the error values in the EKF, and in the maneuver probability model dynamics may need to be tuned to function well with specific tasking configurations, potentially with tasking coefficients tuned to each satellite type. Greater computational resources would likely be necessary to develop general rules for determining the tasking method coefficient values, as a wide variety of orbital scenarios and computationally intensive tracking simulations would need to be run. An initial attempt to generate better results through satellite specific changes can be seen in Appendix B.

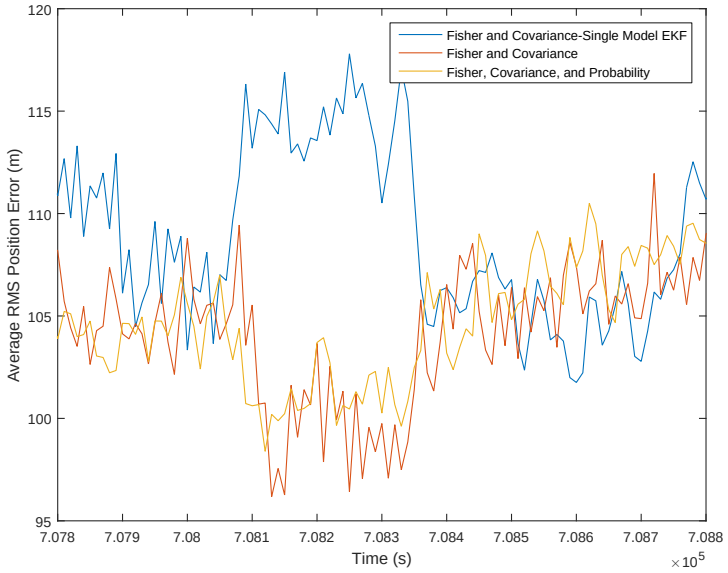

Figure 3.35. Average of all satellites' position error over 100 simulations for all tasking methods near the second LEO maneuver

The results of the implementation of the IMM EKF tracking method with probability dependent tasking demonstrates performance equivalent to single EKF methods away from substantial maneuvers. More importantly, substantial improvements in tracking during periods with major maneuvers are also achieved while mitigating potential major tracking errors that can be the result of sensor limited systems. The improvements in sensor tasking to track maneuvering satellites discussed in this paper seem promising for future developments in the area of SSA.

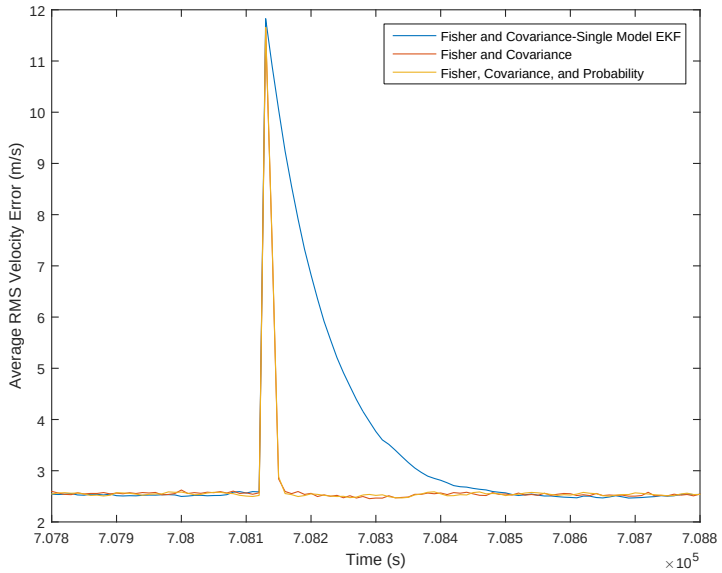

Figure 3.36. Average of all satellites' velocity error over 100 simulations for all tasking methods near the second LEO maneuver

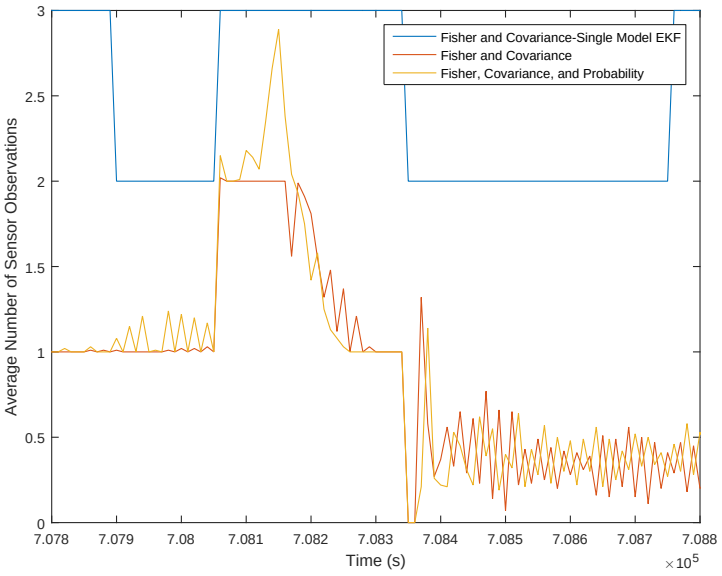

Figure 3.37. Average number of observations of Satellite 11 over 100 simulations for all tasking methods the second LEO maneuver

4. SUMMARY

The tasking of linked sensors to track multiple satellites in an efficient manner is an area of research that has seen substantial recent developments. The use of interacting multiple model extended Kalman filter tracking in Fisher information gain and covariance based satellite tasking techniques has the potential to demonstrate improved satellite tracking performance. Probabilistic maneuver prediction allows for potential satellite maneuvers to be incorporated into the tracking and tasking behavior.

The interacting multiple model extended Kalman filter makes use of the an arbitrary number of range and angle sensor readings at every time step to best update both the maneuvering and non-maneuvering mode state estimates. The two modes differ in their expected state error covariance, with the maneuvering mode having a much higher value. To properly combine these modes to attain the best state estimates, the probability of moving from one mode to the other based on the current estimated state and maneuver trigger boundaries is employed.

The sensor tasking method makes use of the current estimated state and the sensor positions to determine a sensor information gain for each sensor-target pair. This information gain is based on a combination of the Fisher information, current covariance of the estimate, and maneuver probability. These gains can be used as part of a linear programming optimization to determine which combination of sensor observations improves the overall state estimate of all satellites at any give observation step. The direct incorporation of probability into the tasking method, as well as an evaluation of the effects of multiple sensor multiple target systems using interacting multiple model tracking of maneuvering satellites, is the primary focus of this research.

To illustrate the effectiveness of these methods, numerical simulations of a sample multiple satellite configuration are used. The results of these simulations demonstrate that even when tracking more targets than can be targeted by available sensors, the

multiple model method can track maneuvering satellites better than a single model method. Maneuver probability has to be included in the information gain directly to compensate for high covariance fluctuations inherent in the multiple model method, or else serious tracking errors can occur after substantial maneuvers.

Potential future improvements of the simulation aspect of this research could be attained through better maneuvering satellite data. Improved satellite data could be acquired through the use of more advanced simulations or actual processed satellite tracking data. Long term tracking behavior analysis using the tracking methods described in this paper could be properly evaluated. A significant step towards refining these results could result from a deeper analysis into which values of tracking constants and maneuvering probability models result in better performance. Overall, the tasking and state estimation techniques used in this research performed well in simulation and demonstrated that interacting multiple model extended Kalman filter methods can result in substantial improvements in tracking multiple maneuvering satellites using limited sensor resources.

REFERENCES

REFERENCES

[1] Richard Scott Erwin, Paul Albuquerque, lam Hussein, and Sudharman K. Jayaweera. Dynamic sensor tasking for space situational awareness. *American Control Conference (ACC), IEEE*, 2010.

[2] Bruno OS Teixeira, Mario A. Santillo, R. Scott Erwin, and Dennis S. Bernstein. Spacecraft tracking using sampled-data kalman filters. *Control Systems,*, 28.4:78–94, 2008.

[3] Boeing: Space and Intelligent Systems. Space based space surveillance: Revolutionizing space awareness. `http://www.boeing.com/assets/pdf/defense-space/space/satellite/MissionBook.pdf`.

[4] Hengnian Li. *Geostationary Satellites Collocation*. Springer, New York, 2014.

[5] Nicholas H. Hamilton. Formation flying satellite control around the l2 sun-earth libration point. Masters, George Washington University, 1994.

[6] C. C. Chao and H. Bernstein. Onboard stationkeeping of geosynchronous satellite using a global positioning system receiver. *Journal of Guidance, Control, and Dynamics*, 17.4:778–786, 1994.

[7] Sangjin Lee and Inseok Hwang. State-dependent adaptive estimation for impulsively maneuvering spacecraft tracking. *AIAA Guidance, Navigation, and Control Conference*, 2016.

[8] X. Rong Li and Vesselin P. Jilkov. Survey of maneuvering target tracking. part v. multiple-model methods. *Aerospace and Electronic Systems, IEEE Transactions on*, 41.4:1255–1321, 2005.

[9] Tian Kangsheng and Zhu Guangxi. Sensor management based on fisher information gain. *Systems Engineering and Electronics, Journal of*, 17.3:531–534, 2006.

[10] Jian Huang. An object correlation and maneuver detection approach for space surveillance. *Research in Astronomy and Astrophysics*, 12.10:1402, 2012.

[11] Beth L Petrick. Weighting scheme for the space surveillance network automated tasker no. afit/gso/ens/94d-13. Masters, Air Force Institute of Technology, Wright-Patterson AFB OH, 1994.

[12] Jill Tombasco. *Orbit estimation of geosynchronous objects via ground-based and space-based optical tracking.* Phd, University of Colorado, 2011.

[13] Kate Becker, Emmanouil Detsis, Chijioke Nwosa, Vesna Palevska, Minoo Rathnasabathpathy, and Mahsa Taheran. Space situational awareness. Technical report, 2012.

[14] Sangjin Lee and Inseok Hwang. Interacting multiple model estimation for spacecraft maneuver detection and characterization. *AIAA Guidance, Navigation, and Control Conference*, 2015.

[15] Daniel P. Lubey and Daniel J. Scheeresy. Simulation of geo spacecraft undergoing stationkeeping maneuvers. *American Institute of Aeronautics and Astronautics*.

[16] Pratap Misra and Per Enge. *Global Positioning System: Signals, Measurements and Performance*. Ganga-Jamuna Press, Lincoln, Massachusetts, revised second edition, 2011.

[17] Howard D. Curtis. *Orbital Mechanics for Engineering Students*. Butterworth-Heinemann, Oxford, second edition, 2009.

[18] Rui C. Barbosa. Long march 3b lofts laosat-1. `https://www.nasaspaceflight.com/2015/11/long-march-3b-lofts-laosat-1/`.

[19] Ok-Chul Jung, Tae Soo No, Hae-Dong Kim, and Eun-Kyou Kim. A numerical approach for station keeping of geostationary satellite using hybrid propagator and optimization technique. *International Journal of Aeronautical and Space Sciences*, 8.1:122–128, 2007.

[20] Ana Paula Marins Chiaradia, Helio Koiti Kuga, and Antonio Fernando Bertachini de Almeida Prado. Comparison between two methods to calculate the transition matrix of orbit motion. *Mathematical Problems in Engineering 2012*, 2011.

APPENDICES

A. Sensor Specific Tasking Comparison

To better illustrate the differences between tasking methods a set of graphs showing the target satellites of specific sensors along with the satellites visible to that sensor are used. The time around the first and second LEO maneuver as seen in Section 3.6 are shown as trends over shorter time periods are fairly consistent across the whole time period. The sensors are numbered such that Sensors 1 through 4 are the space-based sensors located in each quadrant of the same sun synchronous orbit. Sensors 5 through 9 are the ground-based sensors located at longitudes of 0°W, 45°W, 75°W,120°W, 155°W respectively.

Each tasking method's selected satellite to observe at each time step is represented as a symbol in the tasking matrix. Due to uncertainty in the system there is some variation between simulation runs of which satellite is targeted so the maximum likelihood tasking solution is shown. The black sections in the figures represents the time periods where the indicated target satellites are not visible to a particular sensor. Changes in visibility are primarily due to the LEO target satellites and the orbital sensors movement around the earth causing certain satellites to become obscured. The ground based sensors have a much more consistent set of visible satellites in terms of seeing a certain set of GEO satellites at all times with intermittent views of the LEO target Satellite 11.

A.1 First LEO Satellite Maneuver

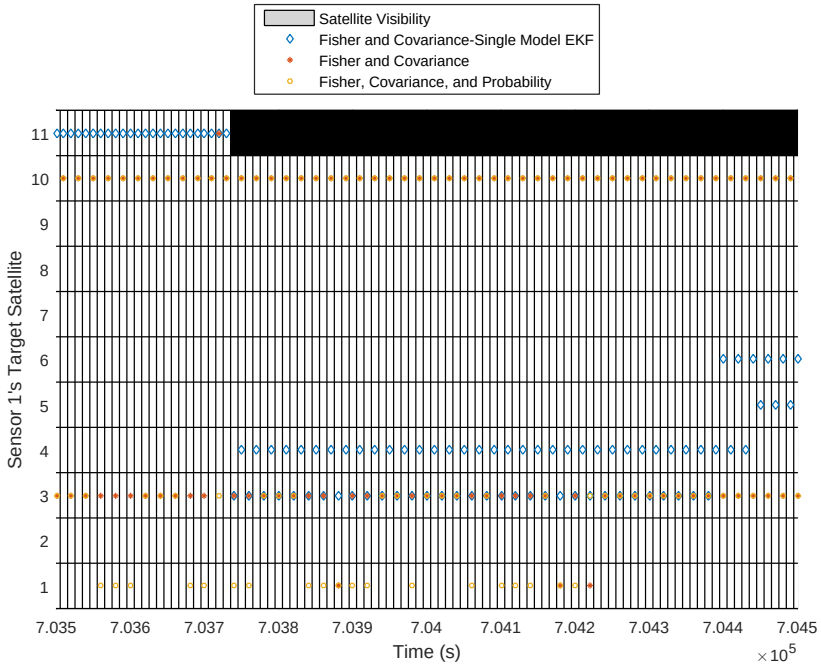

Figure A.1. The target allocation for Sensor 1 during the first LEO satellite maneuver

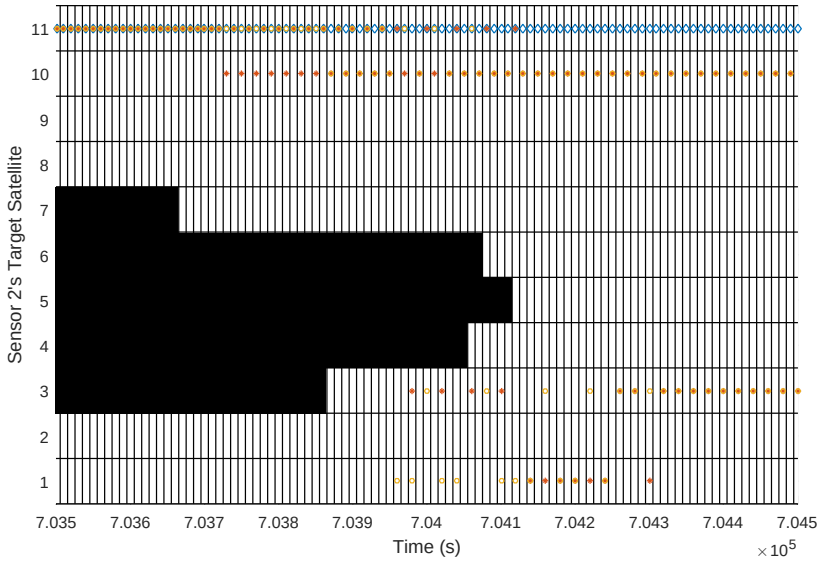

Figure A.2. The target allocation for Sensor 2 during the first LEO satellite maneuver

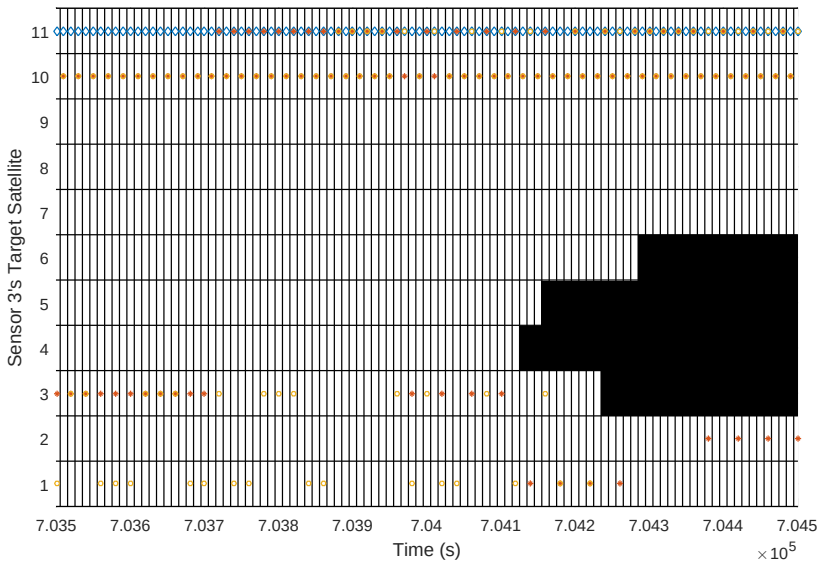

Figure A.3. The target allocation for Sensor 3 during the first LEO satellite maneuver

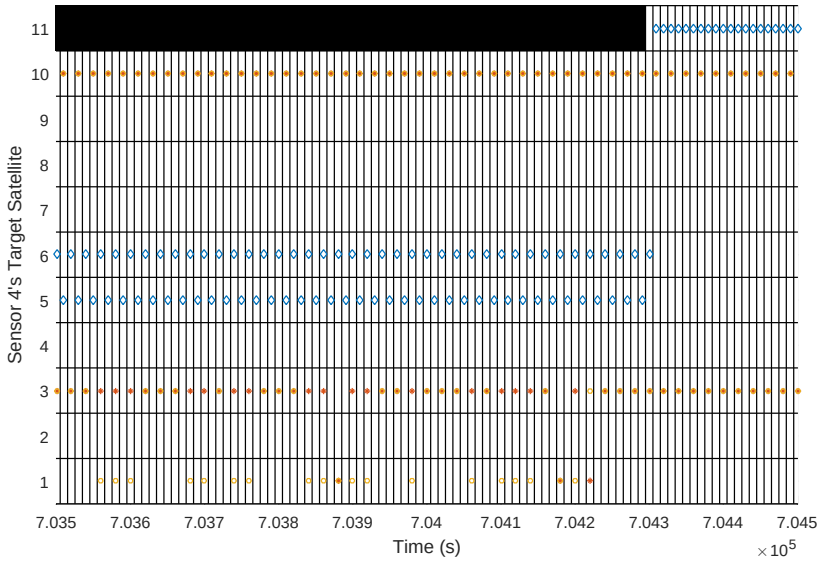

Figure A.4. The target allocation for Sensor 4 during the first LEO satellite maneuver

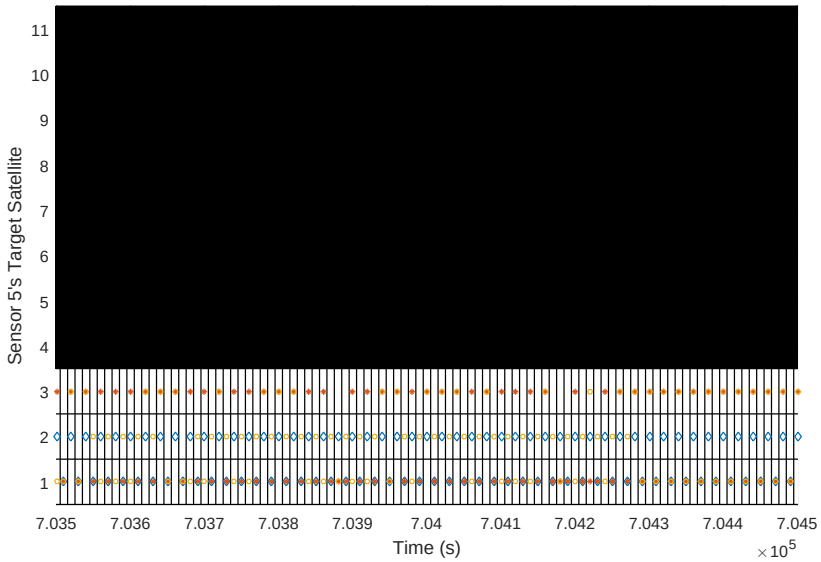

Figure A.5. The target allocation for Sensor 5 during the first LEO satellite maneuver

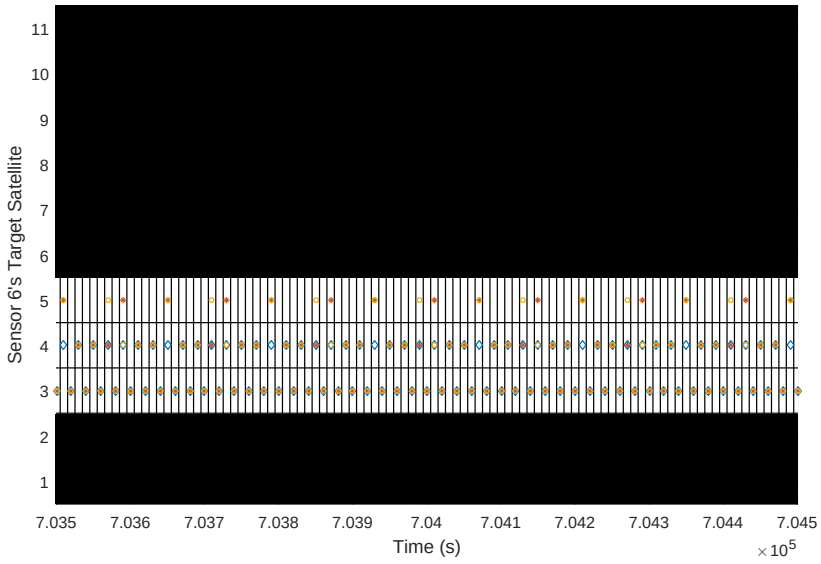

Figure A.6. The target allocation for Sensor 6 during the first LEO satellite maneuver

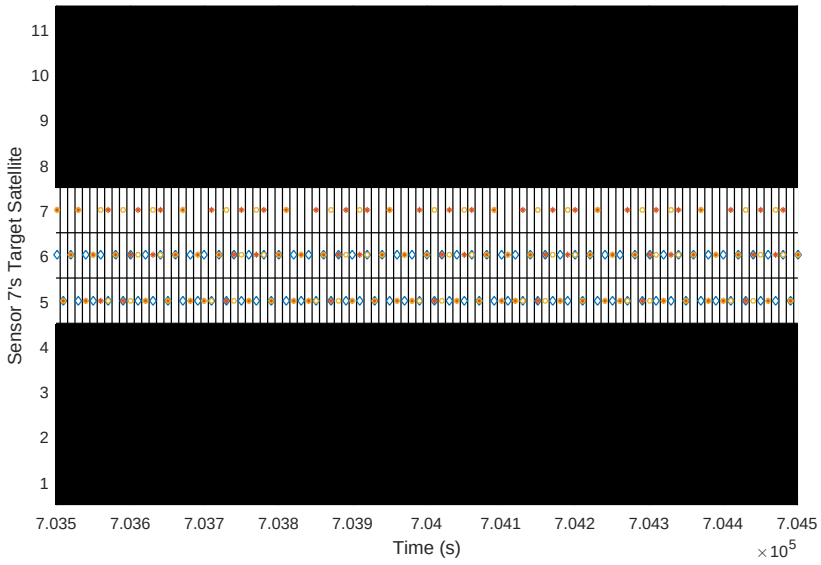

Figure A.7. The target allocation for Sensor 7 during the first LEO satellite maneuver

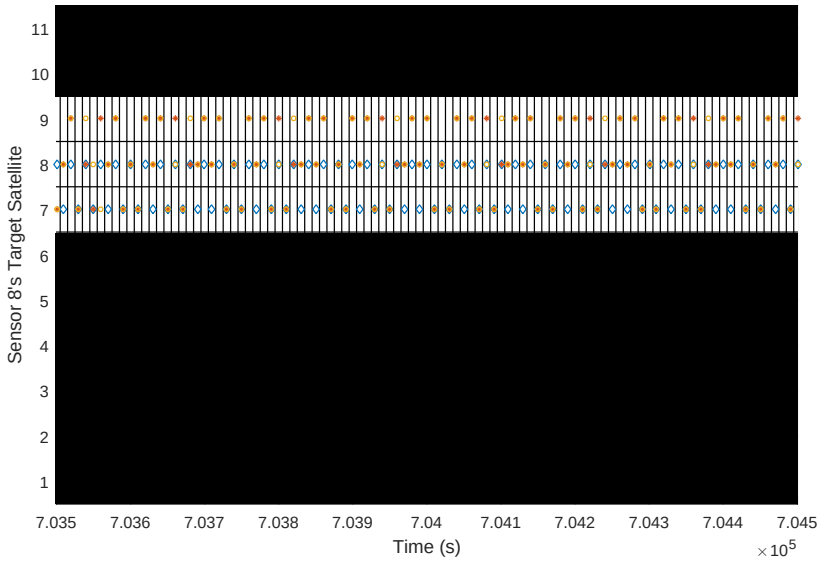

Figure A.8. The target allocation for Sensor 8 during the first LEO satellite maneuver

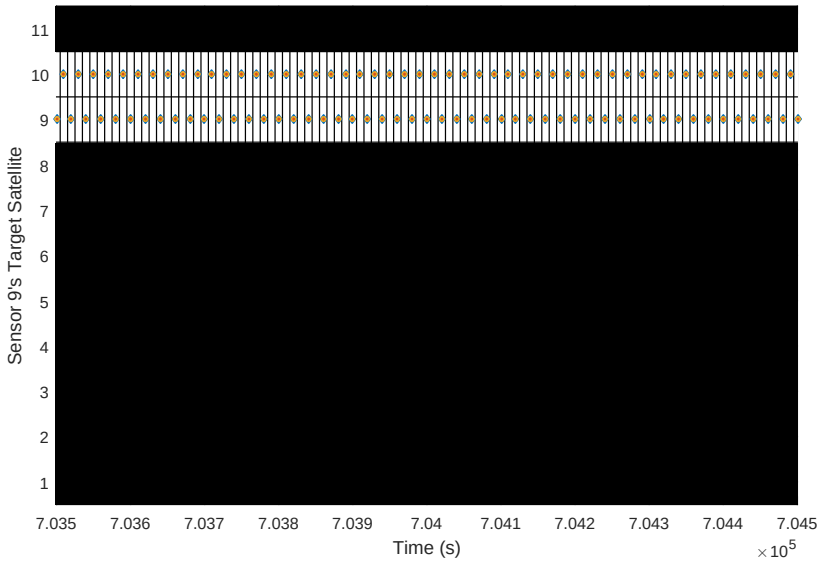

Figure A.9. The target allocation for Sensor 9 during the first LEO satellite maneuver

A.2 Second LEO Satellite Maneuver

Satellite 11 is briefly visible to a ground-based sensor as can be seen in Figure A.15 due to the relatively low field of view of the sensor and the high relative speed of the LEO satellite. This period of visibility is the reason why the second Satellite 11 maneuver does not exhibit the same oscillatory tracking behavior as the first maneuver. The LEO satellite is highly prioritized by the ground-based sensors due to the very high Fisher information gain of that observation due to the close proximity of the sensor and target.

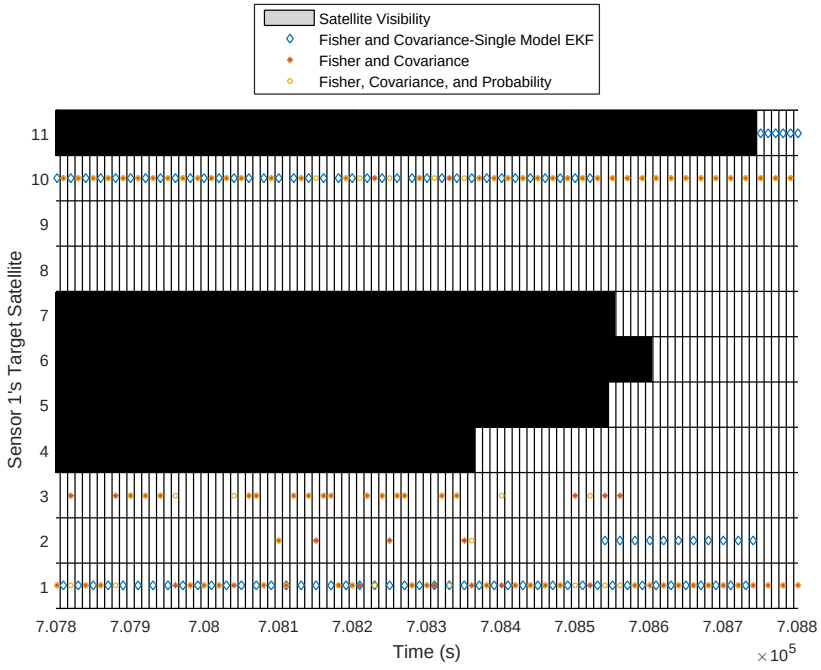

Figure A.10. The target allocation for Sensor 1 during the second LEO satellite maneuver

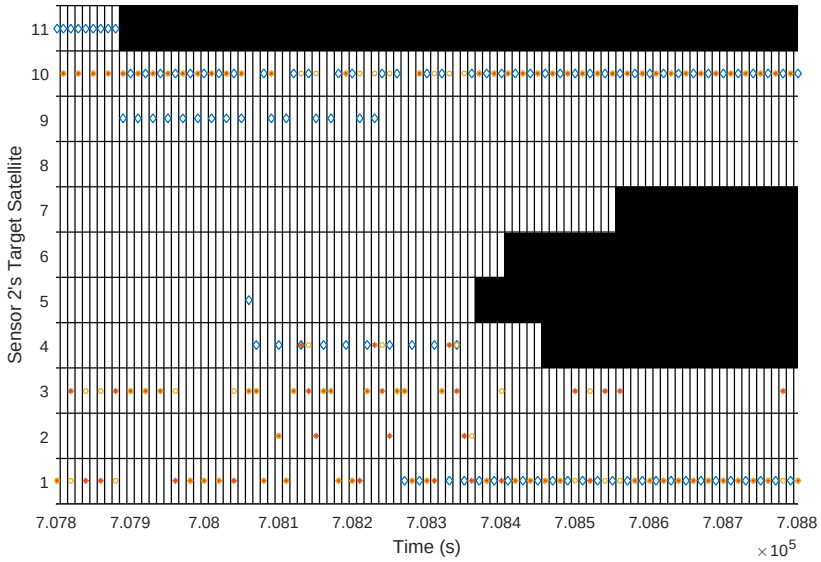

Figure A.11. The target allocation for Sensor 2 during the second LEO satellite maneuver

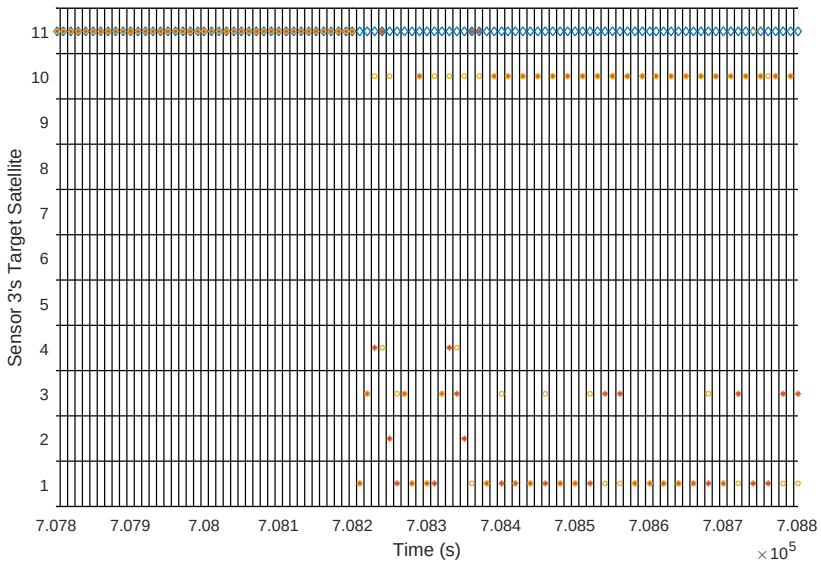

Figure A.12. The target allocation for Sensor 3 during the second LEO satellite maneuver

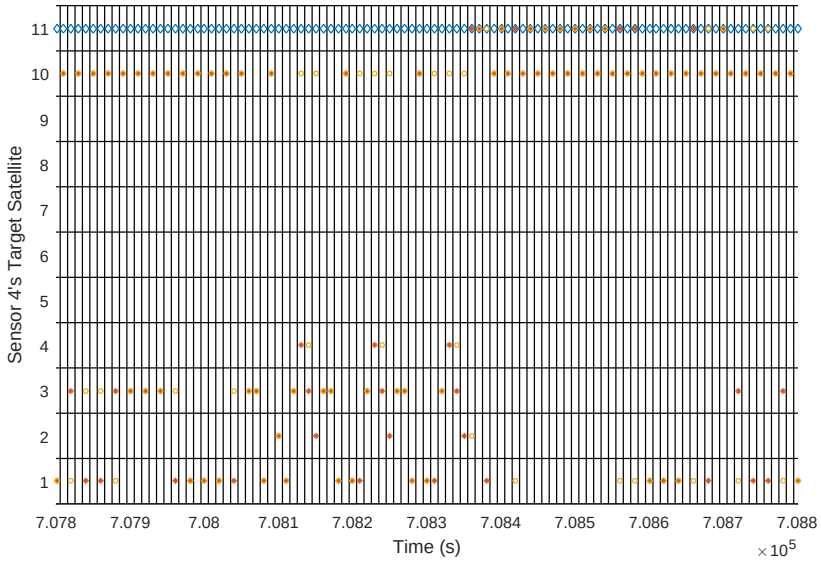

Figure A.13. The target allocation for Sensor 4 during the second LEO satellite maneuver

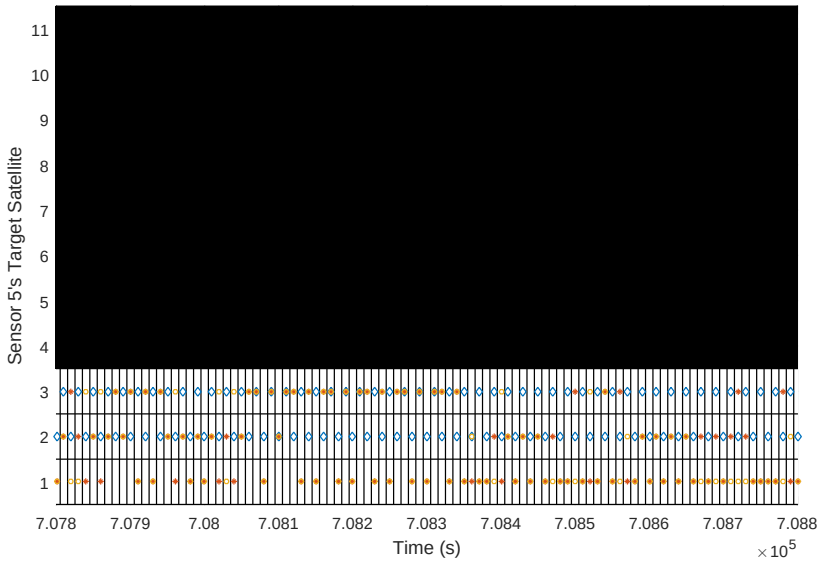

Figure A.14. The target allocation for Sensor 5 during the second LEO satellite maneuver

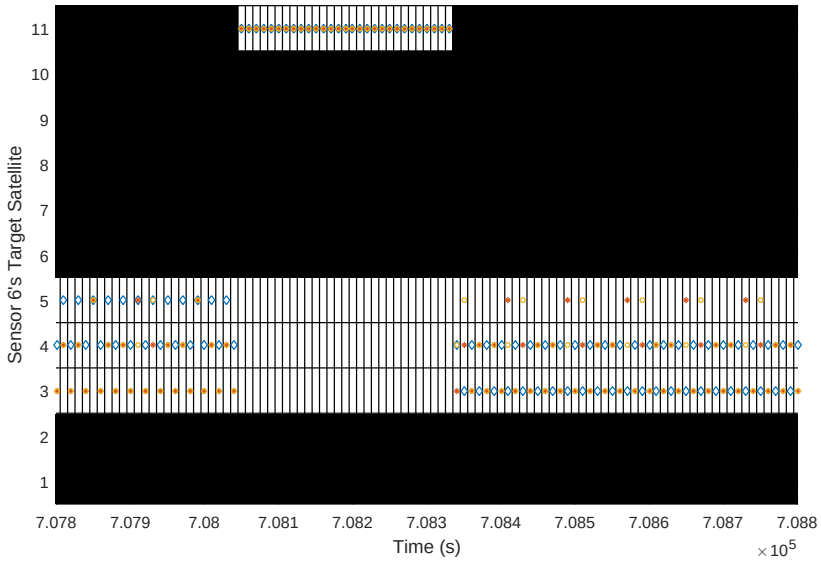

Figure A.15. The target allocation for Sensor 6 during the second LEO satellite maneuver

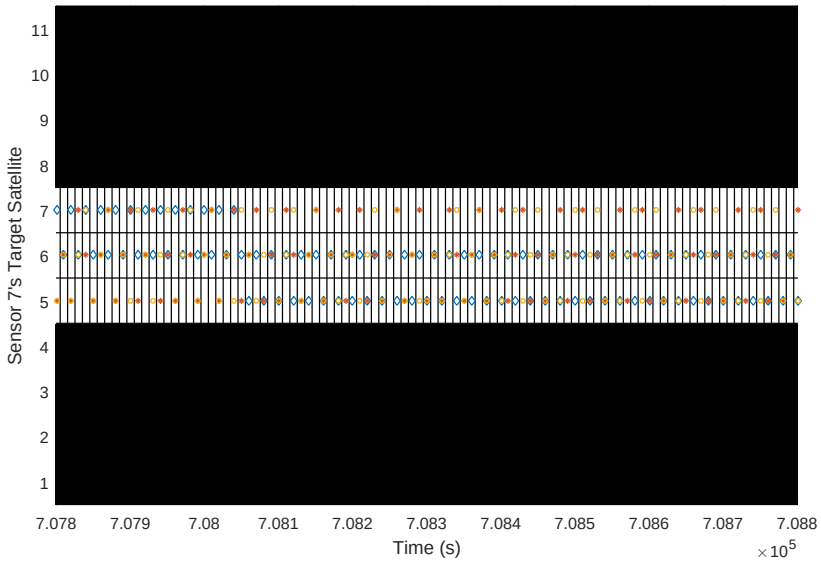

Figure A.16. The target allocation for Sensor 7 during the second LEO satellite maneuver

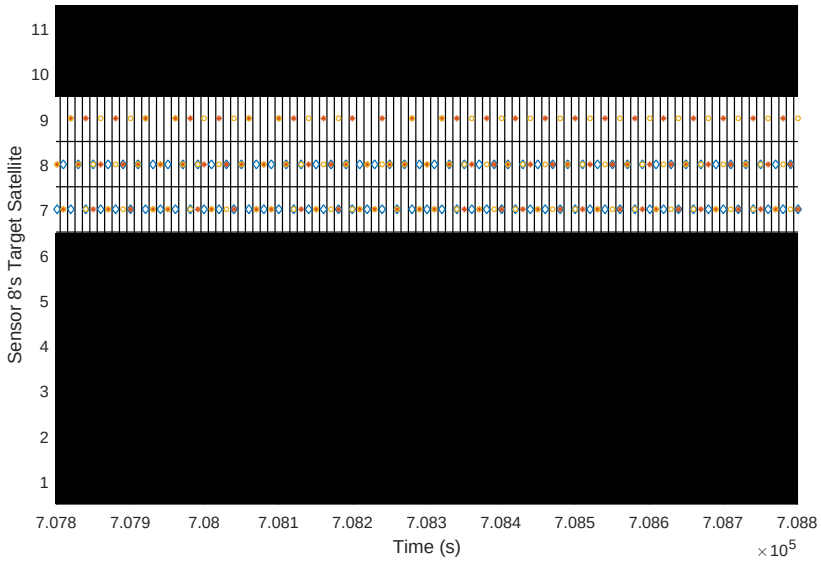

Figure A.17. The target allocation for Sensor 8 during the second LEO satellite maneuver

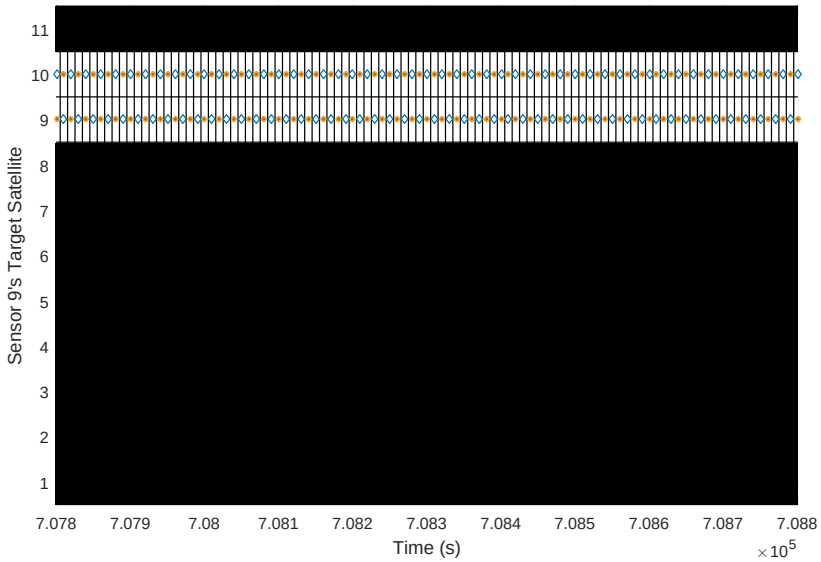

Figure A.18. The target allocation for Sensor 9 during the second LEO satellite maneuver

A.3 Tasking Discussion

The inclusion of Fisher information gain in the tasking method results in sensors tending to favor the target satellites that are closest to them, which is most visible with the single EKF method. This is a desirable behavior as it allows the sensors to target the satellites they are best able to observe compared to other sensors. The estimate covariance component ensures that satellites further away area also observed if more briefly and infrequently. Because of this proximity based priority the LEO satellite tends to be much more highly prioritized which could be adjusted using satellite specific tasking method tuning in future work.

The IMM EKF methods puts a much greater tasking emphasis on geostationary satellites as the satellites near maneuvering point have their higher estimate covariance increased to the point where it is the dominant factor in tasking, reducing the emphasis on targeting the closest satellites. The inclusion of probability directly in the tasking method helps ensure more regular tasking of the LEO Satellite 11 during the first maneuver as it raises the tasking priority to be consistently above that of Satellite 10 as can be seen in Figure A.2. Effectively this is a design trade-off between tracking satellites that are expected to change and satellites that are the easiest to observe for that particular sensor. Based on the particular requirements of the tracking and tasking method this shift in target priority can be adjusted to get the desired results.

B. ADDITIONAL SIMULATION CONFIGURATION

B.1 Alternate Simulation Configuration

In an attempt to illustrate the need for different coefficients for different satellite types in future research a set of alternative simulations are formulated. The motivating configuration change is a much lower state error covariance.

$$\boldsymbol{Q}_1 = \begin{bmatrix} 10^2m^2 & 0 & 0 & 0 & 0 & 0 \\ 0 & 10^2m^2 & 0 & 0 & 0 & 0 \\ 0 & 0 & 10^2m^2 & 0 & 0 & 0 \\ 0 & 0 & 0 & (0.1\frac{m}{s})^2 & 0 & 0 \\ 0 & 0 & 0 & 0 & (0.1\frac{m}{s})^2 & 0 \\ 0 & 0 & 0 & 0 & 0 & (0.1\frac{m}{s})^2 \end{bmatrix} \tag{B.1}$$

To achieve good tracking results with both the single EKF method and the IMM EKF method certain other modifications need to be made to account for this lower error covariance. The lower α is due to the decreased value of the $tr(\hat{\boldsymbol{P}}_i)$ values as is also the reason for the higher β value. The much reduced Υ is due to significant tracking errors that resulted in over valuing potentially maneuvering satellites. Additionally the Σ value for the GEO satellites is reduced to 0.75 to generate better tracking performance in the later part of the simulation period where several GEO satellites are near maneuvering.

To illustrate the positive effects of altering the tracking and tasking methods for different satellite types an additional simulation is done with the maneuvering mode state error covariance of the GEO satellites altered such that it is much lower. This substantially reduces the extra error seen in the later portions of the simulation

Symbol	Value
α	0.25
β	30
Υ	0.05

Table B.1. Alternative tasking coefficients

without this modification. This alteration only effects the two IMM EKF methods so the single EKF results are the same.

$$\boldsymbol{Q}_2 = 10\boldsymbol{Q}_1 \tag{B.2}$$

B.1.1 Single EKF Tasking

An obvious difference of these changes with the single EKF method is that there is a very substantial position error in Figure B.3 around the Satellite 11 maneuvers. The mitigation of errors of this type is one of the goals of the IMM EKF methods and that can be better seen with this lower state error covariance simulation. The velocity error from certain GEO satellite maneuvers is also visible. The overall accuracy is better but the spikes in error seen are much larger indicating that these results would not be acceptable when compared to the non maneuvering error.

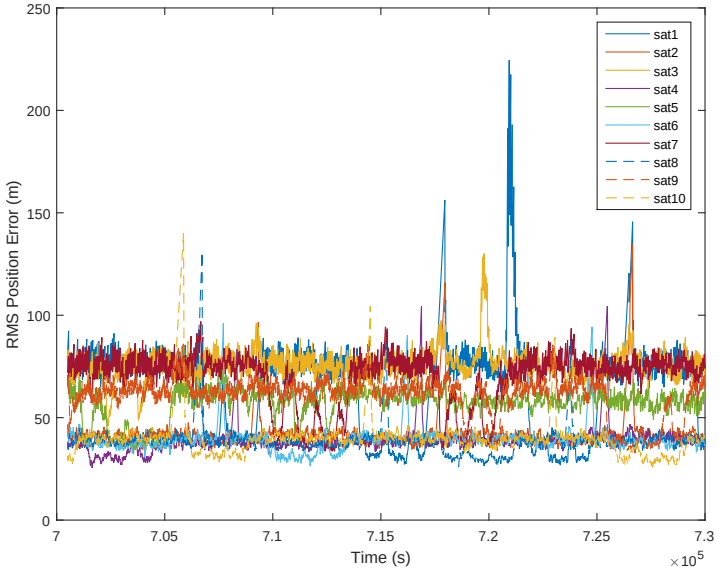

Figure B.1. RMS position error for all satellites averaged over 100 simulations using Fisher information and covariance based sensor tasking with a single EKF estimator

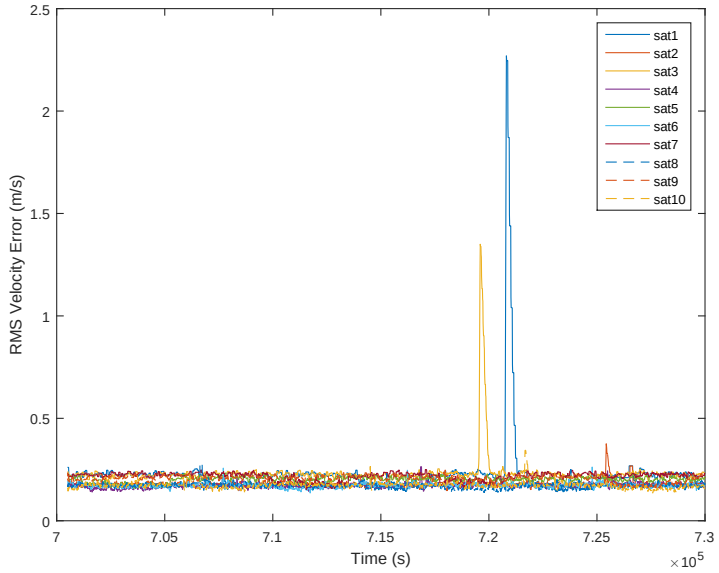

Figure B.2. RMS velocity error for all satellites' except Satellite 11 averaged over 100 simulations using Fisher information and covariance based sensor tasking with a single EKF estimator

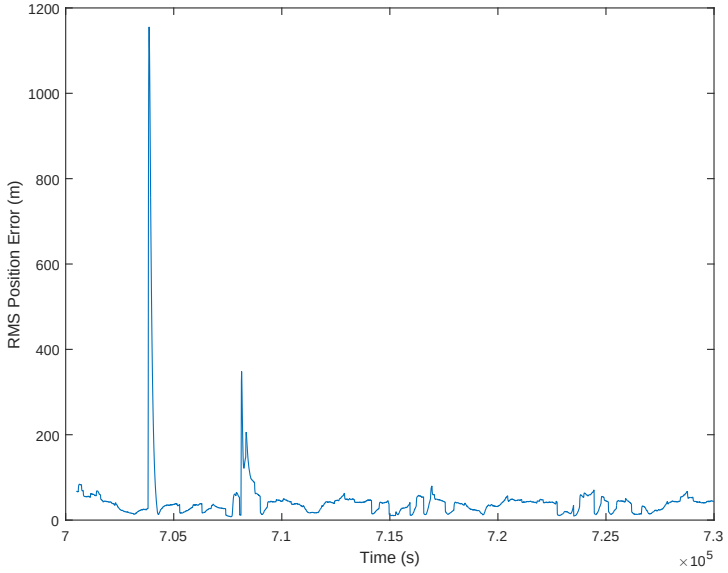

Figure B.3. Satellite 11 RMS position error averaged over 100 simulations using Fisher information and covariance based sensor tasking with a single EKF estimator

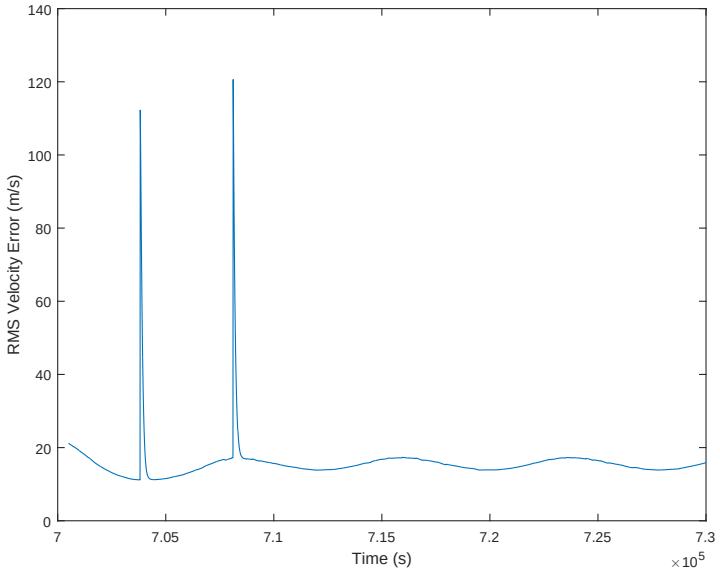

Figure B.4. Satellite 11 RMS velocity error averaged over 100 simulations using Fisher information and covariance based sensor tasking with a single EKF estimator

B.1.2 Fisher and Covariance Tasking

The massive position error seen in Satellite 11 is negated when using the IMM EKF tracking methods (Figure B.8). The position error spikes (Figure B.5) in other satellites are still present and the overall error maximums are roughly comparable to the single EKF. The larger position and velocity errors in the later portions of the simulation are evident as the result of potentially maneuvering GEO satellites. The reduction in the large state error during maneuvers of Satellite 11 is the most significant improvement in this method.

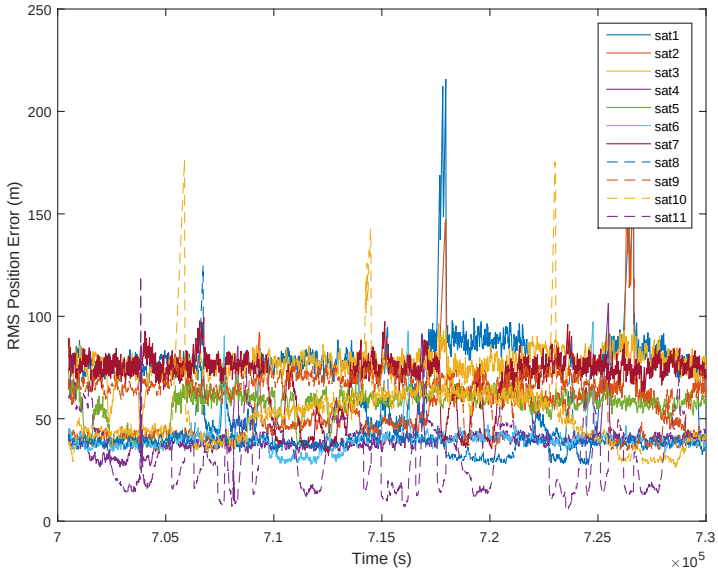

Figure B.5. RMS position error for all satellites except Satellite 11 averaged over 100 simulations using Fisher information and covariance based sensor tasking

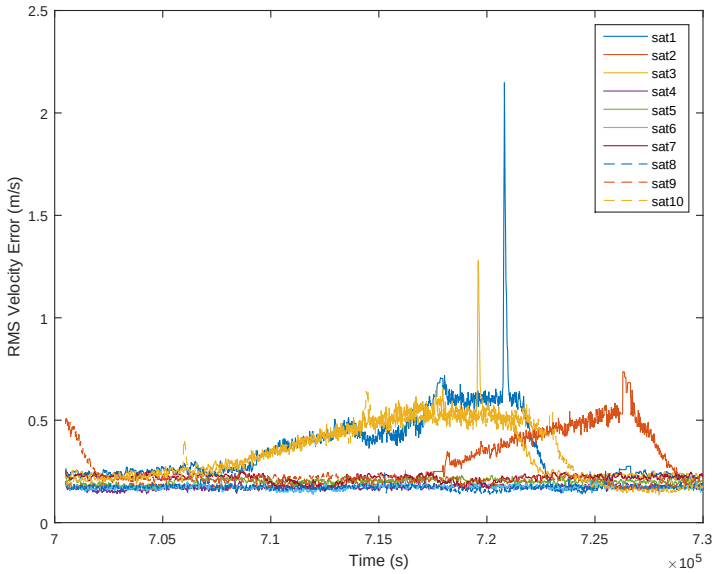

Figure B.6. RMS velocity error for all satellites except Satellite 11 averaged over 100 simulations using Fisher information and covariance based sensor tasking

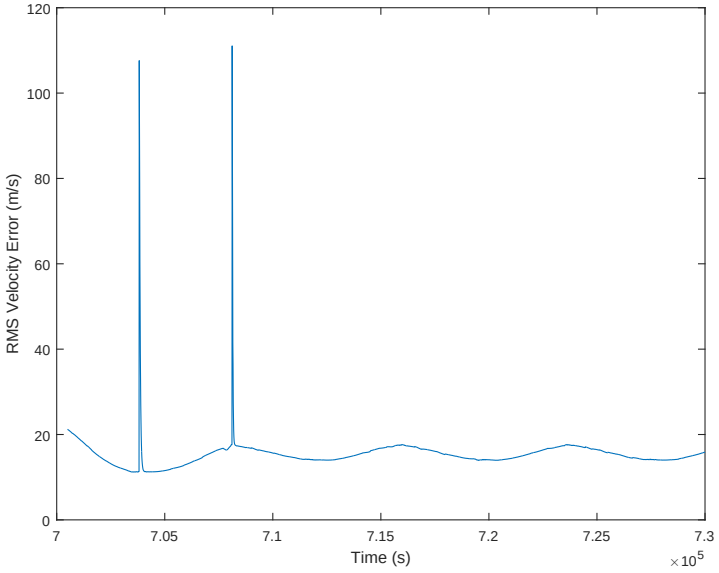

Figure B.7. Satellite 11 RMS velocity error averaged over 100 simulations using Fisher information and covariance based sensor tasking

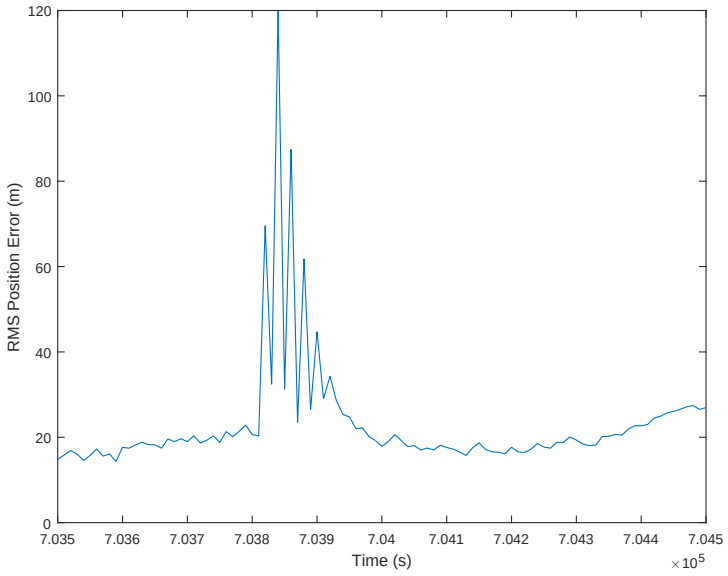

Figure B.8. Satellite 11 RMS position error averaged over 100 simulations using Fisher information and covariance based sensor tasking around the first LEO maneuver

B.1.3 Fisher and Covariance Tasking with altered GEO maneuvering mode

With the altered GEO maneuvering mode state error the large errors in the later portion of the satellite tracking are minimized while maintaining the good tracking of the Satellite 11 maneuver. There is also a clear reduction in the magnitude of position error spikes of the GEO satellites compared to both the single EKF and Fisher and Covariance tasking without the altered GEO maneuvering mode. Because of this satellite specific variable tuning, tracking improvements for all satellites can be seen over previous methods.

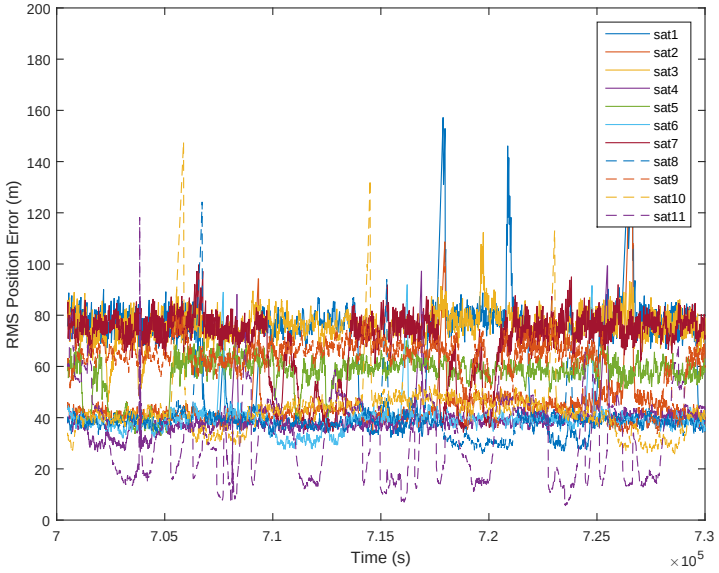

Figure B.9. RMS position error for all satellites except Satellite 11 averaged over 100 simulations using Fisher information and covariance based sensor tasking with an altered GEO maneuvering mode

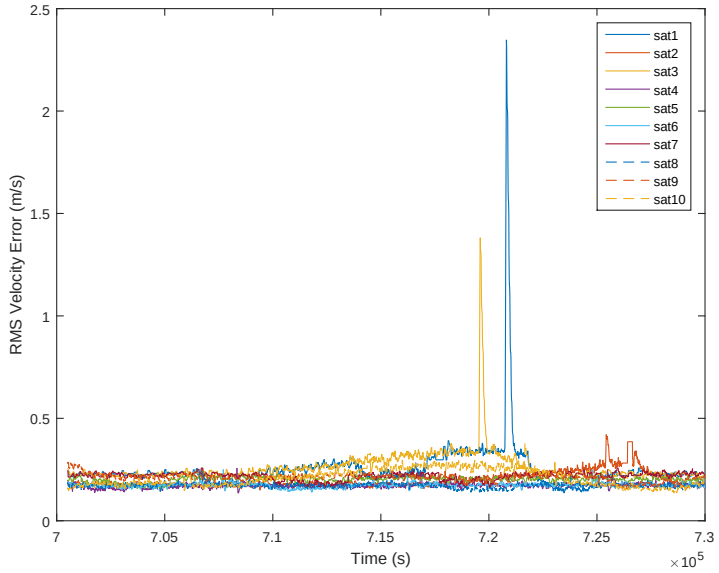

Figure B.10. RMS velocity error for all satellites except Satellite 11 averaged over 100 simulations using Fisher information and covariance based sensor tasking with an altered GEO maneuvering mode

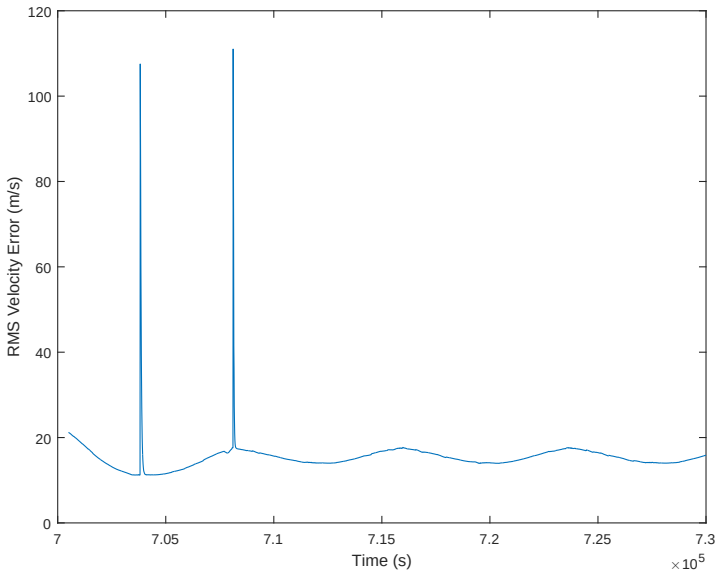

Figure B.11. Satellite 11 RMS velocity error averaged over 100 simulations using Fisher information and covariance based sensor tasking with an altered GEO maneuvering mode

B.1.4 Fisher, Probability and Covariance Tasking

With this particular simulation configuration there is minimal improvement gained by introducing probability based tasking. While probability could potentially be a valuable tool in tuning for other satellite configurations finding an effective method would require future research. Probability elements in the tasking are primarily valuable in dealing with issues where continuous observation, which is less important with the much reduced state error covariances.

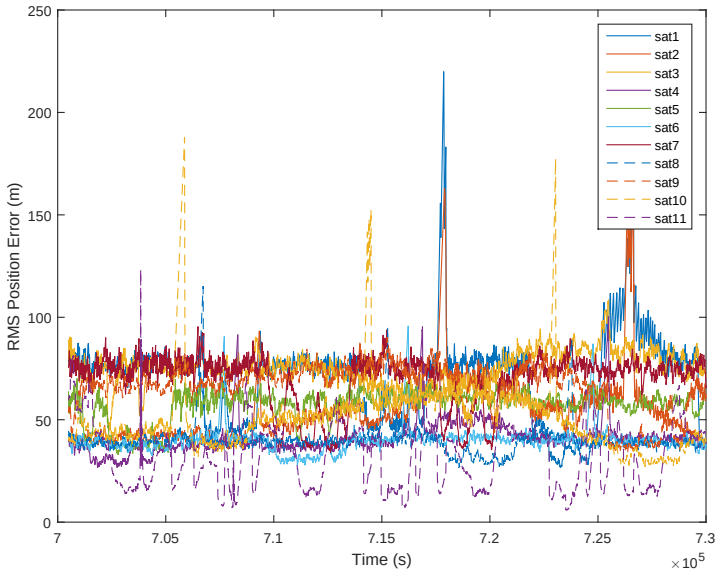

Figure B.12. RMS position error for all satellites averaged over 100 simulations using probability, Fisher information, and covariance based sensor tasking

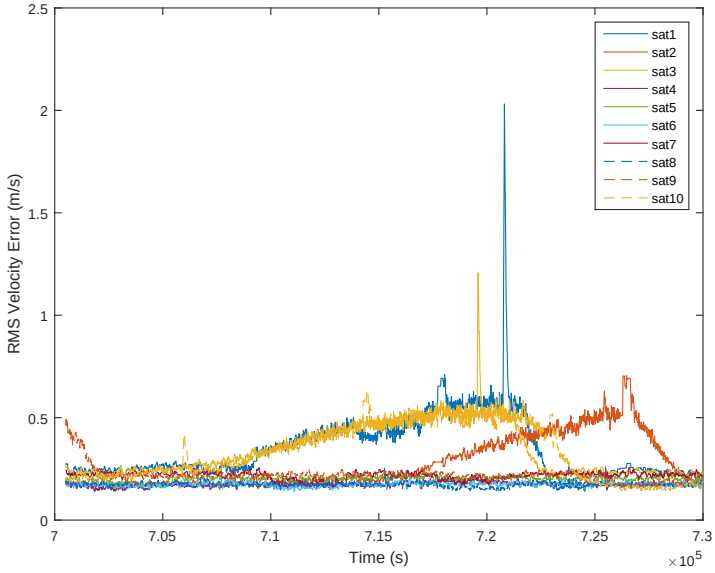

Figure B.13. RMS velocity error for all satellites except Satellite 11 averaged over 100 simulations using probability, Fisher information, and covariance based sensor tasking

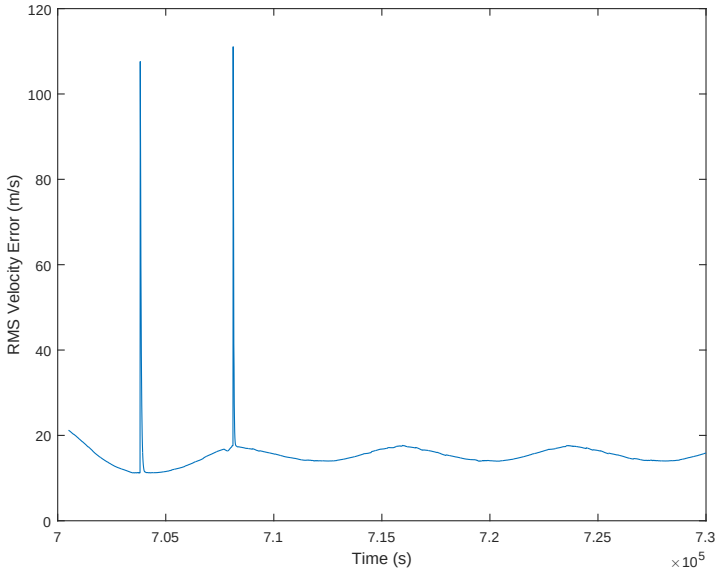

Figure B.14. Satellite 11 RMS velocity error averaged over 100 simulations using probability, Fisher information, and covariance based sensor tasking

B.1.5 Fisher, Probability and Covariance Tasking with altered GEO maneuvering mode

The performance seen here is again nearly identical to the results of the method without probability that made use of the altered GEO maneuvering mode. Indicating that the probability component is not needed in this instance.

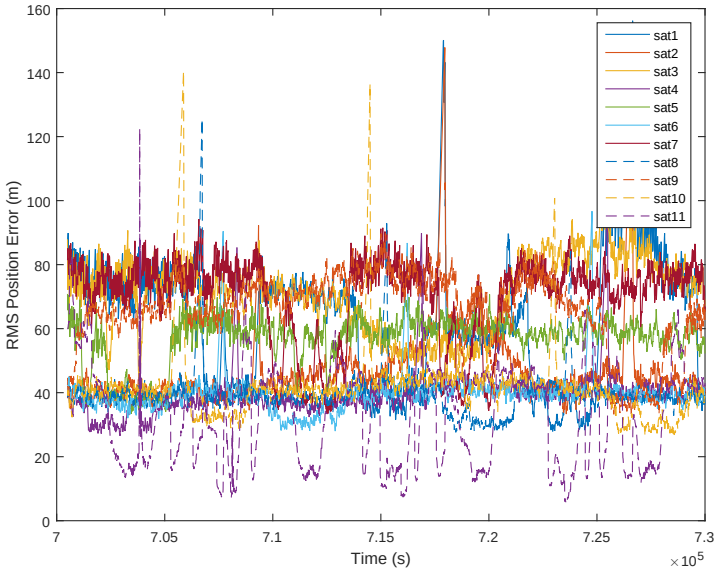

Figure B.15. RMS position error for all satellites averaged over 100 simulations using probability, Fisher information, and covariance based sensor tasking with an altered GEO maneuvering mode

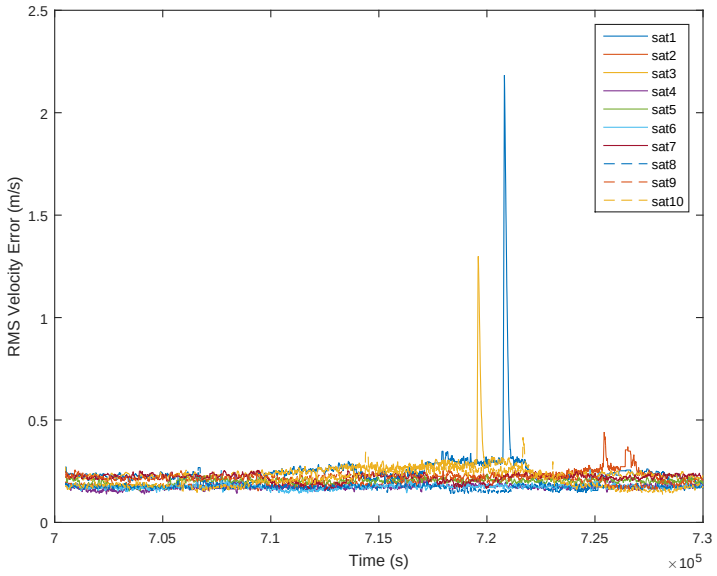

Figure B.16. RMS velocity error for all satellites except Satellite 11 averaged over 100 simulations using probability, Fisher information, and covariance based sensor tasking with an altered GEO maneuvering mode

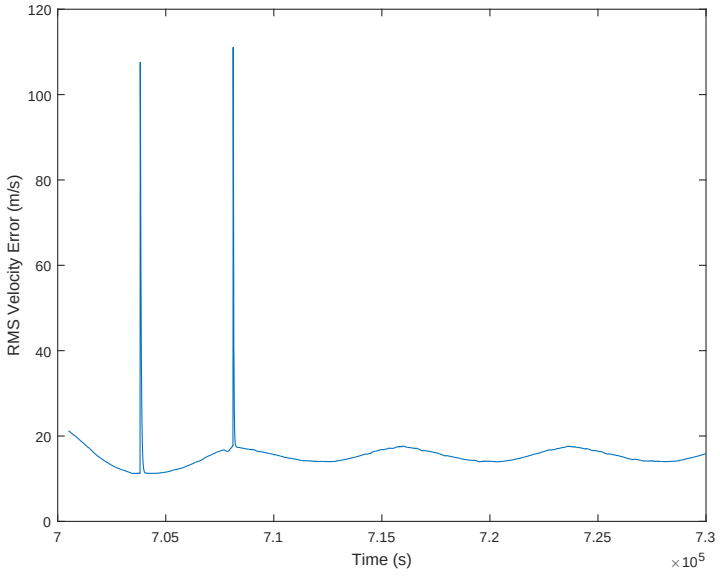

Figure B.17. Satellite 11 RMS velocity error averaged over 100 simulations using probability, Fisher information, and covariance based sensor tasking with an altered GEO maneuvering mode

B.1.6 Method Comparisons

The method comparison demonstrates that the non-maneuvering error values of this configuration are lower than what is seen in the main body of the paper. But there is a substantial increase in error of the IMM EKF methods in certain periods where the GEO satellites are potentially maneuvering (Figure B.18) that is mitigated by altering the tracking behavior of those satellites while preserving the improvements in tracking performance (Figure B.19). The improvement due to IMM EKF methods in position error during the Satellite 11 maneuvers is even more pronounced in these simulations and is on the order of kilometers B.3 which is very substantial on the scale of GEO satellites [1]. The improvements with GEO satellite state error covariance does illustrate that using the same coefficients and tasking model for all satellites in varied systems is not always viable for all tracked satellites. Dynamically developing tasking coefficients for different satellite types would be a promising area of future work to mitigate these issues. As can be seen in Table B.2 the overall performance of the method employing probability and satellite specific tracking method demonstrates the best overall performance of all methods in this paper. However, The differences between the IMM tasking methods was much less pronounced in this configuration as probability based tasking was not required. As a result the difference seen between the IMM EKF methods are primarily the result of simulation variance. This lack of difference indicates that while probability as a tasking component can be a valuable tool, as the main body of this paper illustrated, it is not useful to all tracking and tasking problems.

Method	Error Metric	Value	Standard Deviation
Single EKF	Mean Position Error	$51.9613m$	$6.5992m$
	Max Position Error	$1155.5850m$	–
	Mean Velocity Error	$1.6096\frac{m}{s}$	$0.5792\frac{m}{s}$
	Max Velocity Error	$120.64531\frac{m}{s}$	–
IMM Fisher and Covariance	Mean Position Error	$51.7569m$	$3.3127m$
	Max Position Error	$193.8295m$	–
	Mean Velocity Error	$1.5855\frac{m}{s}$	$0.3772\frac{m}{s}$
	Max Velocity Error	$111.0706\frac{m}{s}$	–
IMM Fisher, Covariance, and Probability	Mean Position Error	$51.6725m$	$3.3175m$
	Max Position Error	$156.1986m$	–
	Mean Velocity Error	$1.5844\frac{m}{s}$	$0.3772\frac{m}{s}$
	Max Velocity Error	$111.08617\frac{m}{s}$	–

Table B.2. Alternate Simulation method error comparison from $700500s$ to $730000s$ with variable $\boldsymbol{Q}_2$

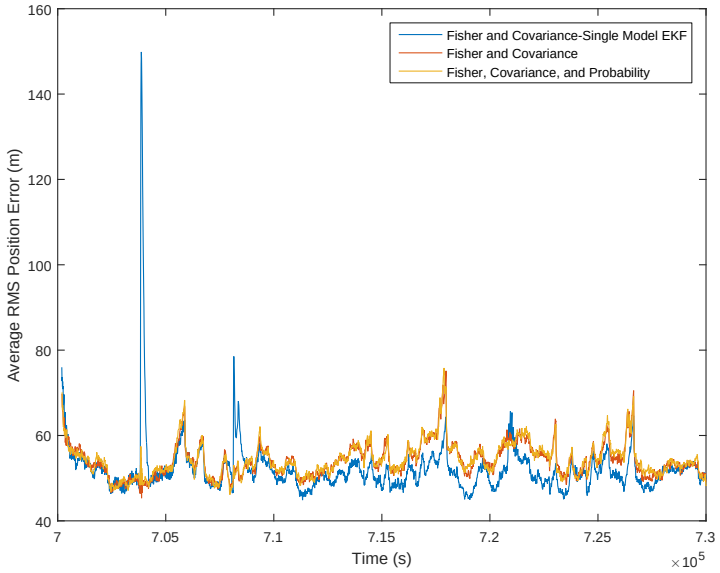

Figure B.18. Average of all satellites' position error over 100 simulations for all tasking methods

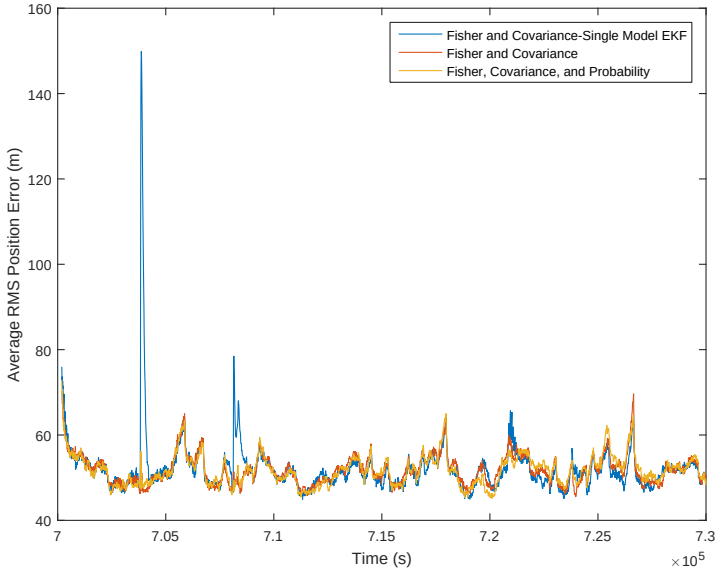

Figure B.19. Average of all satellites' position error over 100 simulations for all tasking methods with an altered GEO maneuvering mode

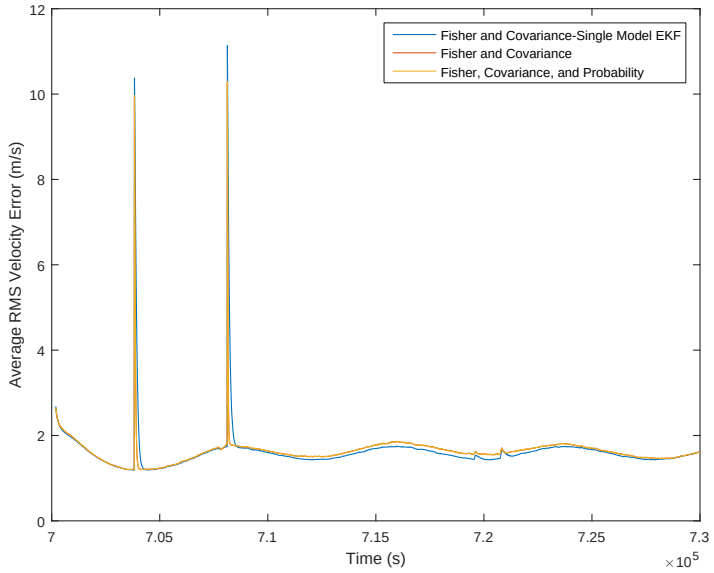

Figure B.20. Average of all satellites' velocity error over 100 simulations for all tasking methods

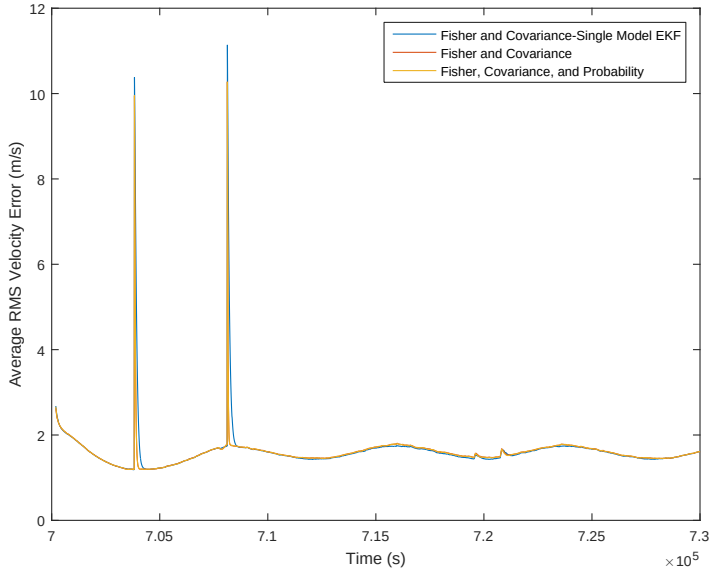

Figure B.21. Average of all satellites' velocity error over 100 simulations for all tasking methods with an altered GEO maneuvering mode

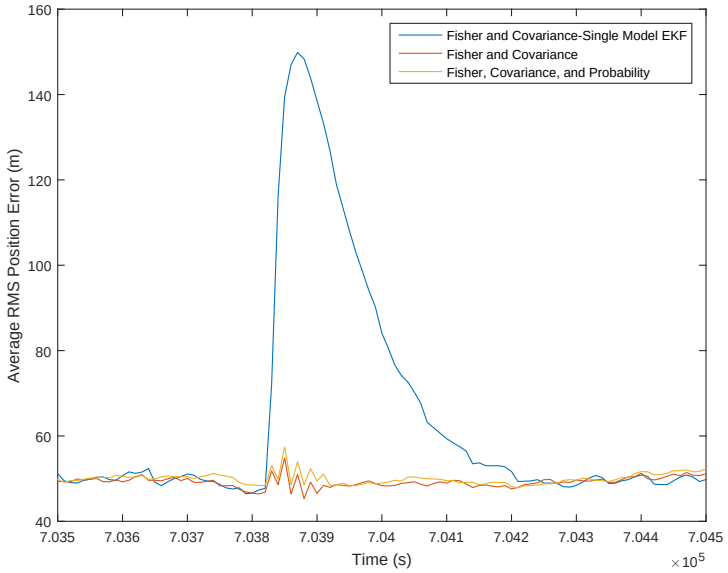

Figure B.22. Average of all satellites' position error over 100 simulations for all tasking methods near the first LEO maneuver

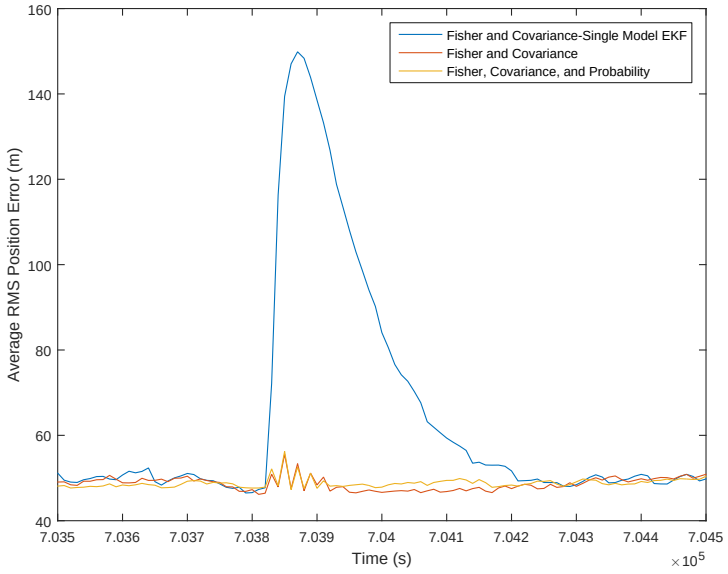

Figure B.23. Average of all satellites' position error over 100 simulations for all tasking methods near the first LEO maneuver with an altered GEO maneuvering mode

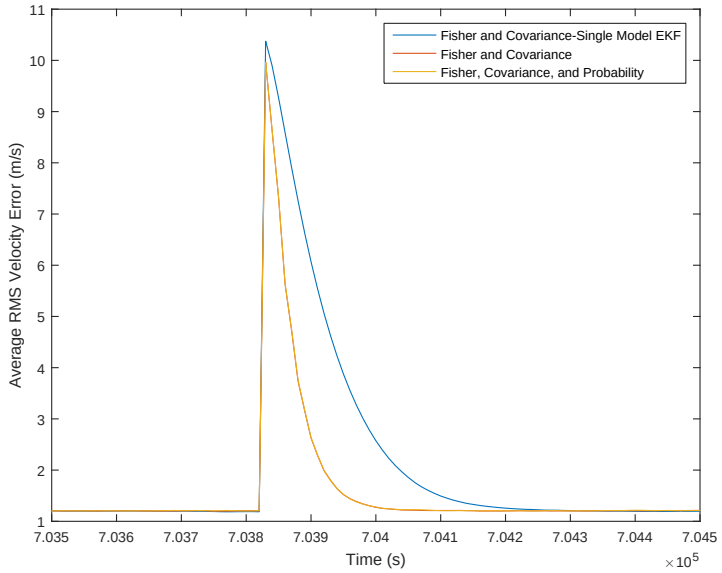

Figure B.24. Average of all satellites' velocity error over 100 simulations for all tasking methods near the first LEO maneuver

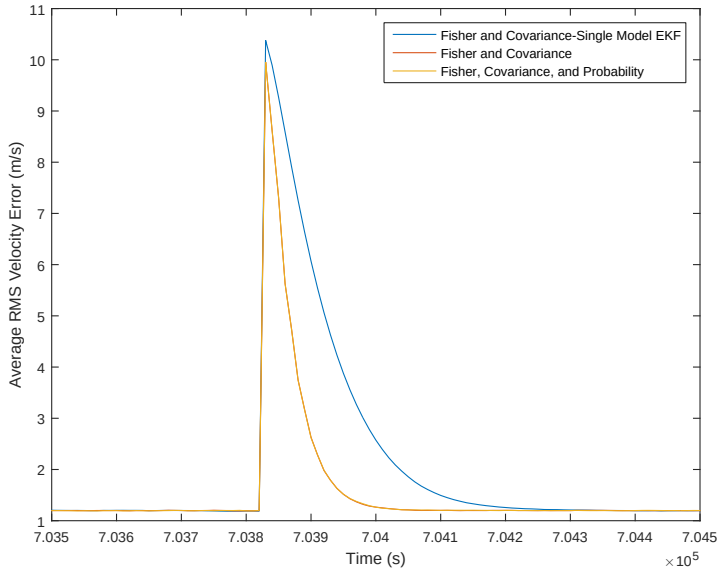

Figure B.25. Average of all satellites' velocity error over 100 simulations for all tasking methods near the first LEO maneuver with an altered GEO maneuvering mode

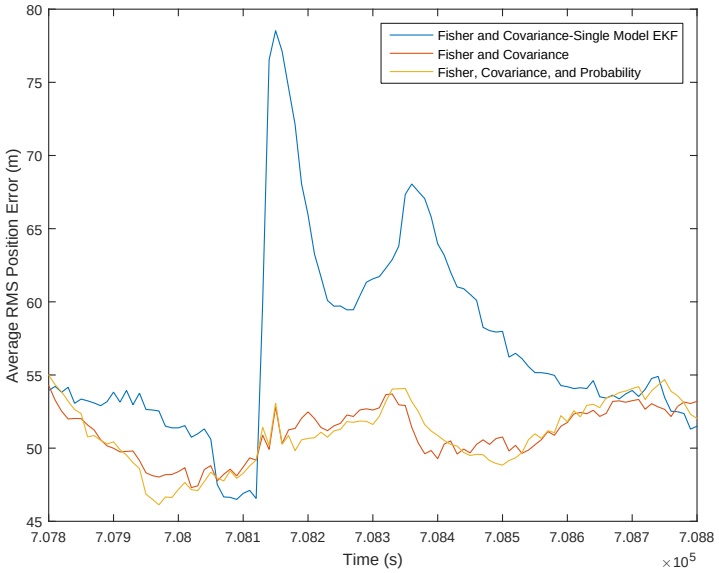

Figure B.26. Average of all satellites' position error over 100 simulations for all tasking methods near the second LEO maneuver

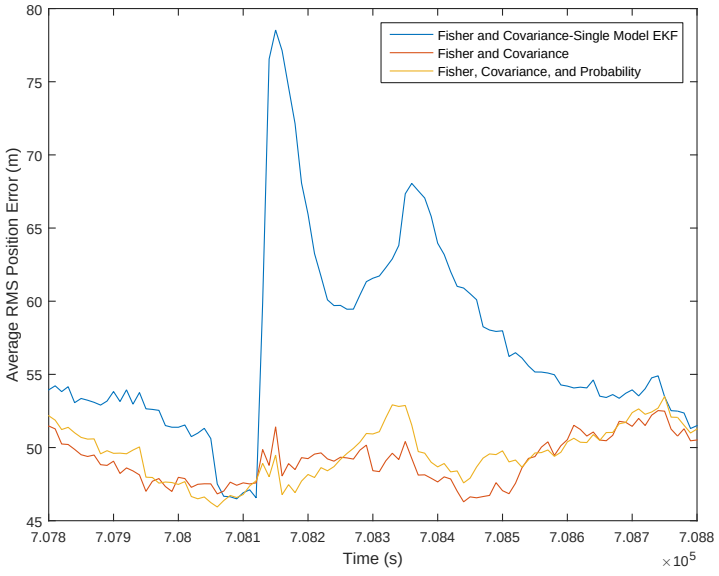

Figure B.27. Average of all satellites' position error over 100 simulations for all tasking methods near the second LEO maneuver with an altered GEO maneuvering mode

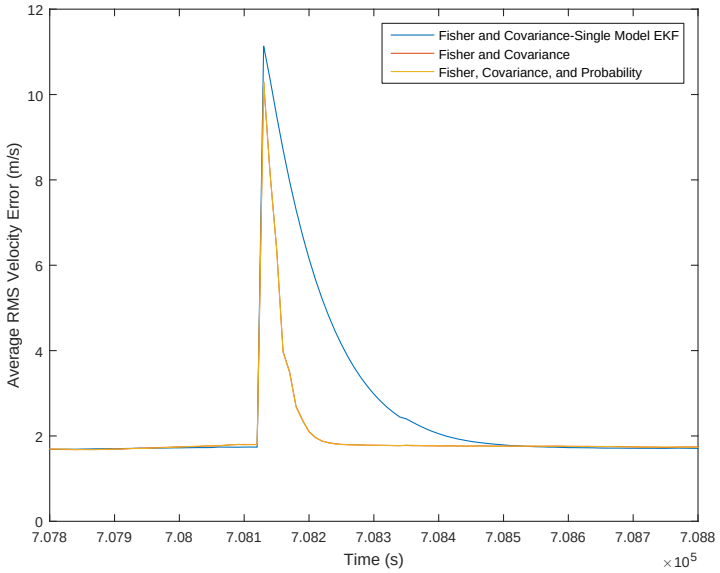

Figure B.28. Average of all satellites' velocity error over 100 simulations for all tasking methods near the second LEO maneuver

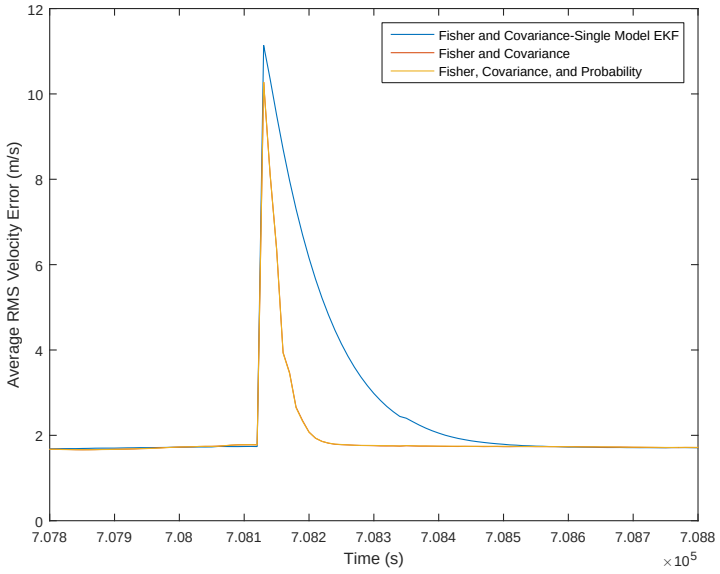

Figure B.29. Average of all satellites' velocity error over 100 simulations for all tasking methods near the second LEO maneuver with altered an GEO maneuvering mode